Attrition Resistant Iron-Based Fischer-Tropsch Catalysts

Final Report

Work Performed Under
Grant No: DE-FG22-96PC96217

for
U.S. Department of Energy
Federal Energy Technology Center
Pittsburgh, PA 15236

by
K. Jothimurugesan
Department of Chemical Engineering
Hampton University
Hampton, VA 23668

James G. Goodwin, Jr.
Department of Chemical and Petroleum Engineering
1249 Benedum Hall
University of Pittsburgh
Pittsburgh, PA 15260

Santosh K. Gangwal
James J. Spivey
Research Triangle Institute
P.O. Box 12194
Research Triangle Park, NC 27709

October 1999

DISCLAIMER

ABSTRACT

Fischer-Tropsch (FT) synthesis to convert syngas ($CO + H_2$) derived from natural gas or coal to liquid fuels and wax is a well-established technology. For low H_2 to CO ratio syngas produced from CO_2 reforming of natural gas or from gasification of coal, the use of Fe catalysts is attractive because of their high water gas shift activity in addition to their high FT activity. Fe catalysts are also attractive due to their low cost and low methane selectivity. Because of the highly exothermic nature of the FT reaction, there has been a recent move away from fixed-bed reactors toward the development of slurry bubble column reactors (SBCRs) that employ 30 to 90 μm catalyst particles suspended in a waxy liquid for efficient heat removal. However, the use of Fe FT catalysts in an SBCR has been problematic due to severe catalyst attrition resulting in fines that plug the filter employed to separate the catalyst from the waxy product. Fe catalysts can undergo attrition in SBCRs not only due to vigorous movement and collisions but also due to phase changes that occur during activation and reaction.

The objectives of this research were to develop a better understanding of the parameters affecting attrition of Fe F-T catalysts suitable for use in SBCRs and to incorporate this understanding into the design of novel Fe catalysts having superior attrition resistance.

A Ruhrchemie iron catalyst of composition $100Fe/5Cu/4.2K/25SiO_2$ was obtained and tested for FT activity in a 1 cm i.d. high pressure fixed bed micro-reactor system. This catalyst will serve as a baseline catalyst for this work from which improvements in attrition resistance and activity will be sought. The effect of silica addition via coprecipitation and as a binder to a doubly promoted FT iron catalysts (100/Fe/5 Cu/4.2K) was studied. The catalysts were prepared

by coprecipitation, followed by binder addition and spray drying at 250°C in a 1 m diameter, 2 m tall spray dryer. The binder silica content was varied from 0 to 20 wt %. A catalyst with 12 wt % binder silica was found to have the highest attrition resistance. The FT activity and selectivity of this catalyst are better than a Ruhrchemie catalyst at 250 °C and 1.48 MPa. F-T reaction studies over 100 hours in a fixed-bed reactor showed that this catalyst maintained around 95% CO conversion with a methane selectivity of less than 7 wt % and a C_5^+selectivity of greater than 73 wt %. The effect of adding precipitated silica from 0 to 20 % pbw (containing 12 wt % binder silica) was also studied. Addition of precipitated silica was found to be detrimental to attrition resistance and resulted in increased methane and reduced wax formation. Based on the experience gained, a proprietary HPR-43 catalyst has been successfully spray dried in 500-g quantity. This catalyst showed 95% CO conversion over 125 h of testing at 250 °C, 1.48 MPa, and 2 NL/g-cat/h and had less than 4% methane selectivity. Its attrition resistance was one of the highest among the catalysts tested.

ACKNOWLEDGMENTS

This study was sponsored by the U.S. Department of Energy (DOE) under Grant No: DE-FG-22-96PC96217. The authors would like to acknowledge with gratitude the guidance provided by the DOE Contracting Officer's Representative, Dr. Richard E. Tischer. The authors also acknowledge the guidance of United Catalysts Inc., and Energy International.

CONTENTS

LIST OF TABLES

LIST OF FIGURES

Attrition Resistant Iron-Based Fischer-Tropsch Catalysts

1.0 INTRODUCTION

Fischer-Tropsch synthesis (FTS) is a set of reactions by which CO and H_2 (syn gas) are converted into a wide variety of hydrocarbons. This synthesis provides the best means currently available for the conversion of coal into synthetic transportation fuels. While over the near to mid term this indirect coal liquefaction route is not likely to be competitive with cheap oil on a global basis, there are a number of commercial activities in this area. SASTECH is making commercially synthetic fuels and chemicals by FTS from coal, China plans to make town gas via this route, and Williams Company is constructing a pilot plant to determining the economics of underground coal gasification, while Shell is using FTS commercially to convert natural gas to high value products. Improvements and innovation in FTS is strategically very important to the U.S. because of its vast coal reserves and because it represents the best way to make high quality liquid products from coal.

Since the gasification of coal gives syn gas relatively lean in hydrogen ($H_2/CO \cong 0.5$-0.7), the use of a catalyst which converts the oxygen of the CO to CO_2 rather than H_2O is preferable. This is achieved by using catalysts which, in addition to being active for FTS, are also active for the water gas shift reaction (WGS):

$$CO + H_2O \rightleftharpoons CO_2 + H_2$$

Fe is the preferred catalyst since it is one of the more active FTS catalysts, active for the WGS reaction, and relatively inexpensive.

Because FTS is so exothermic, one of the major problems in control of the reaction is heat removal. Recent work by industry (Gulf, Statoil, Exxon, SASOL/ SASTECH, Rentech, and others), DOE, and universities has concentrated on the use of slurry-phase reactors, especially

slurry bubble column reactor (SBCRs), which are able to be controlled more easily because of the liquid phase present. Such reactors have relatively simple designs and low initial costs while still permitting high catalyst and reactor productivity.

Obviously, much recent work related to slurry-phase FTS based on coal-derived syn gas has focused on using Fe catalysts. Unfortunately, the use of Fe catalysts in SBCRs have been found to present a number of problems. Because of the difficulty in reducing highly dispersed Fe and its lower FTS activity than Co (which does not posses much WGS activity) or Ru (which is too expensive to use by itself), bulk Fe catalysts have had to be used in order to have sufficient active surface area per catalyst weight. The Fe catalysts used in SBCRs have been usually prepared by precipitation, one of the typical methods of preparation of Fe catalysts for use in fixed bed reactors.

The problems encountered in using precipitated iron catalysts are mainly due to two major characteristics: (a) their low density and (b) their attrition properties. Since SBCRs are used to produce high alpha (α) FTS products, there is a need to easily and inexpensively separate the catalyst from the liquid products. The apparent density of typical precipitated Fe catalysts is estimated to be very close (near 0.7 g/cm^3) to that of Fischer-Tropsch wax (about 0.68 g/cm^3) at reaction conditions (Donnelly, 1989). While this is beneficial for keeping the catalyst slurried, catalyst separation from the products can be difficult since the catalyst does not settle well.

Although internal/external filtration systems can be incorporated with slurry reactors, plugging of the filters by Fe catalyst particles is encountered. This is due to the low attrition resistance of the Fe catalyst and the significant breakage of the Fe particles. Fe catalysts are subject to both chemical as well as physical attrition in a SBCR. Chemical attrition can be caused due to phase changes that any Fe catalyst goes through ($Fe_2O_3 \rightarrow Fe_3O_4 \rightarrow FeO \rightarrow$ Fe metal $\rightarrow$ Fe

carbides) potentially causing internal stresses within the particle and resulting in weakening, spalling or cracking. Physical attrition can result due to collisions between catalyst particles and with reactor wall. Catalyst particles of irregular shapes and non-uniform sizes produced by conventional methods are subject to greater physical attrition. Recently, there has been an in-depth development of precipitated Fe catalysts for use in the slurry phase at the University of Kentucky (O'Brian et al., 1995). However, none of the catalysts produced by this route appears to offer much improvement in attrition resistance.

1.1 Use of Fe Catalysts in SBCRs

Recent work by industry (Gulf, Statoil, Exxon, SASOL/SASTECH, Rentech, and others), DOE, and universities has concentrated on the use of slurry-phase reactors, especially SBCRs. The advantages of the SBCRs are (i) the ability to use low H_2/CO ratio synthesis gas, (ii) the ability of the liquid phase to efficiently withdraw the heat of reaction and thereby control reaction temperature, (iii) high catalyst and reactor productivity, (iv) favorable conditions for catalyst regeneration, and (v) simple construction and low investment cost.

Much recent work related to slurry-phase FTS based on coal-derived syngas has focused on using Fe catalysts. The major problem encountered in the use of Fe catalysts in SBCRs is their tendency to undergo attrition which can result in fouling/plugging of downstream filter and equipment and make the separation of the catalyst from the oil/wax product very difficult if not impossible.

To date, the only group reporting any success in solving this problem is SASTECH. They have patented a wax-catalyst separation system for use external to the reactor. However, it appears that this may be only part of the solution and that catalyst "pretreatment" also plays an important role. Unfortunately, not only are all of the details proprietary, they are owned by a

foreign company. Also, even if some combination of improved catalyst and external separation system is successful, the need for a separate separation system beyond in-system filters creates added cost for this process.

1.2 Catalyst Attrition

The factors which affect attrition dynamics include the properties of the catalyst particles, the reactor environment, and the types of breakage mechanics. Spherical particles are less likely to attrit than irregularly shaped particles. The size of the particle and the size distribution of the entire catalyst particle population also influence attrition. In general, larger particles are more easily attrited than smaller ones. However, there is no systematic relationship between particle size, size distribution, and friability. The porosity of the particle influences its friability. Also, pores filled with liquids are more likely to rupture due to changes in state of the liquid caused by temperature or pressure changes. Catalyst particle hardness provides a general measure of the particles ability to resist wear and its susceptibility to fracture (Lee et al., 1993).

In addition to the physical properties of the catalyst, the reaction environment can have a major impact on attrition by causing solid-state phase transformations in the catalyst. During activation of the polycrystalline precipitated Fe catalyst, iron oxide transforms from hematite to magnetite and finally into Fe^{o} and iron carbide phases. While the transformation from hematite to magnetite is extremely rapid, the magnetite-to-carbide transition is much slower (Shroff et al., 1995). Because of the multiplicity of phases, grain boundaries phase growth kinetics, significant stresses can be introduced into the Fe particle leading to breakage.

1.3 Fe Catalyst Preparation

The preparation of the early precipitated iron catalyst developed by Ruhrchemie and used in the fixed-bed reactors at SASOL as well as the more recent work carried out on these catalyst

to improve their performance has been reviewed extensively (Dry 1981, Anderson 1984, Lang, et al., 1995). The work done on precipitated iron catalysts intended specifically for liquid-phase synthesis has also been reviewed (Kolbel 1980). Basically, these iron catalysts are prepared by precipitation from a preheated solution of iron and copper nitrates (40 g Fe and 2 g Cu per liter) with sodium carbonate (Dry 1981). The addition of sodium carbonate is carried out with vigorous stirring for several minutes until the pH reaches 7-8. Sodium is removed by washing with hot distilled water in a filter press. The resulting precipitate is slurried in water and impregnated with a potassium waterglass solution to provide 25 g SiO_2 per 100 g Fe. SiO_2 is present as a structural promotor. The precipitated silica is adsorbed onto or reacted with the high area Fe_2O_3 and excess potassium removed by the addition of sufficient HNO_3 to give 0.5 g K_2O per 100 g Fe after filtration. The catalyst is filtered, extruded , and dried to less than 10 wt% water (Dry 1981). If no silica is added or if it is to be added in forms other than potassium waterglass, alkali addition to the precipitate is carried out using a dilute potassium carbonate solution. Precipitation with ammonia or ammonium carbonate solution may be preferable in order to eliminate the promoter effect of retained sodium carbonate, greater ease of filtration, and use of 40% less water is in the washing process (Kolbel 1980).

The structure of the catalyst is affected by the concentrations of the different solutions, the time of precipitation, and the control of temperature and pH during the precipitation process. Silica stabilizes the iron oxide by preventing crystal growth and results in higher surface area catalysts. The porosity of the catalyst is also dependent on the amount of shrinkage during the drying process. The pore volume can be increased more than two fold when the precipitate is re-slurried in acetone and then dried. However, the physical strength is an inverse function of the pore volume (Dry 1981). The non-uniform particle sizes and, especially, the irregular shapes of

the catalyst particles produced by precipitation lead to high production of catalyst fines by abrasion. Although the addition of silica to catalysts produced by precipitation may improve their physical and mechanical properties, especially their hardness, it does not make them suitable for operation in a SBCR. Their low density (~0.7 g/cm^3) which is close to the density of FT wax (0.68 g/cm^3) makes it difficult to separate them from the wax following reaction although it helps to keep them slurried.

Supported metal catalysts on attrition resistant supports such as alumina or silica are commonly used in the refining and chemical industry. The attrition resistance of these supports is due in major part to their ability to be produced in a spheroidal shape, their refractory properties, and their strength. While supported Co catalysts have been found to be very effective for FTS and, in fact, are being used by Shell in their plant in Malaysia, supported Fe catalysts have been found to be less effective for FTS compared to precipitated ones (Dry 1981; Anderson 1984; Bukur, D.B., et al., 1990 a, b). This is due to an increased difficulty in reducing the Fe, the lower inherent activity of Fe, an interaction of promoters such as alkali with the support making higher concentrations of these promoters necessary, and the presence of small pores which can be clogged by wax during reaction thereby eliminating active Fe sites within the pores. Other tradition routes for preparing Fe catalysts appear even less attractive.

1.4 Spray Drying

Spray drying is a technique which is widely used to produce up to 60 mesh spheroidal materials starting from colloidal or uniform size powders (Stiles 1983). Spray dried catalysts are used in fluidized bed reactors because of their spheroidal shape, excellent hardness, abrasion resistance, and size uniformity. Spray drying consists of first producing a slurry of catalyst precursor dispersed in a solution of the oxide precursor which will form the hard phase of the

catalyst. The oxide material must be in the form of discrete subcolloidal or very small colloidal particles preferably less than 0.5 nm. The slurry is then spray dried to form porous microspheres which are calcined to produce the micron-size particles.

1.5 Catalyst Pre-Treatment

Before synthesis, a catalyst precursor is subjected to a pretreatment, the purpose of which is to bring the catalyst into an active form for synthesis. The pretreatment of Fe is not as straight forward as that for Ru, Co or Ni. The pretreatment for iron FT catalysts is not clearly understood (Srivastava et al., 1990; Rao et al., 1992; Soled et al., 1990). Part of the confusion stems from the fact that the nature and composition of iron catalysts undergo changes during reaction. These changes depend on the temperature, time of exposure to the reactant feed, nature of the reactor system, composition of the feed and activation conditions (time and temperature). The common pretreatment conditions employed in the case of iron catalysts are H_2 reduction, CO reduction (and carbiding), or reduction in the reactant gas. Recent work at the Federal Energy Technology Center has focused on the effect of catalyst pretreatment on the catalysts synthesis behavior in stirred tank slurry reactor (Pennline et al., 1987; Zarochak and McDonald, 1987).

Several phases of iron are known to exist when iron-based catalysts are subjected to F-T synthesis conditions (Amelse et al., 1978, 1984; Blanchard et al., 1982; Dictor and Bell, 1986; Dwyer and Somorjai, 1978; Jung et al, 1982; Niemantsverdriet et al., 1980; Raupp and Delgas, 1979; Teichner et al., 1982; Zou et al., 1992; Jung and Thomson, 1992;1993; Sault, 1993; Sault and Datye, 1993; Butt, 1990; Bukur et al., 1995a; 1995b; O'Brien et al., 1995). These include metallic iron (α -Fe), iron oxides (hematite, α-Fe_2O_3; magnetite, Fe_3O_4 and Fe_xO), and iron carbides, of which at least five different forms are known to exist. These include O-carbides (carbides with carbon atoms in octahedral interstices, ϵ-Fe_2C, ϵ'-$Fe_{2.2}C$, and Fe_xC) and TP-

carbides (carbides with carbon atoms in trigonal prismatic interstices, χ -$Fe_{2.5}C$ and Fe_3C). The formation and distribution of these phases depend on the reaction conditions, reaction times, and state of the catalyst (reduced/unreduced, supported/unsupported , etc.). However, the role of each of these phases during the reaction has not been resolved. As has been discussed earlier, the various phase changes which occur for Fe during pretreatment and reaction may play a significant role in the catalyst attrition.

1.6 Project Objectives

The objectives of the project were to (1) develop a better understanding of the parameters affecting attrition resistance of Fe F-T catalysts suitable for use in SBCRs and (2) incorporate this understanding into the design of Fe catalysts having superior attrition resistance. The goal was to develop an Fe catalyst, without sacrificing FTS activity and selectivity, which can be used in a SBCR having only an internal filter for separation of the catalyst

2.0 DESCRIPTION OF PROJECT TASKS

TASK 1: Catalyst Preparation

The objectives of this task were to prepare precipitated iron catalyst with various levels of binder and precipitated silica. Several parameters were varied in the catalyst preparation to study their effect on the catalyst attrition, activity and selectivity. Section 3.1 describes the detailed catalyst preparation procedure employed in this study.

TASK 2: Catalyst Performance Evaluation

The objectives of this task were to evaluate the performance of various catalyst compositions under similar conditions in a fixed-bed microreactor. Section 3.3 describe the

experimental apparatus and procedures employed throughout the project. Catalyst comparisons were carried out at the following operating conditions:

Pretreatment: CO, 280°C, 16h

Temperature: 250°C

Pressure: 1.48 MPa

SV: 2 nL/(g of cat/h)

H_2/CO: 0.67

The catalyst was tested over a period of 100 to 125 h.

TASK 3: Catalyst Characterization

The objectives of this task were to characterize the fresh, reduced and used catalysts. Section 3.2 describes the various analytical techniques employed for catalyst characterization throughout the project. A detailed attrition study of the catalysts is reported in Appendix A.

TASK 4: Slurry Reactor Testing

The objectives of this task were to determine the catalyst performance (activity, selectivity, longevity and attrition) in a slurry reactor.

3.0 EXPERIMENTAL APPROACH

3.1 Catalyst Preparation

A standard Ruhrchemie precipitated Fe catalyst (Identified as Batch 52119) was obtained from the U.S. Department of Energy (DOE) as a benchmark catalyst. The composition of this catalyst was 100 Fe/5 Cu/4.2 K/25 SiO_2. It contained 25 parts by weight (pbw) precipitated silica. It was obtained as a 1/8 in. extrudate and was crushed to 50 to 100 μm particles prior to use.

In this study, all catalysts were prepared with the same ratio of iron, copper, and

potassium (100 Fe/ 5 Cu/4.2 K) as the benchmark catalyst, but with differing levels of binder and precipitated silica. Three types of catalysts were prepared as shown in

Table 1.

Table 1. Catalyst Designation and Binder Content

Catalyst Series	Binder Silica (wt %)	Precipitated Silica (pbw)
Fe-bSi(x)	x	0
Fe-pSi(y)	12	y
Ruhrchemie	0	25
HPR	Proprietary Composition	

Catalyst preparation involved four steps: preparation of the iron, copper, and silica (when added) precursor; incorporation of potassium; addition of binder silica; and finally spray drying. Two types of silica-containing iron catalysts were prepared and the procedure is shown in Figure 1. The first series of catalyst contained binder silica but no precipitated silica and had a composition of 100Fe/5Cu/4.2 (plus binder silica). The binder silica preparation and addition method is proprietary. These catalysts were prepared by coprecipitation using an aqueous solution containing $Fe(NO_3)_3.9H_2O$ and $Cu(NO_3)_3.2.5H_2O$ in the desired Fe/Cu atomic ratio, which was precipitated by adding ammonium hydroxide. The resulting precipitate was then filtered and washed three times with deionized water. The potassium promoter was added as aqueous $KHCO_3$ solution to the undried, reslurried Fe/Cu coprecipitate. To this catalyst, five different levels of binder silica were added: 4,8,12,16 and 20 %. These catalysts were then spray dried at 250°C using a large bench-scale Niro spray dryer, 3 ft diameter x 6 ft high. Finally, the spray dried catalyst was calcined at 300°C for 5 h in a muffle furnace. These catalysts are designated Fe-bSi(x), denoting that they contain x % binder silica.

The second series of catalysts contained both precipitated and binder silica. Four such catalyst were prepared containing 5,10,15 and 20 pbw precipitated silica (yielding catalysts of

the composition 100Fe/5Cu/4.2K/ySiO_2, where y is 5,10,15 or 20). The precipitated silica was added as a dilute solution of $Si(OC_2H_5)_5$ to the nitrate solution described above. To each of these catalysts, 12 % binder silica was added. These catalysts are designated Fe-pSi(y). These catalysts were then spray dried and calcined in the same way as those above. Finally, HPR series of iron precipitated catalyst was prepared. The preparation of HPR series of catalyst were proprietary.

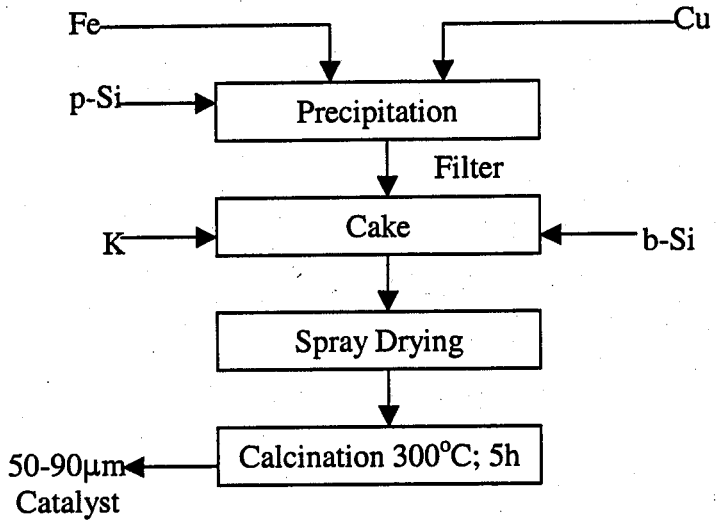

Fig: 1 Catalyst Preparation Procedure

3.2 Catalyst Characterization

Detailed physical and chemical characterization of the fresh, reduced and used catalysts were carried out using the following analytical techniques.

The BET surface area of the catalysts was determined by N_2 physisorption using a Micromeritics Gemini 2360 system. The samples were degassed in a Micromeritics Flow Prep 060 at 120°C for 1 h prior to each measurement. The SEM micrograph was taken using a Cambridge Stereoscan 100. X-ray powder diffraction patterns were obtained using a Phillips

PW1800 x-ray unit using CuKα radiation. Analyses were conducted using a continuous scan mode at a scan rate of 0.05° 2θ per second.

For determination of the reduction behavior and the reducibility of the catalysts, TPR experiments were carried out using a Micromeritics 2705 TPR/TPD system. A sample close to 0.2 g was dried and degassed under high purity Ar at 400°C for 1h followed by cooling to ambient temperature. Reduction was achieved under H_2/Ar gas mixture (volume ratio 5/95). Total gas flow was 40 cc/min and temperature program was 25 to 900°C at a heating rate of 10°C/min. Hydrogen consumed by the catalyst was detected using a thermal conductivity detector (TCD) and recorded as a function of temperature.

The attrition of the catalysts was measured using a three-hole air-jet attrition tester per ASTM-D-5757-95. This test method is applicable to spherically or irregularly shaped particles that range in size between 10 and 180 micrometers, have skeletal densities between 2.4 and 3.0 g/cm^3, and are insoluble in water. Particles less than 20 microns are considered fines. The heart of the system is the vertical attriting tube, a stainless steel tube 710 mm long with an inside diameter of 35 mm. There is an orifice plate attached to the bottom of this tube with three 2-mm long drilled sapphire square-edged nozzles. The nozzles are precision drilled 0.381+/- 0.005 mm in diameter. Above the attriting tube is the settling chamber, a 300-mm long cylinder with a 110-mm inside diameter. Finally, there is a fines collection assembly made up of a 250-mL filtering flask and an extraction thimble. There is additional peripheral equipment required to provide the source of humidified air (30-40% relative humidity) that the test method requires. To conduct a test, a sample of dried powder is humidified and attrited by means of three high velocity jets of humidified air. The fines are continuously removed from the attrition zone by elutriation into a fines collection assembly. The attrition index (AI) is calculated from the

elutriated fines to give a relative estimate of the attrition resistance of the powdered catalyst as may be observed in commercial use.

The full test protocol calls for 45 g of a screened and dried representative sample to be humidified with 5 g of demineralized water to produce 50 g of water equilibrated sample. This sample is run in the apparatus for 5 hours, with an intermediate change of the fines filter at one hour elapsed time. The AI is based on the fines loss after 1 hour and 5 hours.

3.3 Apparatus and Procedures

The catalysts prepared were tested in a laboratory scale high-pressure and high temperature fixed bed reactor which is shown in Figure 2. Briefly, the fixed-bed reactor was constructed of 1-c.m-i.d. stainless steel tube. The iron F-T catalysts were pretreated under flowing CO at 280°C for 16 h before reaction. Following catalyst pretreatment, the reactor temperature was decreased to 50°C. CO flow was stopped, and synthesis gas was introduced at a gas space velocity of 2.0 NL/g-cat/h. The synthesis gas was a premixed gas of CO and H_2 (H_2/CO=0.67) containing 5 % Ar as an internal standard for product analysis. The reactor system was then pressurized to 1.48 MPa. The reactor temperature was then increased gradually to 250°C. This is referred to as the conditioning period. After achieving, the desired process condition of 250°C, 1.48 MPa, 2.0 NL/g-cat/h and H_2/CO=0.67, the catalyst was tested over a period of 100 to 125 h.

The product gas was analyzed by an online Hewlett-Packard (HP) 5890 Series II plus gas chromatograph (GC), with advanced Chemstation control and capabilities. The hydrocarbons C_1-C_{15} and the oxygenates were analyzed using an HP-1 100 m x 0.25 mm x 0.5 μm capillary column and detected by a flame ionization detector (FID). The CO, CO_2, and Ar were separated by a 2.6 ft x 1/8 in. Haysep Q column detected by TCD.

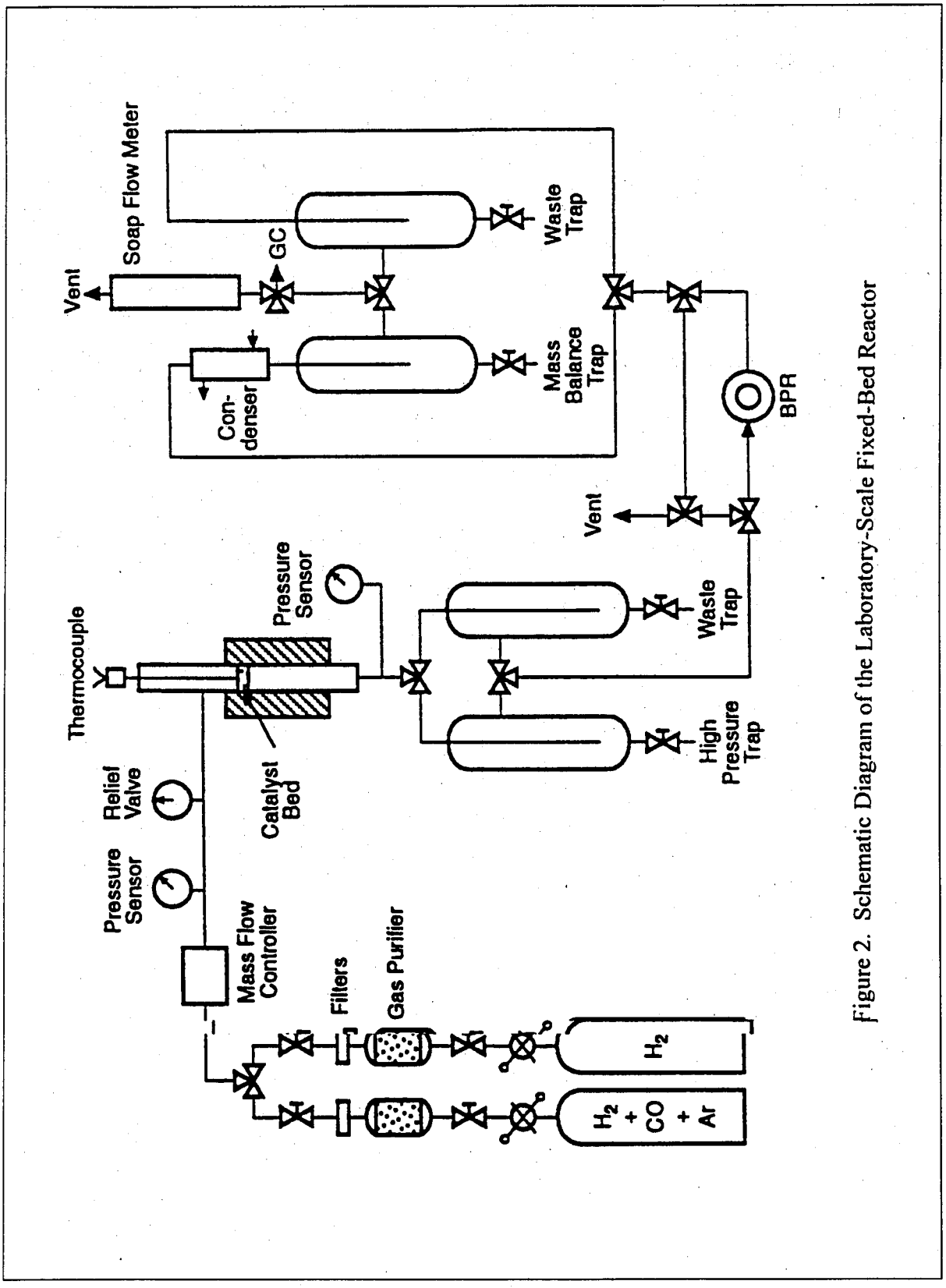

Figure 2. Schematic Diagram of the Laboratory-Scale Fixed-Bed Reactor

4.0 RESULTS AND DISCUSSIONS

Scanning electron microscopy (SEM) of binder and precipitated silica catalysts are shown in Figure 3. The catalyst is roughly spherical in shape, typical of a spray drying process, with diameters ranging from 30 to 90 μm.

The attrition resistance of the silica binder based catalysts (with no precipitated silica) increased (attrition reduced) as binder level was increased up to 12 % as shown in Table 2. It then decreased when the binder level was increased to 20 %, indicating an optimum binder level of about 10 to 12 %. For this reason, this material was used as the basis for preparing the Fe-pSi(y) series of catalysts with various levels of precipitated silica. The Fe-pSi series containing precipitated silica was prepared with 12 % binder silica. As precipitated silica content increased from 5 to 20 parts by weight, the attrition became so severe that it plugged the attrition tester during 5 h test. It is clear that from these results, the addition of precipitated silica causes more attrition. An HPR series of proprietary catalysts was prepared to further improve attrition resistance. As can be seen, these catalysts have significantly improved attrition resistance, even better than the Fe-bSi series of catalysts. Finally, an HPR-43 material was prepared as a larger 500-g batch to demonstrate scalability of the proprietary preparation technique.

Table 3 shows the BET surface areas of the fresh and reduced catalysts, the hydrogen uptake, pore volume, bulk density and the porosity of all the catalysts synthesized. The BET surface area of the catalysts increased with both binder silica and precipitated silica concentration. In general, the addition of silica to iron FT catalysts is known to improve stability of the porous iron oxide/hydroxide network (Bukur et al., 1995a). Silica enters the pores of the original network of the catalysts, thus providing a rigid matrix which helps prevent a complete collapse of the pore structure of the catalyst. However, after reduction with CO at 280°C for

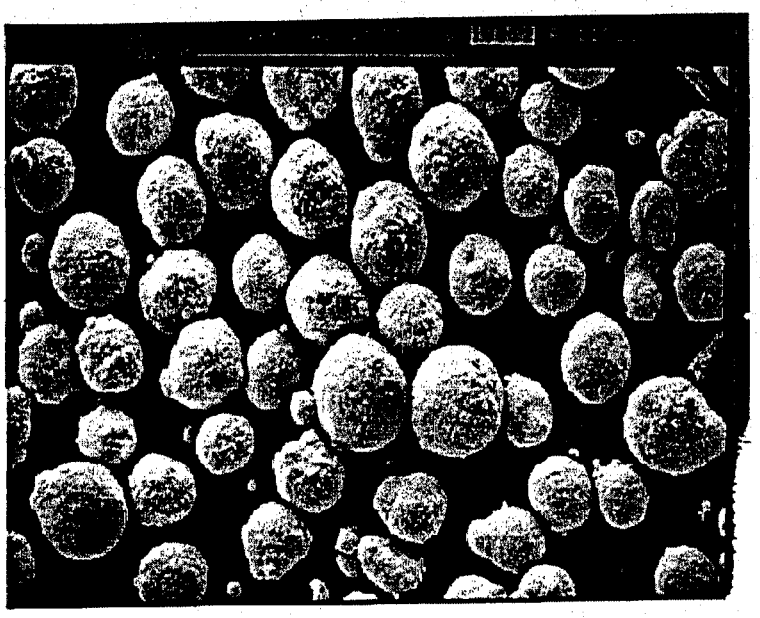

Fig.3 (a)

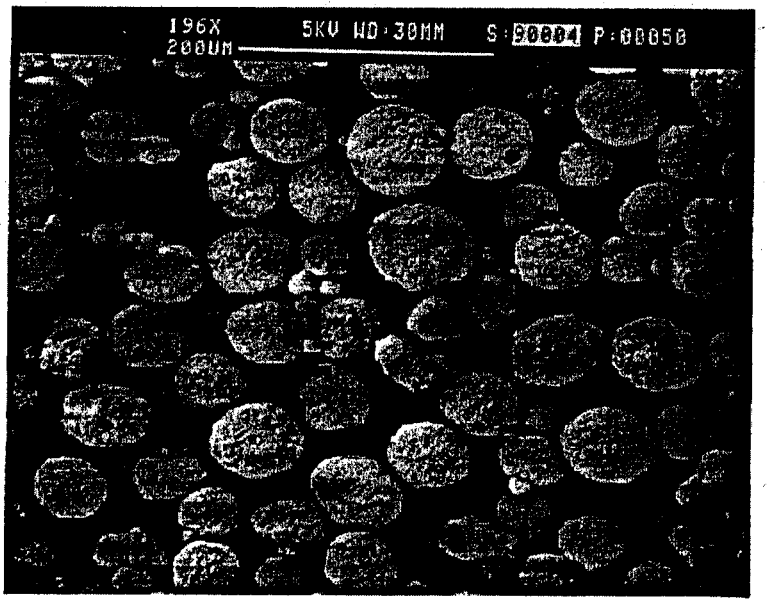

Fig. 3 (b)

Figure 3. SEM Image of the Spray Dried Precipitated Iron Catalysts (a) Fe-bSi(12) (b) Fe-pSi(15)

Table 2. ASTM Fluid Bed Test Results

Catalyst Designation	Attrition loss (wt %)	
	1 h	5 h
Fe-bSi(4)	24.4	32.6
Fe-bSi(8)	25.7	35.4
Fe-bSi(12)	12.8	22.7
Fe-bSi(16)	22.0	30.1
Fe-bSi(20)	34.9	35.0
Fe-pSi(5)	24.2	37.3
Fe-pSi(10)	31.0	39.6
Fe-pSi(15)	42.1	*
Fe-pSi(20)	39.1	*
HPR-39	4.7	10.0
HPR-40	4.1	9.7
HPR-41	6.4	17.7
HPR-42	5.2	15.5
HPR-43	7.6	14.6
Ruhrchemie	NM	NM

NM=Not measured

* Tester plugged due to severe attrition

Table 3. Physical and Chemical Properties of Fe Catalysts

Catalyst Designation	BET Surface Area, m^2/g		TPR Measurements H_2 Desorbed, mmol/g.cat	Pore Volume, mL/g	Bulk Density, g/mL	Porosity, %
	Fresh	Reduced				
Fe-bSi(4)	80.3	35.6	24.3	NM	NM	NM
Fe-bSi(8)	95.7	50.8	23	NM	NM	NM
Fe-bSi(12)	121	68.7	20.6	NM	NM	NM
Fe-bSi(16)	151	103	19	NM	NM	NM
Fe-bSi(20)	172	98.9	18.4	NM	NM	NM
Fe-pSi(5)	163	116	18.8	0.54	0.95	51.3
Fe-pSi(10)	168	144	17.9	0.54	0.89	48.5
Fe-pSi(15)	189	163	17.7	0.62	0.95	59.8
Fe-pSi(20)	218	181	17.6	0.64	0.92	58.2
HPR-39	107.8	NM	NM	NM	NM	NM
HPR-40	81.4	NM	NM	NM	NM	NM
HPR-41	60.5	NM	NM	NM	NM	NM
HPR-42	79.8	NM	NM	NM	NM	NM
HPR-43	81.5	NM	NM	0.11	2.41	27.4
Ruhrchemie	300	NM	NM	NM	NM	NM

NM=Not measured

16 h, the surface area of the reduced catalyst was lower than that of the fresh catalyst. This may be due to the formation of carbonaceous deposits, which causes blocking of the pores of the catalyst. The catalysts prepared had pore volumes in the 0.54 to 0.65 cm^3/g range and the bulk densities in the 0.89 to 0.95 g/cm^3 range. These densities are higher than typical precipitated catalysts that have bulk densities of about 0.7 g/cm^3 and should allow easier separation from wax which has a density of about 0.68 g/cm^3.

The reduction behavior of the FT catalysts was studied by TPR and the profiles for binder and precipitated silica catalysts are shown in Figure 4. There were slight variations among the catalysts, with all showing peaks at 320 and 750°C. The peak at 320°C corresponds to the reduction of $Fe_2O_3 \rightarrow Fe_3O_4$, and the peak at 750°C corresponds to the reduction of Fe_3O_4 to metallic iron. Thus, it can be seen that the reduction of Fe_3O_4 to Fe is more difficult step requiring temperatures greater than 600°C for its occurrence in temperature-programmed mode. The small shoulder peak at roughly 250°C is due to the reduction of $CuO \rightarrow Cu$. A summary of the TPR characterization results for all the catalysts studied is given Table 3. The hydrogen uptake generally decreased with silica content, though the effect of the precipitated silica is much less than the effect of the binder silica. The higher H_2 consumption by the Fe-bSi catalysts compared to the Fe-pSi indicates a greater extent of reduction for catalysts containing binder silica.

X-ray powder diffraction patterns of the fresh, CO-activated sample after activation, and after 100 h of FT synthesis for the binder and precipitated silica catalysts are shown Figures 5 and 6. The pattern has been plotted over 2θ value ranging from 5° to 75°. The pattern in Figures 5 and 6 shows that the "fresh" samples are identical and are comprised of α-Fe_2O_3. The catalyst activated at 280°C, with CO for 16 h exhibits the peaks for Fe_3O_4 and $\chi Fe_{2.5}C$. The "used"

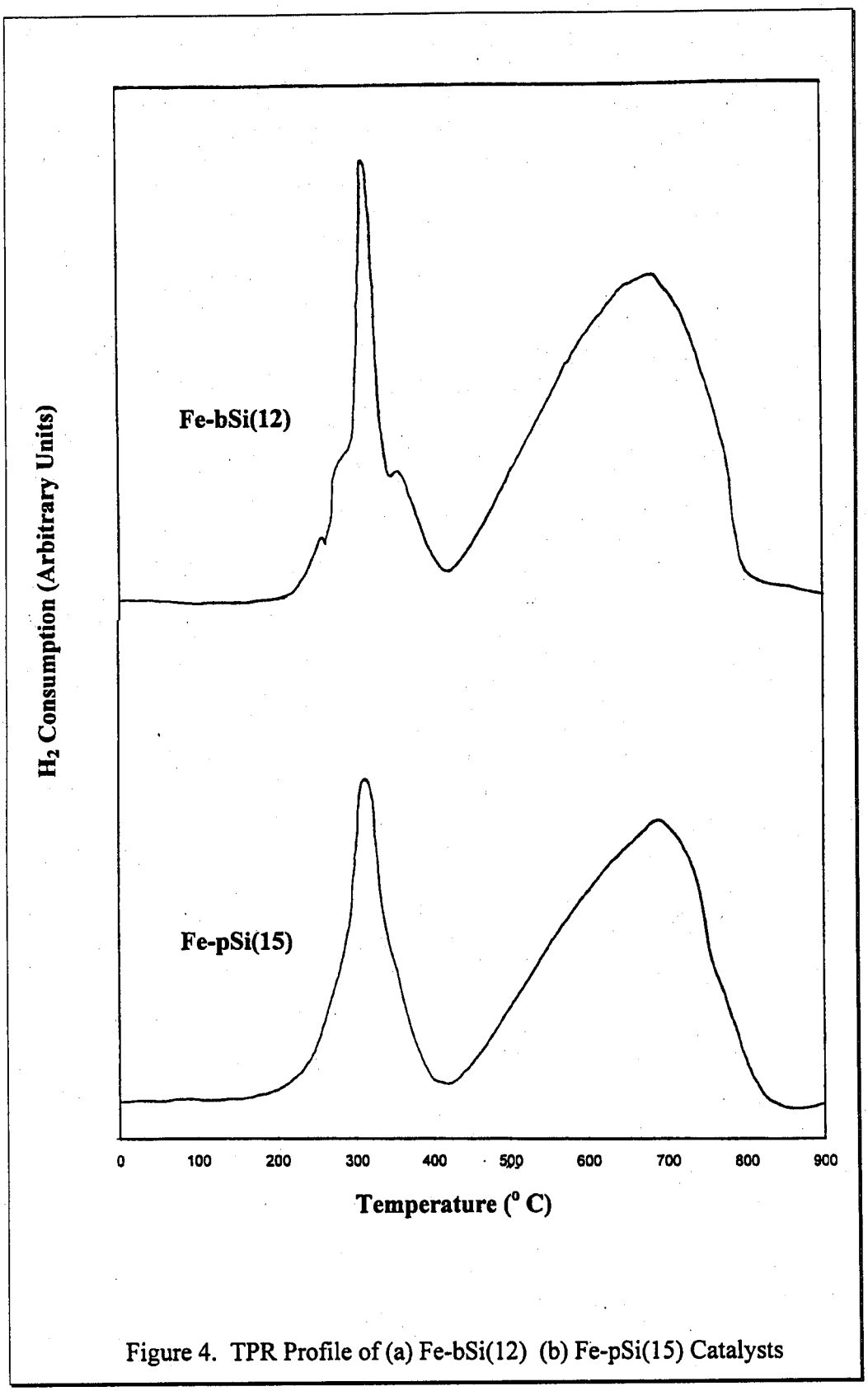

Figure 4. TPR Profile of (a) Fe-bSi(12) (b) Fe-pSi(15) Catalysts

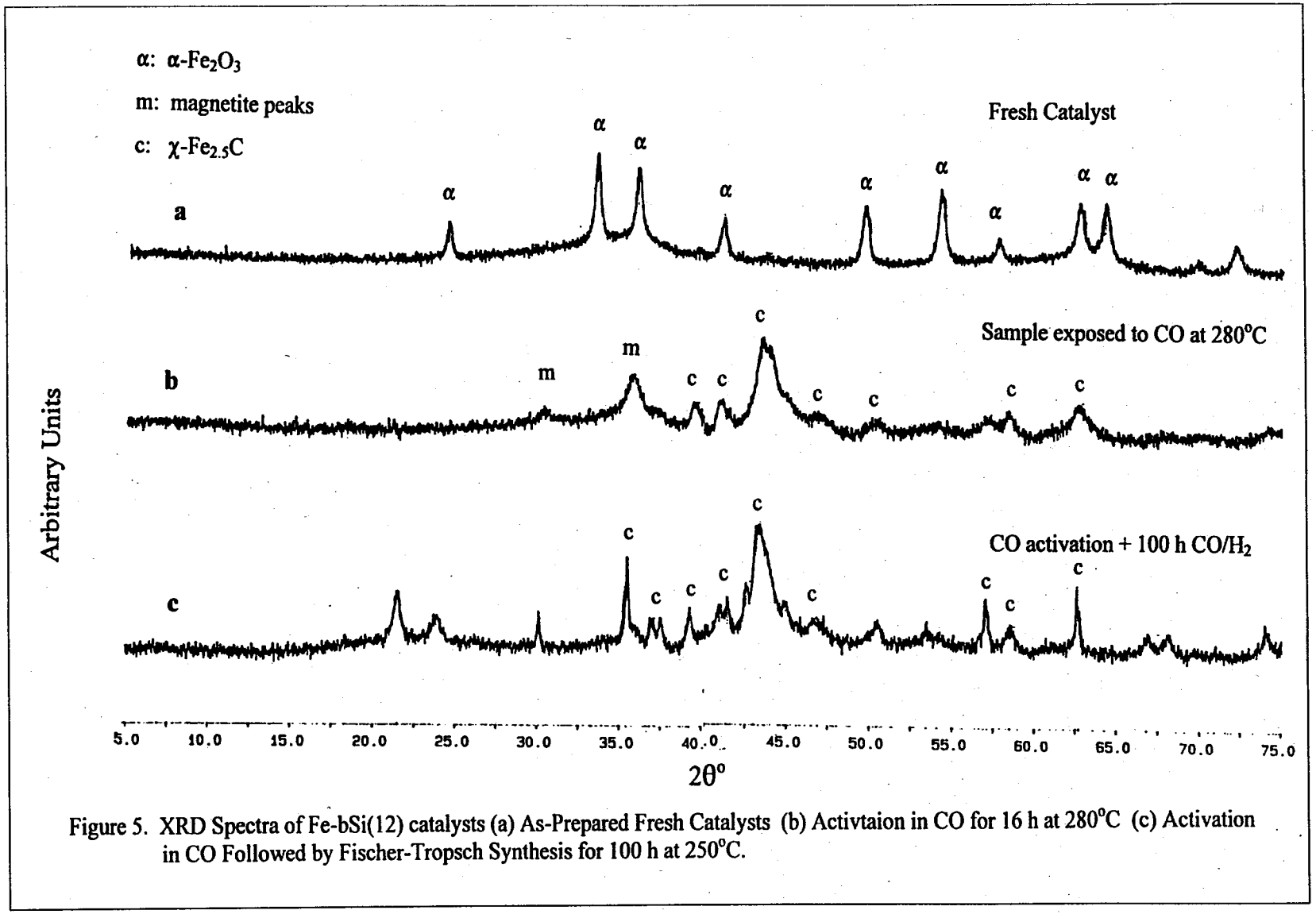

Figure 5. XRD Spectra of Fe-bSi(12) catalysts (a) As-Prepared Fresh Catalysts (b) Activtaion in CO for 16 h at 280°C (c) Activation in CO Followed by Fischer-Tropsch Synthesis for 100 h at 250°C.

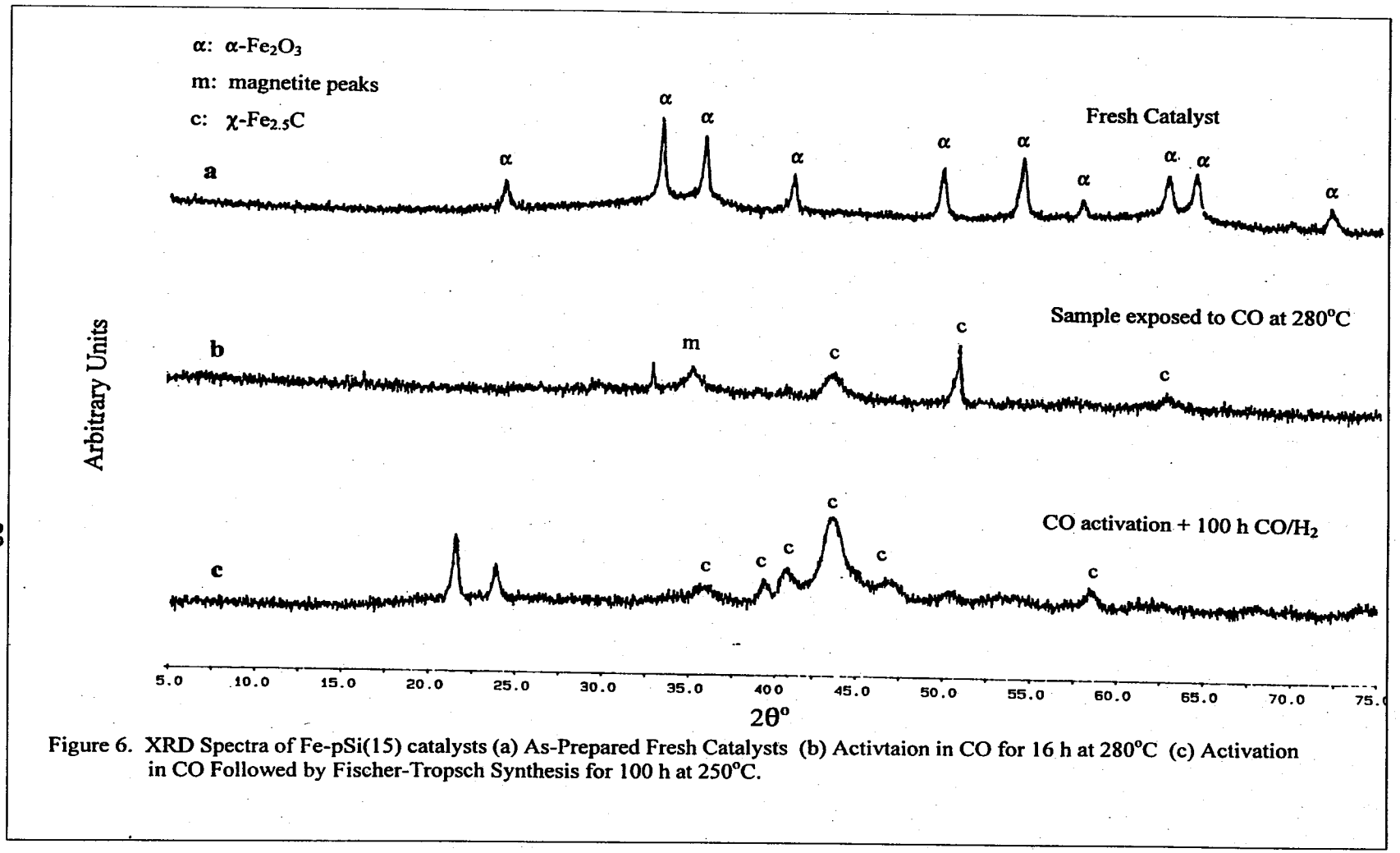

Figure 6. XRD Spectra of Fe-pSi(15) catalysts (a) As-Prepared Fresh Catalysts (b) Activtaion in CO for 16 h at 280°C (c) Activation in CO Followed by Fischer-Tropsch Synthesis for 100 h at 250°C.

sample contain mainly $Fe_{2.5}C$.

The CO conversions plot are shown Figures 7 and 8. All catalysts tested were more active than the Ruhrchemie catalyst. Table 4 shows the CO conversion and hydrocarbon selectivity for the various catalysts, along with the data on Ruhrchemie catalyst for comparison. Following a short induction period, during which steady state was achieved, there was no significant change with time in CO conversions or hydrocarbon selectivities reported in Table 4 over the test duration, typically 100 to 125 h, for any of the catalysts. The alpha value for all catalysts tested range from 0.87 to 0.91. All catalysts tested were more active than Ruhrchemie. The selectivity varied with silica type and content. There was a beneficial effect of binder silica up to 8 to 12 % on selectivity (reduced methane, nearly constant C_5^+). However, as binder silica content increased above 12 %, the C_1 and C_2 to C_4 selectivities increased at the expense of C_5^+ selectivity. As the precipitated silica content increased (at 12 wt % binder silica), the selectivity to C_1 to C_{11} products increased. However, the C_5 to C_{11} selectivity for the catalysts containing precipitated silica was higher than the selectivity for those catalysts containing only binder silica.

HPR-43, a proprietary catalyst, showed the lowest methane selectivity and nearly the highest CO conversion. As stated earlier, this catalyst was scaled up to 500-g quantity. This catalyst showed 95 % CO conversion over 125 h of testing at 250°C, 1.48 MPa, and 2 NL/g.cat/h and had a less than 4 % methane selectivity. Its attrition resistance was one of the highest among the catalysts tested.

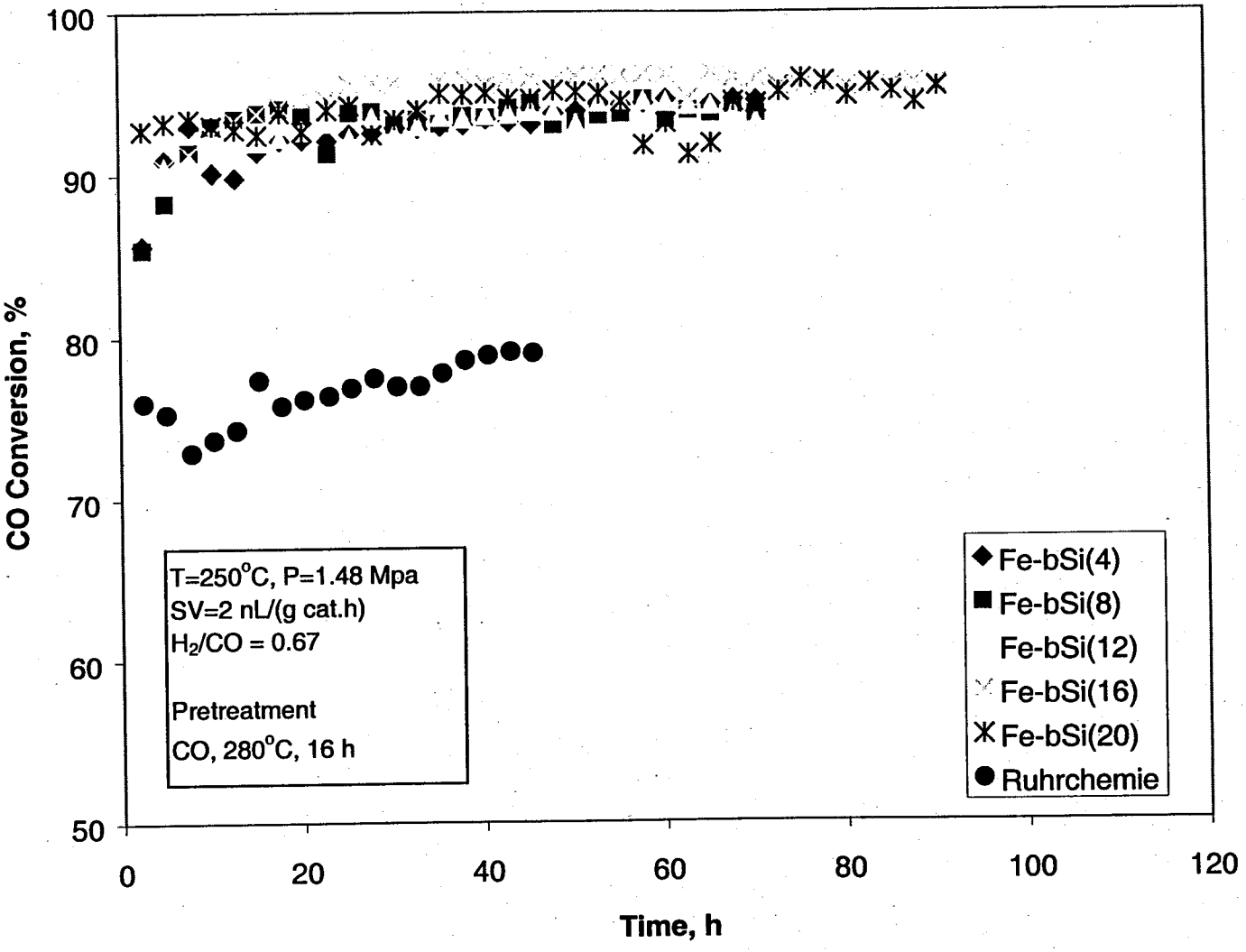

Figure 7. Effect of Binder Silica on Synthesis Gas Conversion and Catalyst Stability

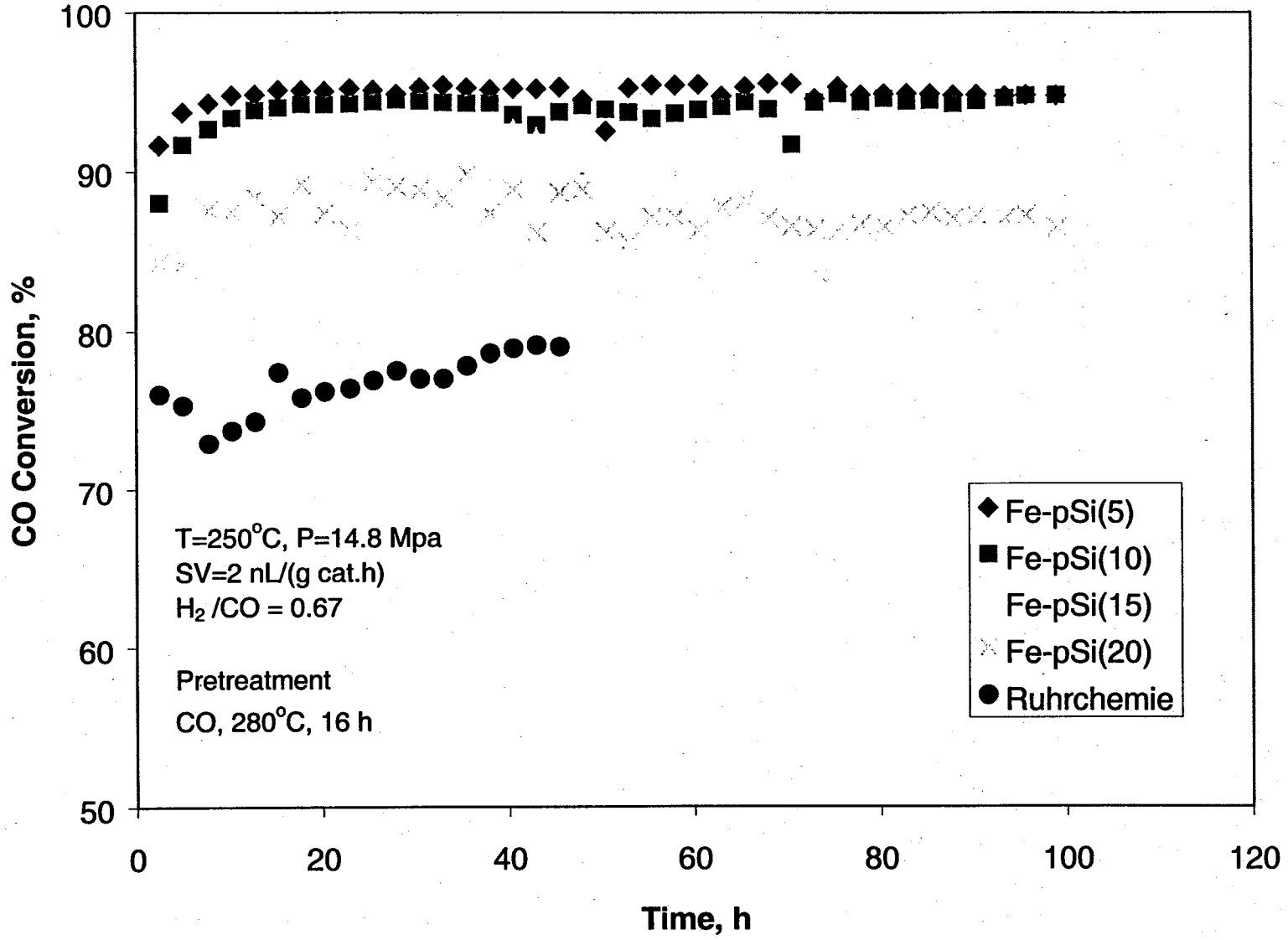

Figure 8. Effect of Precipitated Silica on Synthesis Gas Conversion and Catalyst Stability

Table 4. Catalyst Activity and Selectivity

Catalyst Designation	CO Conversion (%)[a]	Selectivity				α
		C_1	C_2-C_4	C_5-C_{11}	C_{12}^+	
Fe-bSi(4)	94.3	7.4	18.1	12.7	61.8	0.92
Fe-bSi(8)	94.1	6.8	17.6	13.0	62.5	0.91
Fe-bSi(12)	94.3	6.8	19.6	12.8	60.8	0.89
Fe-bSi(16)	95.5	9.9	25.0	17.3	47.8	0.87
Fe-bSi(20)	94.5	9.6	23.5	17.6	49.3	0.87
Fe-pSi(5)	95.5	8.8	23.2	22.0	46.0	0.87
Fe-pSi(10)	94.4	10.2	23.5	26.5	39.8	0.86
Fe-pSi(15)	90.1	10.2	22.4	30.5	36.9	0.87
Fe-pSi(20)	88.2	9.5	20.1	32.8	37.7	0.88
HPR-43	95.0	3.9	17.7	23.8	54.6	0.90
Ruhrchemie	86	8.3	21.3	14.3	56.1	0.90

[a] Measured at 250°C, 1.48 MPa, 2 NL/g.cat/h, H_2/CO=0.67

5.0 CONCLUSIONS AND FUTURE WORK

The addition of binder silica to precipitated 100Fe/5Cu/4.2K FT catalyst followed by spray drying increases the attrition resistance significantly. Within the range of the non-proprietary catalysts tested here, the optimum binder silica content is 10 to 12 wt %. The FT activity and selectivity of this catalyst are better than a Ruhrchemie catalyst at 250°C and 1.48 MPa. The addition of precipitated silica to catalyst containing 10 to 12 % binder silica decreases attrition resistance and increases methane selectivity. Based on the experience gained, a proprietary HPR-43 catalyst has been successfully spray dried in 500-g quantity. This catalyst showed 95 % CO conversion over 125 h of testing at 250°C, 1.48 MPa, and 2 NL/g.cat/h and had a less than 4 % methane selectivity. Its attrition resistance was one of the highest among the catalysts tested.

Future research needs to continue to focus on further increasing iron catalyst attrition resistance, activity, and selectivity for example by evaluating the effect of pretreatment, binder type, and promoter content. Hampton University, University of Pittsburgh, and Research Triangle Institute have reached an intelluctual property and commercialization agreement to further develop the iron catalyst. HPR-43 prepared and scaled up under this grant using a spray drier. Final catalyst activity and selectivity of HPR-43 is being evaluated in a slurry reactor at a host private company site. A patent application is being prepared for the iron catalyst. An agreement has been developed with the private company to evaluate the catalyst in a slurry reactor, both CSTR and SBCR. Initial test results reported by the private company have been promising. HPR-43 promises to be much more attrition resistant than the iron catalyst tested by DOE at the Laporte slurry reactor pilot plant. The private company also plans to carry out comparision testing of attrition, activity, and selectivity for HPR-43 and the iron catalyst tested at Laporte

6.0 REFERENCES

Amelse, J.A., Schwartz, S.T., and Butt, J.B., J. Catal., 87, 179(1984).

Amelse, J.A., Butt, J.B., and Schwartz, L.H., J. Phys. Chem., 82, 558(1978).

Anderson, R.B., The Fischer-Tropsch Synthesis; Academic Press: Orlando, FL, 1984.

Blanchard, F., Reymond, J.P., Pommier,B., and Tecichner, S.J., J. Mol.Catal., 17, 171(1982).

Bukur, D.B., Okabe, K., Rosynek, M.P., Li, C., Wang, D., Rao, K.R.P.M., and Huffman, G.P., J. Catal., 155, 353(1995a).

Bukur, D.B., Nowicki, L., Manne, R.K., and Lang, X., J. Catal., 155, 366(1995b)

Bukur, B.D., Mukesh, D., and Patel, S.A., Ind. Eng.Chem.Res., 29, 194(1990a).

Bukur, D.B., Lang, X., Mukesh, D., Zimmerman, W.H., Rosynek, M.P., and Li, C., J. Catal.,29, 1588(1990 b).

Butt, J.B., Catal .Lett., 7, 61(1990).

Dictor, R., and Bell, A.T., J. Catal., 97, 121(1986).

Donnelly, T.J., and Satterfield, C.N., Appl.Catal., 56, 231(1989).

Dry, M., in Catalysis:Science and Technology, Vol.1, ed.by Anderson, J.R., and Boudart,M., Springer-Verlag, NY, 1981

Dwyer, D.J., and Somorjai,G.A., J.Catal., 52, 291(1978)

Jung., H.J., Walker,Jr., P.L., and Vannice, M.A., J. Catal., 75, 416(1982).

Jung,H., and Thomson, W.J., J. Catal., 134, 654(1992)

Jung,H., and Thomson, W.J., J. Catal., 139,375(1993).

Kolbel, H., and Ralek, M., Catal.Rev.-Sci.Eng., 21, 225(1980).

Lang, X., Akgerman, A., and Bukur, D.B., Ind.Eng.Chem.Res., 34, 73(1995).

Lee., S.K., Jiang, X., Keener, T.C., and Khang, S.J., Ind.Eng.Chem. Res., 32, 2758(1993).

Niemantsverdriet, J.W., Van der Kraan, A.M., Van Dijk, W.L., and Van der Baan, H.S., J. Phys. Chem., 84, 3363(1980).

O'Brien, R.J., Raje, A., Keogh, R.A., Spicer, R.L., Xu, L., Bao, S., Srinivasan, R., Houpt, D.J., Chokkram, S., and Davis, B.H., Coal Liquefaction and gas Conversion Contractors' Review Conference, 1995.

Pennline, H.W., Zarochak, M.F., stencel, J.M., and Diehl, J.R., Ind.Eng. Chem.Res., 26, 595(1987)

Rao, V.U.S., Stiegel, G.J., Cinquegrane, G.J., and Srivastava, R.D., Feul Proc.Technology, 30, 83(1992).

Raupp, G.B., and Delgass, W.N., J. Catal., 58, 348(1979).

Sault, A.G., J. Catal., 140, 121(1993).

Sault, A.G., and Datye, A.K., J. Catal., 140, 136(1993).

Shroff, M.D., Kalakkad, D.S., Coulter, K.E., Kohler, S.D., Harrington, M.S., Jackson, N.B., Sault, A.G, and Datye, A.K., J. Catal., 156, 185(1995).

Soled,G., Iglesia, E., and Fiato, R.A., Catal. Lett., 7, 271(1990).

Srivastava, R.D., Rao, V.U.S., Cinquegrane, G., and Stiegel, G.J., Hydrocarbon Processing, 1990.

Stiles, A.B., Catalyst Manufacture., Marcel Dekker, Inc., New York, 1983

Teichner, S.J., Reymond, J.P., and Meriadeau, P., J. Catal., 75, 39(1982).

Zarochak, M.F., and McDonald, M.A., in Seventh DOE Indirect Liquefaction Contractors Meet.Proc., Pittsburgh, Dec 7-9, p.96(1987).

Zou, W., Robinson, K., and Gonzalez., R.D., J. Catal., 136, 621(1992)

APPENDIX A

Final Report by University of Pittsburgh

Attrition Resistant Iron-Based Fischer-Tropsch Catalysts

FINAL REPORT

Work Performed Under
Grant No. DE-FG22-96PC96217

For
U.S. Department of Energy
Federal Energy Technology Center
Pittsburgh, PA 15236

By

Rong Zhao
James G. Goodwin, Jr.
Department of Chemical and Petroleum Engineering
University of Pittsburgh
Pittsburgh, PA 15260

October 1999

DISCLAIMER

ABSTRACT

Fischer-Tropsch Synthesis (FTS) is one of the major indirect routes for converting syngas ($CO+H_2$). Iron Catalysts are the preferred catalysts for the conversion of syngas based on coal, due to their water gas (WGS) capabilities. Since FTS is highly exothermic, slurry bubble column reactors (SBCRs) has been suggested for this reaction due to their excellent heat removal capability. However, the catalyst attrition encountered, especially when iron catalyst is used, has hindered the application of SBCRs. To improve the physical strength of the iron catalysts, the spray drying technique has recently been used for preparation of iron SBCR Fischer-Tropsch (F-T) catalysts. However, the effects of such preparation in the improvement of catalyst attrition resistance are still not clear.

In this study, two series of spray dried iron F-T catalysts having the composition $Fe/Cu/K/SiO_2$ have been studied to better understand the characteristics important for attrition resistance. XRD results confirmed that the catalysts after calcination are in the same hematite Fe_2O_3 phase. Crystallinity and BET surface area were found not to be relevant to the catalyst attrition performance. TPR results indicated little or no SiO_2 and metal interaction. However, the porosity of the catalysts was found to be relevant to the catalyst attrition resistance. After acid leaching of the catalysts, further study of the SiO_2 in the catalyst showed a porous and uniform SiO_2 construct is suggested to provide the best attrition resistance for the catalysts.

Since phase change during reaction has always been a concern for iron catalysts in terms of attrition resistance, some of the catalysts were carburized and tested using the jet cup. The attrition resistance was found to actually improve after carburization.

ACKNOWLEDGMENTS

This study was sponsored by the U.S. Department of Energy (DOE) under Grant No: DE-FG-22-96PC96217. The authors would like to acknowledge with gratitude the guidance provided by the DOE Contracting Officer's Representative, Dr. Richard E. Tischer.

CONTENTS

1.0 INTRODUCTION

Fischer-Tropsch synthesis (FTS) is one of the major indirect ways of converting coal into a wide variety of hydrocarbons. Iron-based catalysts are the preferred catalysts for FTS based on coal and have been a research focus for FTS recently (Bukur et al., 1990; 1996; Schulz et al., 1994; Kalakkad et al., 1995; Huang et al., 1993). Such catalysts are relatively inexpensive, possess reasonable activity for FTS, and have high WGS activity compared to cobalt catalysts. This enables iron Fischer-Tropsch (F-T) catalysts to process low H_2/CO ratio syngas without an external shift reaction step.

In the development of FTS over the past 20 years, the application of slurry bubble column reactors (SBCRs) has drawn much attention. This is due to their excellent heat removal capability of SBCRs during reaction. Since FTS is a highly exothermic reaction, the use of SBCRs can largely solve the reaction control problem. However, commercial application SBCRs is just now being to be applied. One of the major drawbacks in the industrial application of SBCRs is catalyst attrition, especially when iron catalysts are used (Bhatt et al., 1997). The attrition of catalysts in SBCRs causes filter plugging problems as well as lower product quality. The use of supported iron catalysts can improve the catalyst attrition resistance, but at the expense of lower specific catalyst activity.

In order to try to improve the physical strength of the catalysts without sacrificing their activity, the spray drying technique has been recently used in the preparation of iron F-T catalysts (Srinivasan et al., 1996; Jothimurugesan et al., 1999). This improvement in physical strength by use of spray drying has stimulated much interest in preparing iron F-T catalysts by this technique as well. In practice, many parameters are relevant to final catalyst attrition resistance, such as solids concentration in the slurry, calcination temperature etc. Different preparation conditions result in different catalyst morphology, BET surface area, and porosity,

which can affect not only the catalyst attrition resistance, but also the catalyst activity. The effects of each preparation parameter on the performance of a catalyst are therefore complex.

In the present research, the structures of two series of spray-dried Fe catalysts were studied. The goal was to investigate the relationship between the structure of the catalysts and binder material and their attrition resistances. At the absence of iron phase change, such understanding can help us to better address the impact of the catalyst physical properties on catalyst strength and separate these phase effects from further studies of Fe catalyst attrition performance under reaction conditions. Preliminary results had indicated significant differences in attrition resistance and it was desired to better understand these differences. The effects of type and concentration of refractory silica (precipitated or binder silica), as well as morphology and porosity of particles on attrition resistance of spray dried iron catalysts are addressed.

2.0 EXPERIEMENTS

2.1. Catalyst Preparation

The iron catalysts were prepared at Hampton University and then it was shipped to University of Pittsburgh for attrition tests. In brief, two series of iron catalysts were prepared for this study. One series of catalysts were prepared without precipitated silica but with different weight percentages of binder silica. The other series of catalysts were prepared with different levels of precipitated silica and with 12 wt % of binder silica. For both series, catalysts were prepared having compositions of $100Fe/5Cu/4.2K/xSiO_2$ by weight. First precipitation from an aqueous solution containing $Fe(NO_3)_3.9H_2O$, $Cu(NO_3)_2.2.5H_2O$, $Si(OC_2H_5)_4$ (if added to give precipitated SiO_2) in the desired ratio by the addition of ammonium hydroxide. This precipitate was then slurried with the binder SiO_2 precursor. The final step was to spray dry the catalysts at 250°C in a Niro Spray drier, which is scalable spray drier. After spray drying, the catalysts were

then calcined at 300°C for 5 hours in a muffle furnace. The detailed preparation conditions and procedures can be found in section 3.1 of the main text.

In this report, the following nomenclature is used: the letter **p** represents precipitated silica while the letter **b** stands for binder silica. For example, a catalyst designated as Fe-bSi(12) refers to an iron catalyst prepared without precipitated silica but with 12 wt % binder silica. Since the concentrations of Cu and K were not varied relative to Fe, they are not addressed in the nomenclature used. In addition, since two different types of SiO_2 was used in the preparation of catalysts, i.e. precipitated and binder SiO_2, the term SiO_2 study refers to either or both of them.

In order to study the precipitated and/or binder silica incorporated in the catalysts, acid leaching was performed by treating the catalysts using an HCl solution. After the iron dissolved, the SiO_2 remaining was washed 5 times using deionized water. After filtration, the SiO_2 was dried under vacuum condition at room temperature in order to avoid any possible agglomeration caused by heating.

3. CATALYST CHARACTERIZATION

3.1 Attrition Resistance

The attrition resistance of the catalysts were evaluated using the jet cup test, a proposed ASTM method and one which has been demonstrated to cause attrition characteristic in an SBCR (Zhao et al., 1999). In the present study, 5 grams of each sample were used for the attrition tests, which were all performed using the air flow rate of 15 *l*/min with a relative humidity of 60 % at room temperature for 1 hour. The detailed attrition assessment study for SBCR catalysts, system configuration and test procedure can be found in Appendix B. The fines were collected by a thimble filter at the outlet of the jet cup chamber and were analyzed for particle size distribution together with the particles remaining in the chamber.

3.2. Particle Morphology

Particle morphology was obtained for each catalyst (as prepared and after attrition testing) and acid-leached sample using a Philips XL30 FEG Scanning Electron Microscope (SEM). The samples were coated with palladium before measurement to avoid charging problems.

3.3. Particle size Distribution

A Leeds & Northrup Microtrac Model 7990-11 laser particle size analyzer was used in order to measure the particle size distributions. Both size distributions of the samples as prepared and after jet cup testing were measured. Each sample was put into 50 ml of deionized water and dispersed using an ultrasonic bath. The results of several measurements of the same sample averaged in order to minimize the error. The detailed sampling and measuring procedures were described in Appendix B.

Since size distribution in attrition studies are usually plotted as weight (or volume) percentage versus average projected area diameter of particles, change in the volume moment, a type of average particle size commonly used to represent a particular PSD, has been selected as a useful indicator of the attrition process. The volume moment, x_{VM}, can be calculated by (Allen, 1997).

$$x_{VM} = x_{WM} = \frac{\sum dM}{\sum dV} = \frac{\sum x^4 dN}{\sum x^3 dN} \qquad (1)$$

where, x_{VM} is the volume moment, x_{WM} the weight moment, M the size moment, V the particle volume, and N the number of particles of size (diameter) x.

3.4. BET Surface Area and Pore Size Distribution

The BET surface area and pore size distribution (micropore and mesopore) of the catalysts were determined by N_2 physisorption using a Micromeritics ASAP 2010 automated

system. The samples were degassed in the Micromeritics ASAP 2010 at 100°C for 1 hour, and then 300°C for two hours prior to each measurement. These parameters were determined for both catalyst samples as prepared and after attrition tests.

3.5. Reducibility

The reducibility of the iron catalysts as prepared were measured by temperature programmed reduction (TPR) using an Altamira AMI-1 systems. The TPR measurements were carried out using 5% H_2 in Ar with a flow rate of 30 cc/min and the temperature was ranged from 30°C up to 900°C at a ramping rate of 5°C/min.

3.6. Phase and Crystallinity

X-ray powder diffraction patterns were obtained using a Philips PW1800 x-ray unit using Cu|Kα radiation. Analysis was conducted for each catalyst sample as prepared and some samples after acid leaching using a continuous scan mode at a scan rate of 0.05° (2θ) per second.

4.0 RESULTS

The attrition resistance results for all the iron catalysts studied are summarized in Table 1. It can be seen that catalysts without precipitated silica in general are relatively more attrition resistant compared to the catalysts with precipitated silica. For the series of catalysts with precipitated silica, the attrition resistance obviously decreased with an increase in the

Table 1. Jet cup attrition resistance test results of the spray dried iron catalysts.

Catalyst	Coprecipitaed Silica (pbw)	Binder Silica (wt%)	Fines (wt%) [(a)]	Original Volume Moment (μm) [(c)]	Volume Moment after Test (μm) [(c)]	Net change in Volume Moment (%)
Fe-bSi(4)	0	4	26.6	78.0	39.2	49.7
Fe-bSi(8)	0	8	21.8	86.7	45.4	47.6
Fe-bSi(12)	**0**	**12**	**8.5**	**88.8**	**67.8**	**23.6**
Fe-bSi(16)	0	16	18.2	69.91	47.6	31.9
Fe-bSi(20)	0	20	51.6	63.5	23.7	62.7
Fe-pSi(5)	5	12	26.6	103.0	37.3	63.8
Fe-pSi(10)	10	12	33.9	83.0	34.1	58.9
Fe-pSi(15)	15	12	39.6	90.2	27.7	69.3
Fe-pSi(20)	20	12	41.3	85.9	30.1	65.0
Co/SiO_2 [(d)]	N/A	N/A	31.07	79.88	45.16	43.47

(a) Fines wt% = weight of fines collected/weight of total catalyst recovered

(b) Weight increased = (total weight recovered / weight of loading) x 100% (due to the humidity of the air).

(c) Volume Moment is a volume mean diameter of the particles.

(d) Co035 is a Davison silica supported 20wt% cobalt catalyst, which was used for develop the procedure.

concentration of the precipitated silica. On the other hand, for the series of catalysts without precipitated silica, an optimum concentration of binder silica was observed in terms of improvement of the catalyst attrition resistance. The catalyst with 12 wt% of binder silica but no precipitated silica, Fe-bSi(12), appears to be the most attrition resistant one among all the catalysts tested. A cobalt catalyst with 20 wt% of cobalt prepared using incipient wetness of a spray dried silica is also listed in Table 1 as a benchmark. This cobalt catalyst was found to be suitable for use in an SBCR (Zhao et al., 1999). The comparison of the attrition results shows that some of the spray dried iron catalysts in their calcined state are physically as strong as, or stronger than, the cobalt catalysts. These iron catalysts are there for considered to have strong potential for SBCR use.

The XRD results of these catalysts verify that the components of the fresh catalysts are rather the same, consisting primarily of hematite Fe_2O_3 (Figure 1). A sample of hematite Fe_2O_3 (purity 99.98%), Aldrich Chemicals, Co., was also examined by XRD as a benchmark (see also Figure 1). Compared to this pure Fe_2O_3 sample, the iron catalysts was obviously less XRD crystalline. Other components, even the SiO_2 (binder silica and/or precipitated silica) were not detectable by XRD results for any of the catalysts.

The reducibility of the catalysts was determined using TPR and the results are listed in Table 2. The TPR results indicate that H_2 consumption during TPR decreased with an increase in the concentration of the binder silica. However, this change was due mainly to decrease in the overall concentration of iron oxide in the catalysts. The reducibilities of the iron catalysts were approximately the same (as an iron basis) for all the catalysts. In Figure 2, a typical reduction curve is shown. This curve is similar to other in the literature (Jothimurugesan et al., 1999). The first peak is considered to be the reduction of Fe_2O_3 to Fe_3O_4 and the second peak to be the

Figure 1. XRD results of the iron catalysts as prepared and Fe_2O_3 as benchmark

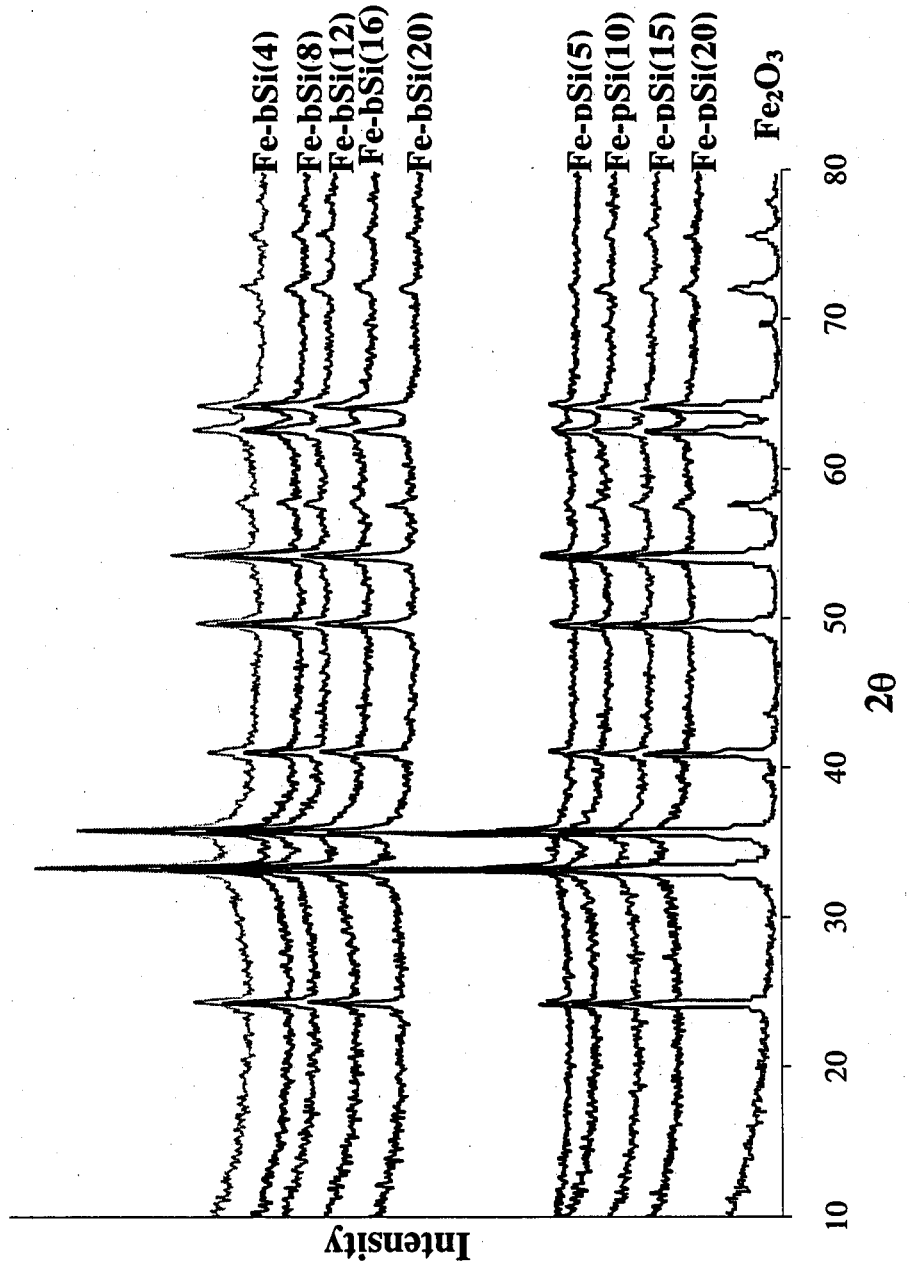

Table 2. TPR results of spray dried iron catalysts.

Catalyst	H_2 TPR (mmol H_2/g cat)	Reducibility (%)
Fe-bSi(4)	39.0	0.74
Fe-bSi(8)	38.8	0.76
Fe-bSi(12)	34.5	0.70
Fe-bSi(16)	34.9	0.74
Fe-bSi(20)	34.1	0.74
Fe-pSi(5)	34.6	0.74
Fe-pSi(10)	32.8	0.73
Fe-pSi(15)	33.1	0.77
Fe-pSi(20)	31.6	0.76

Figure 2. A typical TPR result [Fe-bSi(16) as prepared]

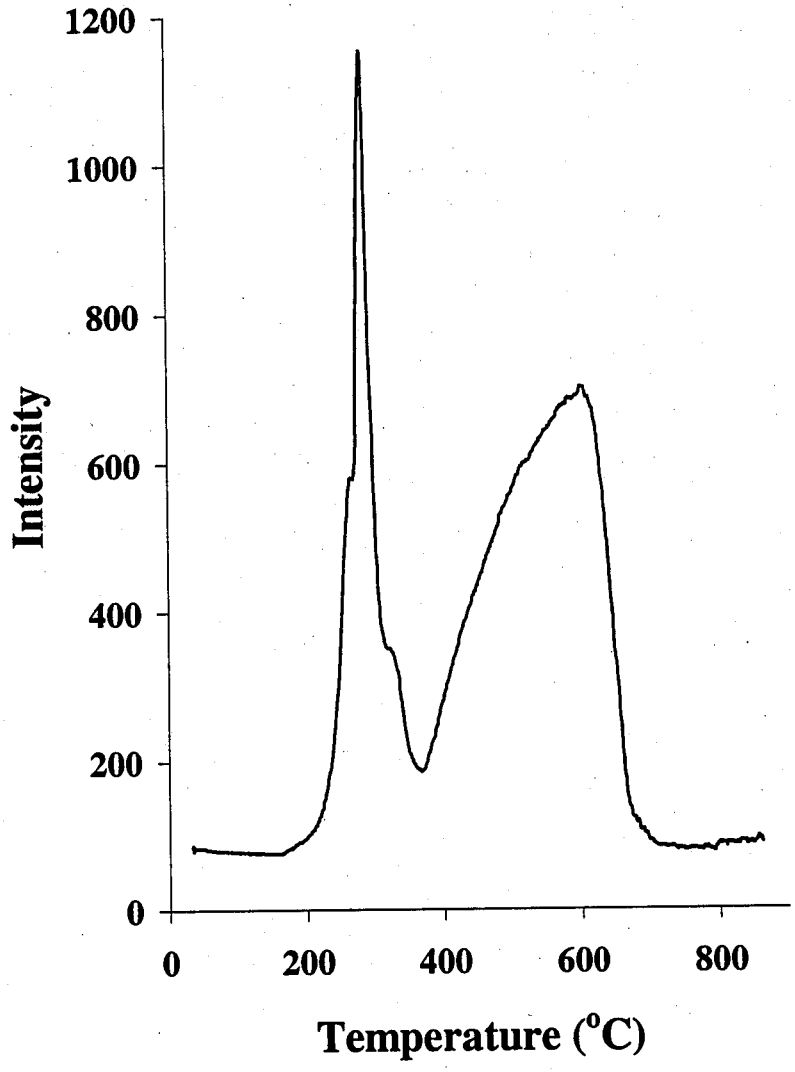

reduction of Fe_3O_4 to metallic iron. The small shoulder before the first peak has been suggested to be due to the reduction of the CuO.

The BET surface areas and average pore sizes were measured for both catalysts as prepared and after attrition tests using N_2 physisorption. As shown in Table 3, the BET surface areas, for each series of catalysts, generally increased with an increase in the concentration of SiO_2. The series with precipitated silica had relatively higher surface areas compared to the series without precipitated silica. The pore volumes (micropore and mesopore) slightly increased with an increase in the concentration of SiO_2. The series of catalysts with precipitated silica appears to have had higher pore volumes compare to the series without precipitated silica. The average pore sizes (calculated using 2*pore volume/surface area) varied slightly for all the catalysts. In general there was a decrease in average pore size for both series of catalysts, as SiO_2 content increased-related obviously to the large increase in BET surface area. After the jet cup tests, the average pore sizes remained unchanged for all the catalysts compared to those of the catalysts as prepared, while the BET surface areas slightly decreased after the test for most catalysts.

Figure 3 and Figure 4 illustrate the morphologies of the catalyst with and without precipitated silica, respectively. For each catalyst, micrographs of the particles both as prepared and after attrition testing are shown. It is apparent that the particles were more spherical (less agglomeration) with the increase of binder concentration for both series of catalysts. There are relatively less agglomeration observed for the series of catalysts with precipitated silica and some "donut"-shape particles (the particles with holes) can be observed (where the arrows pointed in Figure 3). Such "donut"-shape particles are not observed for the series of catalysts without precipitated silica, even for those having higher concentration of binder silica.

Table 3. BET surface areas and average pore sizes of the iron catalysts.

Catalyst	BET Surface Area (m^2/g)		Pore Volume (cm^3/g)		Average Pore Radius (A)	
	Fresh	Attrited	Fresh	Attrited	Fresh	Attrited
Fe-bSi(4)	101.3	94.23	0.29	0.28	43.6	44.7
Fe-bSi(8)	124.6	108.1	0.28	0.26	35.3	36.1
Fe-bSi(12)	146.2	137.1	0.28	0.29	32.0	33.9
Fe-bSi(16)	176.6	173.1	0.37	0.34	33.8	33.3
Fe-bSi(20)	158.3	168.2	0.33	0.34	37.3	37.7
Fe-pSi(5)	179.4	180.5	0.34	0.34	35.2	35.8
Fe-pSi(10)	190.8	177.1	0.37	0.35	36.9	37.3
Fe-pSi(15)	216.8	188.7	0.36	0.33	30.8	33.4
Fe-pSi(20)	245.0	243.9	0.39	0.40	30.2	32.6

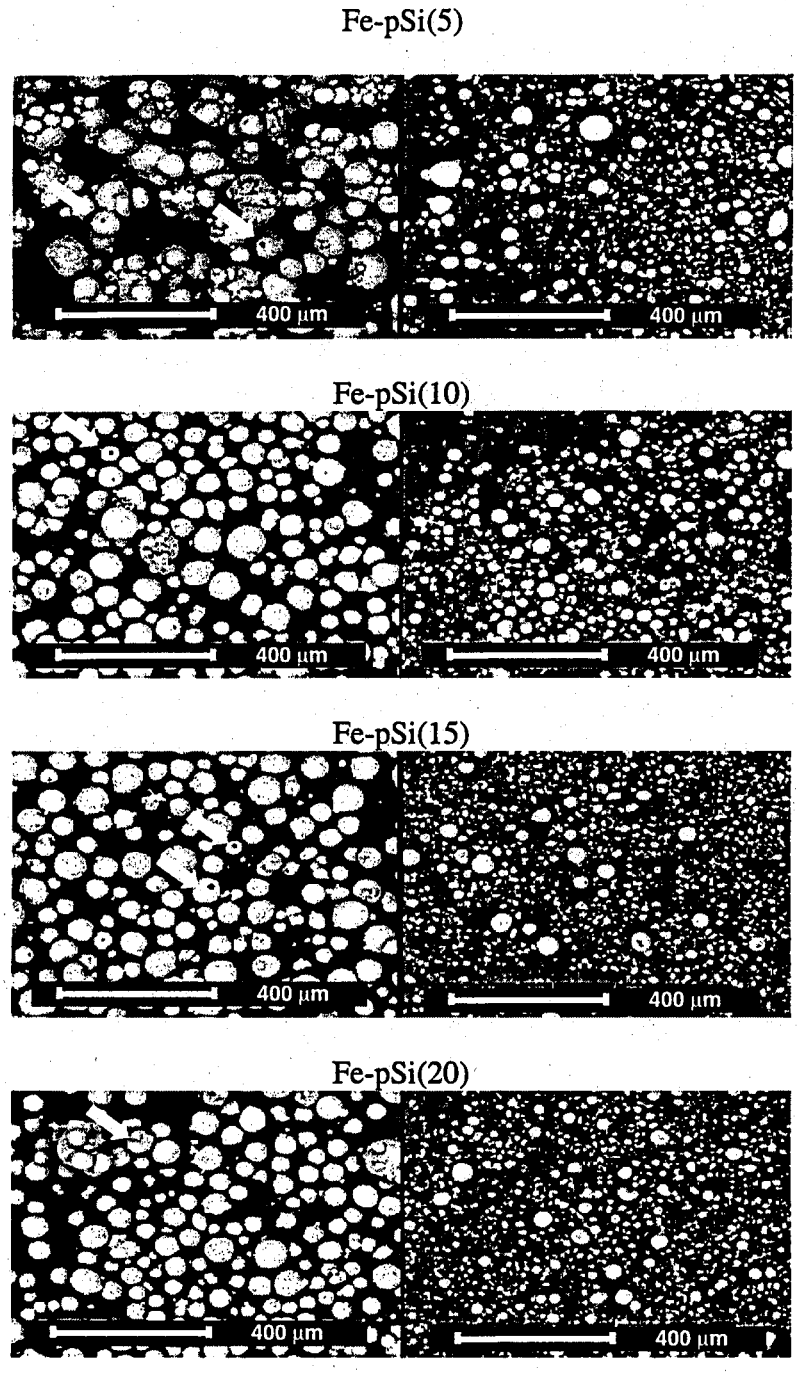

Figure 3. Morphology of the series of iron catalysts with precipitated silica

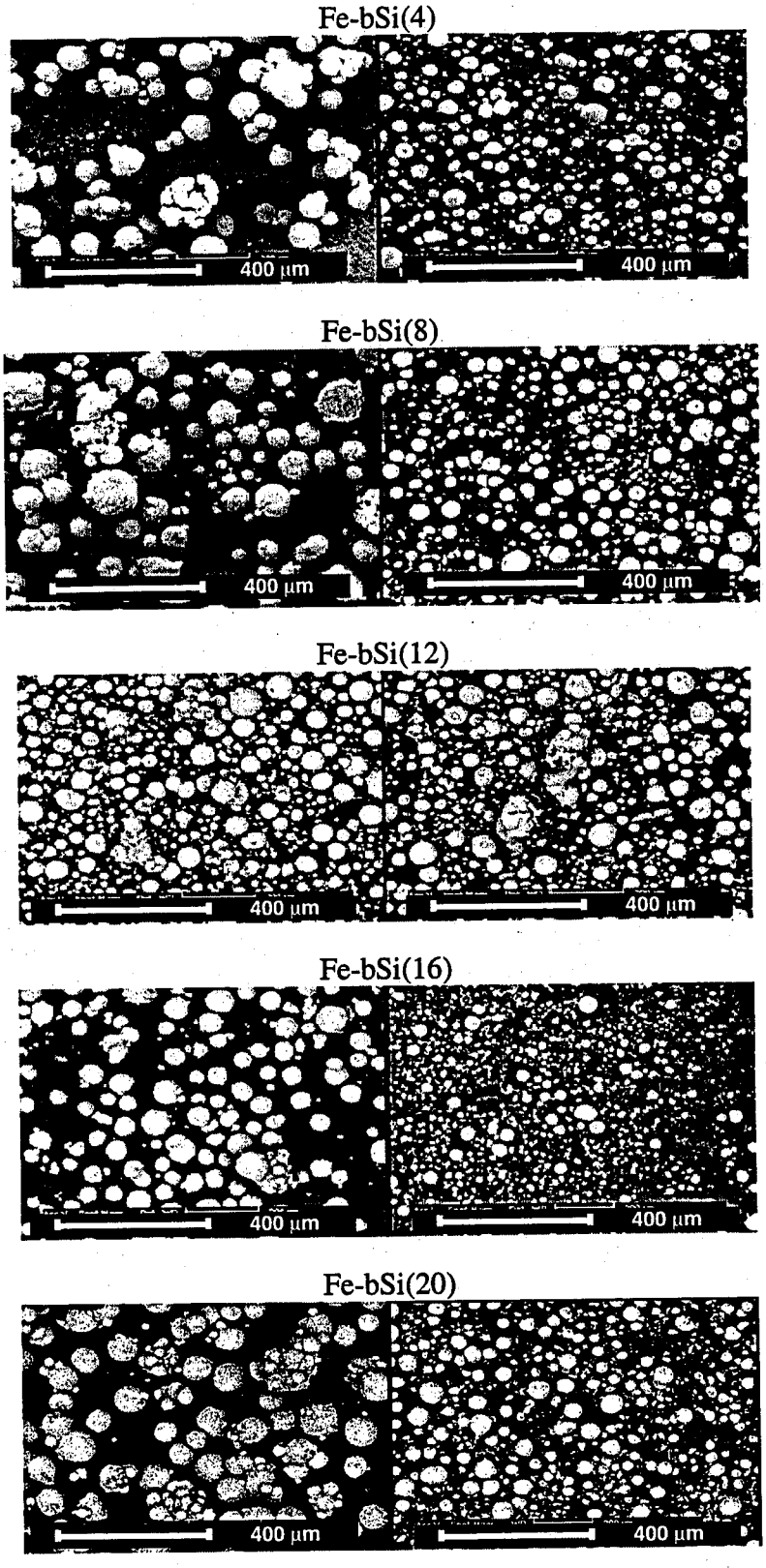

Before Attrition After Attrition

Figure 5. Morphology of binder silica catalysts.

When comparing the particles before and after attrition, it appears that the agglomerates formed during catalyst preparation were broken apart during the attrition test (Figures 3 and 4). The particle size obviously decreased for most catalysts after the attrition tests, especially for the series of catalysts with precipitated silica. The apparent decrease in the particle sizes was similar as seen by SEM and determined using laser diffraction. The only catalyst that did not change much in particle size was Fe-bSi(12), as also seen by particle size analysis. For this catalyst, some agglomerates still remained even after the jet cup test.

In order to study the phase and morphology of the supports, which plays an important role in attrition resistance of the catalysts, both series of catalysts were treated using acid leaching. This is due to the strong signal of iron oxide during XRD or SEM measures make the analysis of the supports very difficult. The XRD results of the supports are shown in Figure 5. The single peak in the XRD patterns shows that iron oxide is almost completely resolved during acid leaching. The supports are identified as silica, but are found all to be not crystallized.

The morphology of the supports was further studied using SEM. The results are summarized in Figure 6 and 7 for the supports of the series of catalysts with or without precipitated silica, respectively. The supports for the catalysts without precipitated silica (Figure 7) agglomerated more after dry compared to those without precipitated silica (Figure 6). The supports of the catalyst Fe-bSi(12) seem to agglomerate the least in series of catalyst without precipitated silica. On the contrary, the supports of the series of catalysts with precipitated silica seem to form individual spherical particle with very seldom agglomeration. There are also "donut"-shape particles that can be observed for the supports of the series of catalysts with precipitated silica (where the arrows pointed at in Figure 6).

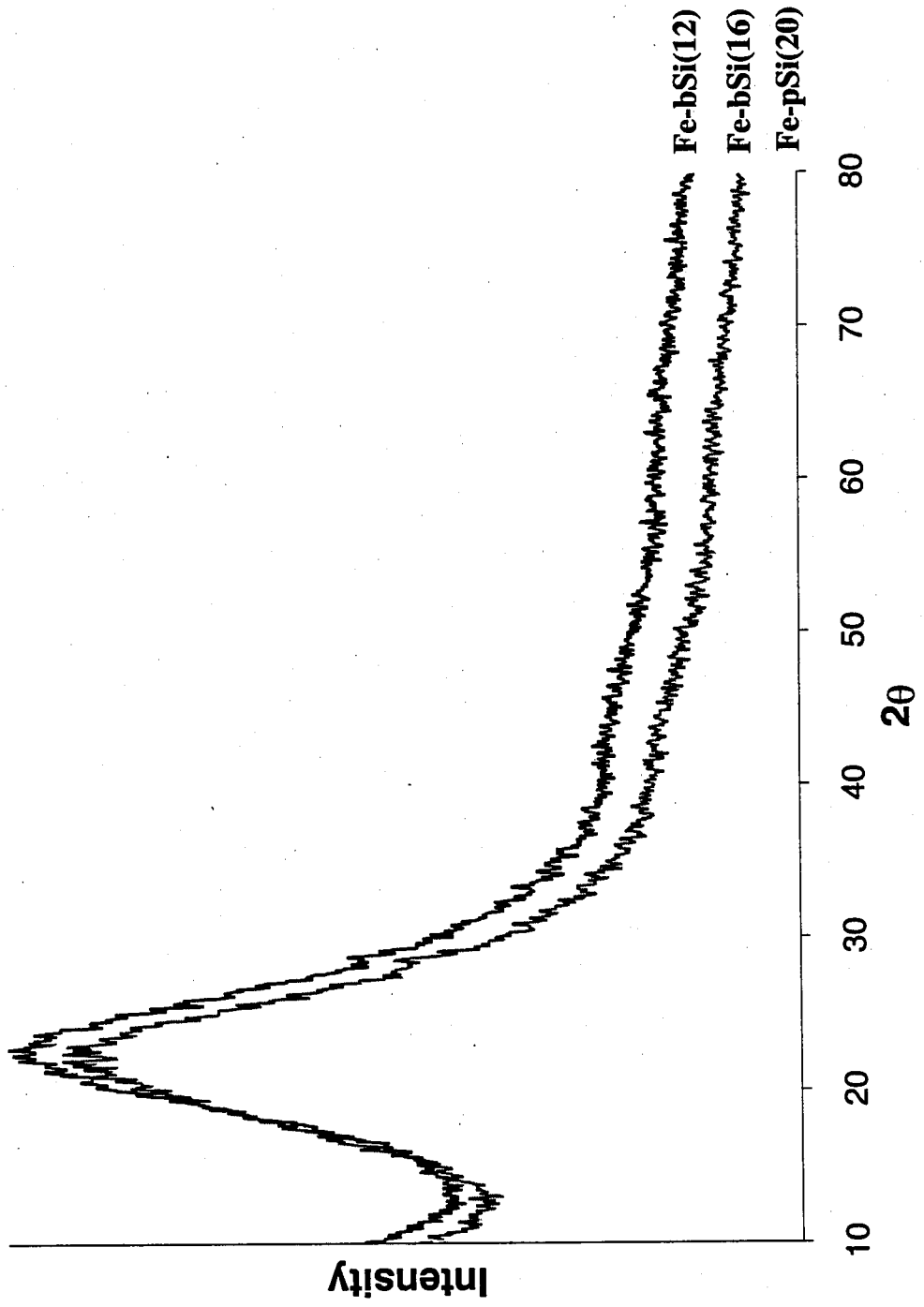

Figure 5. XRD results of some of the silica supports of the iron catalysts

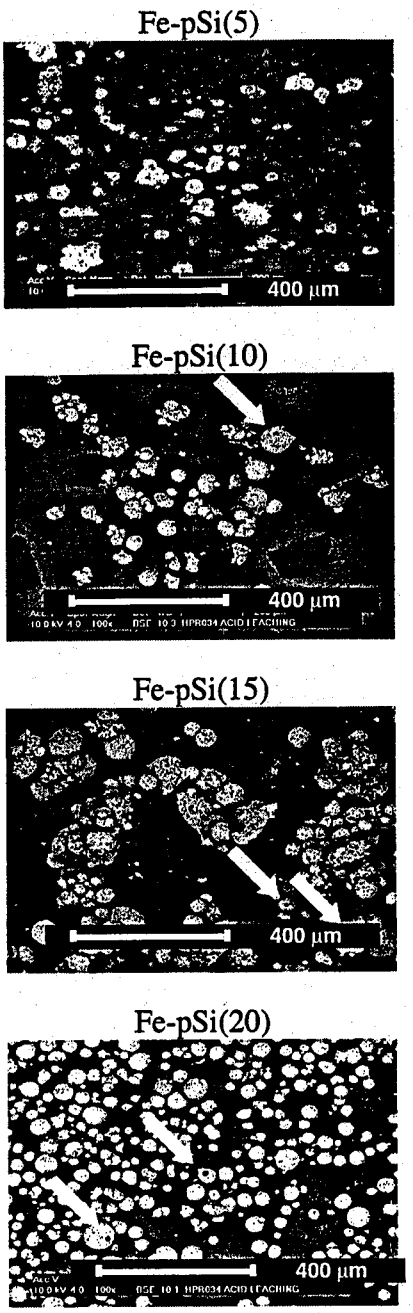

Figure 6. Morphology of the supports of the series of iron catalysts with precipitated silica

Fe-bSi(4)

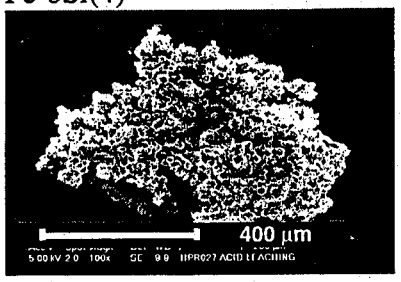

Fe-bSi(8)

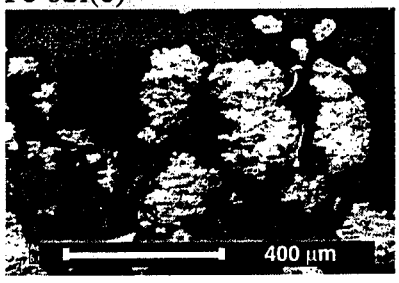

Fe-bSi(12)

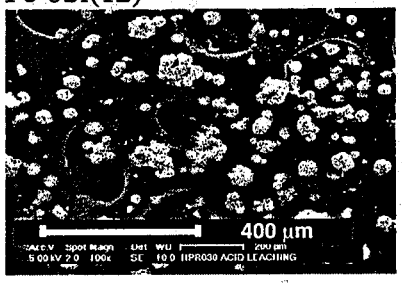

Fe-bSi(16)

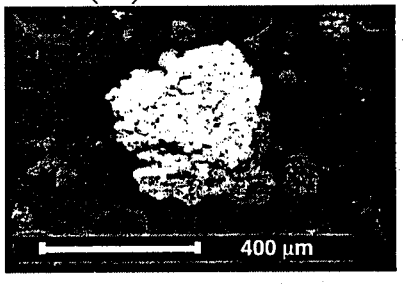

Fe-bSi(20)

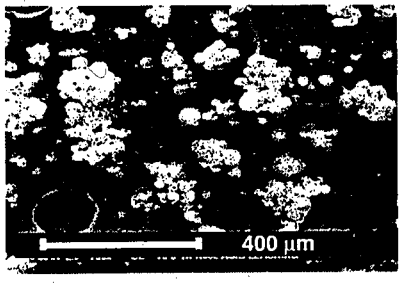

Figure 7. Morphology of the supports of the series of iron catalysts with binder silica

5.0 Discussion

Although the catalysts tested were prepared under similar conditions using spray dry technique, the attrition resistances vary in a large range (Table 1). After the addition of the precipitated silica, not only is the overall catalyst attrition resistance worse than that of the catalysts without precipitated silica, but also the attrition resistance decreases with the increase in the concentration of precipitated silica. Without the addition of the precipitated silica, it is not very clear how catalyst attrition resistance is affected by the concentration of the binder silica, even though there seems to be a trend of an optimum concentration of binder silica at ca. 12 wt %. In order to find out why and how the type and concentration of the supports have such an effect on attrition resistance, some further studies were performed.

As we expected, the XRD results (Figure 1) shows that the iron phase present in all the catalysts after calcination is Fe_2O_3. It is less likely that the difference in attrition resistance was due to any phase difference. Nor is the crystallinity of the iron oxide found to be responsible for the differences in the catalyst attrition resistance. It is shown in Figure 1 that iron oxide in the catalysts are not as crystal as the pure Fe_2O_3 elements, but slight differences were found for all the catalysts.

To find out any possible support and metal interaction, the TPR analysis was carried out. The calculated results (Table 2) showed that the reducibilities of the catalysts are very close. The addition of precipitated silica does not appear to affect the catalyst reducibility. These results suggest an unlike interaction of the supports and iron metal.

It is apparent from the XRD and TPR results that the catalysts as prepared are not very different chemically, except for the concentrations of the components. Therefore, the physical properties of these catalysts have drawn more attention in our studies. The morphology of the

catalysts was determined using SEM (Figure 3 and 4). To our surprise, the sphericity of the catalysts is found to have insignificant effects on the attrition resistance. For the catalysts with precipitated silica (Figure 3), the catalysts are more spherical compared to the ones without precipitated silica (Figure 4), whereas the attrition resistances of the ones without precipitated silica are relatively better (Table 1). Further study of the catalyst structure at higher magnitude using SEM did not show any differences among the catalysts. Since iron oxide is the dominant phase in the particles, iron oxide crystals are the only elements observed.

Although the BET surface areas are found different for these catalysts, they do not appear to affect the attrition resistance of the catalysts. In general, the surface area increases with the increase in the support concentration for both series of catalysts. On the other hand, when plot the average pore size with the attrition resistance (weight loss of fines during jet cup tests), it appears for the series of catalyst without precipitated silica that the attrition resistance decrease with the increase of average pore size. On the contrary, the series of catalysts with precipitated silica, similar trend was not observed .

From the above analysis, it seems that the porosity of the catalyst particles appears to have some impact on the attrition resistance. Yet the mechanisms of the structure effects are not clear from the data above. It is known that the iron oxide itself does not have much attrition resistance, the supports incorporated in the catalyst particles obviously are the key elements in the attrition performance of the catalysts. It is therefore interesting to find out whether such structure of the supports also present in these iron catalysts and whether any egg-shell type structure of the supports also present in these iron catalysts and whether the formation of such structure is the key factor in the attrition resistance improvement as well.

Since the signals of iron oxide is much stronger than those of the silica supports during XRD and SEM measurements, the catalysts were therefore treated using HCl solution in order to resolve the iron oxide. The XRD results of some of the supports after acid leaching (Figure 5) show that the supports are all silica. The supports are also found not crystallized, which is considered to be due to the low calcination temperature of the catalysts.

The study of the support morphology (Figure 6 and 7) shows that the supports for the catalysts appeared to be relatively smaller compared to the catalysts as prepared, especially for the catalysts without precipitated silica. The supports of the catalysts without precipitated silica appear to agglomerate more easily compared to those of catalysts with precipitated silica. When the supports were observed at higher magnification, it was found that these agglomerates were made of spherical particles (~30-40 μm in diameter) and some "amorphous" material (Figure 8). The XRD results (Figure 5) show that both of the spherical particles and the "amorphous" material should be silica, since no other elements present in the XRD patterns. It is, therefore, interesting to notice that silica exist in the catalyst particles seems to have two types: one forms the skeletal structure that appear to be spheres, the other appear to be more "amorphous" which causes agglomeration of the supports during drying.

For the supports of the catalysts with precipitated silica (Figure 9), the "amorphous" silica is seldom observed. Since the lacking of such "glue", these supports were not agglomerated much after the acid leaching. At higher magnification, it can be observed that the particles are spherical in shape and appear to be more porous (Figure 9) compared to the supports of the catalysts without precipitated silica (Figure 8). "Donut"-shape particles can also be found for the supports of catalysts with precipitated silica (Figure 6), whereas this type of particles is seldom observed for those of the catalysts without precipitated silica (Figure 7). It is

Figure 8. Morphology of the supports of the series of iron catalysts with binder silica at higher magnification

Fe-bSi(4)

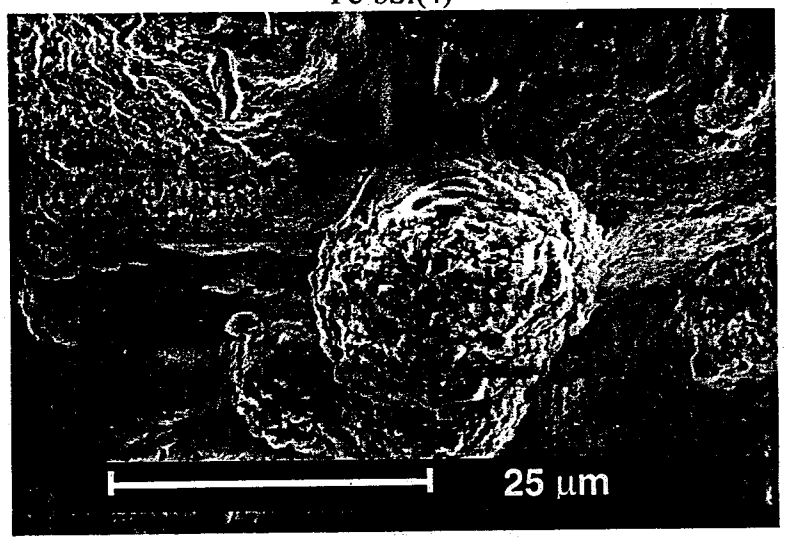

Fe-bSi(8)

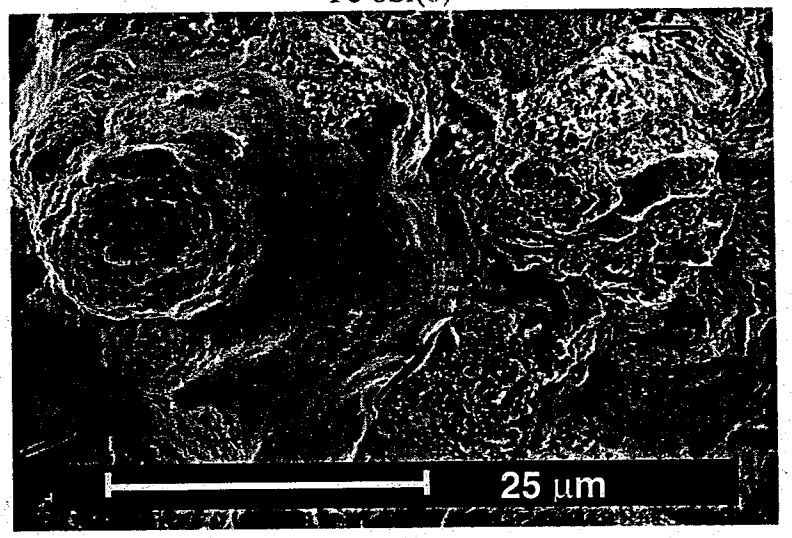

Fe-bSi(16)

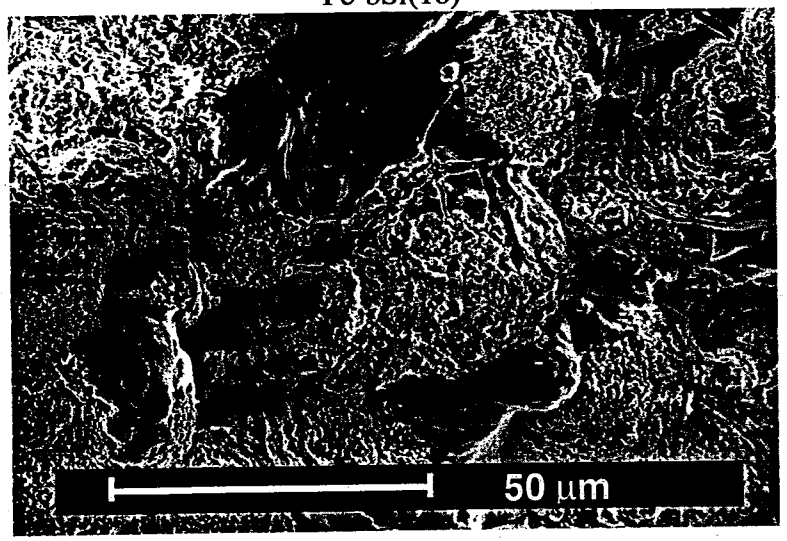

Fe-bSi(20)

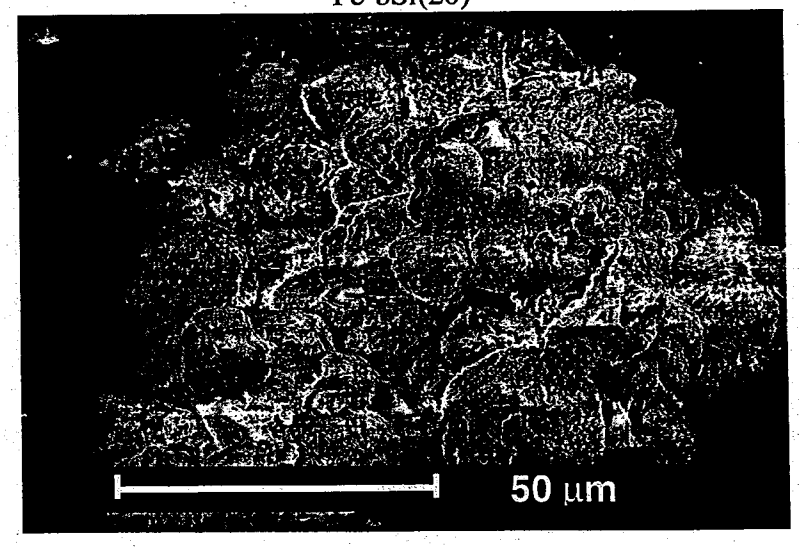

Figure 9. Morphology of the supports of the series of iron catalysts with precipitated silica at higher magnification

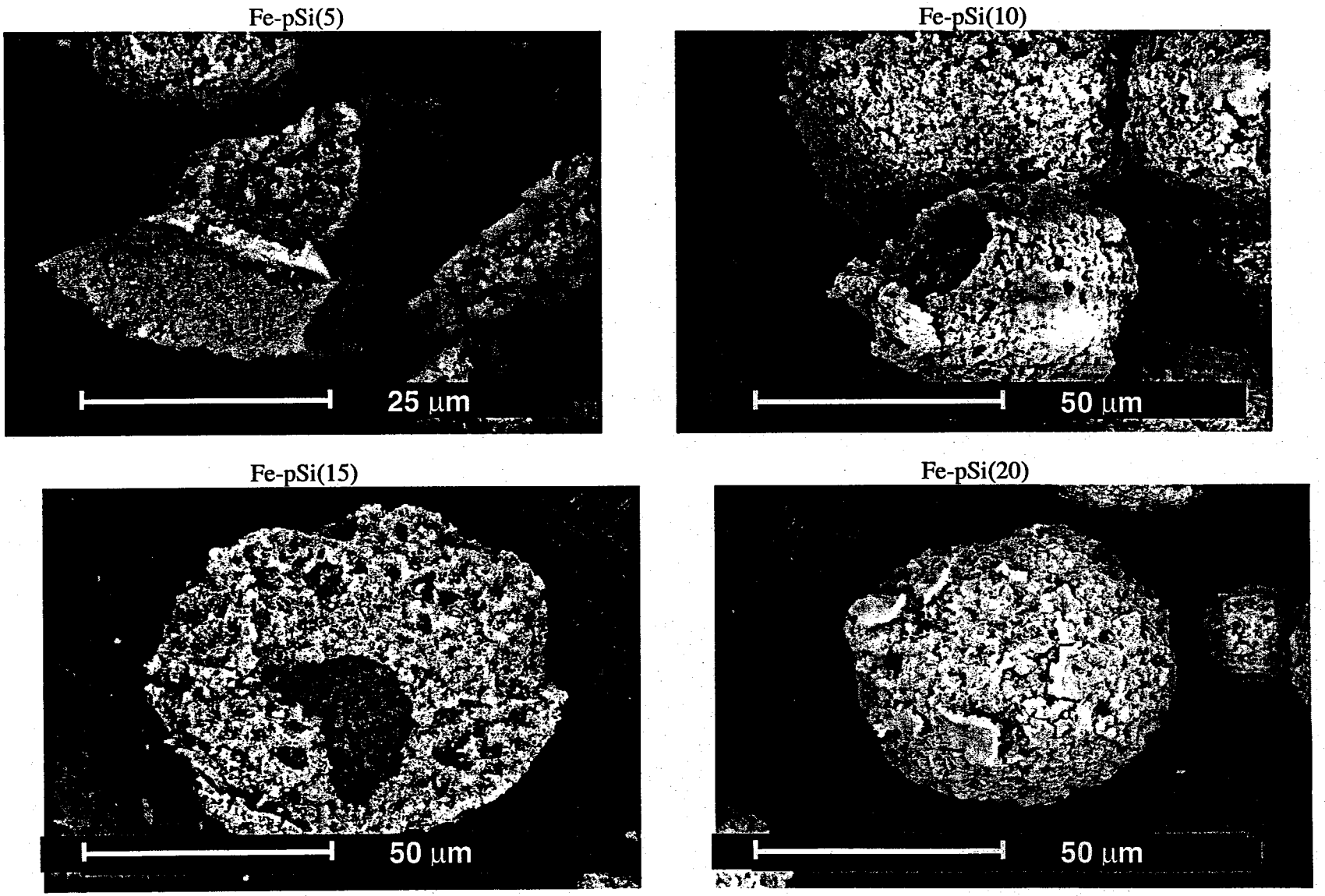

therefore speculated that addition of precipitated silica eliminated the existence of the "amorphous" silica and helped the silica to form a more porous structure. The increase in concentration of precipitated silica further increases the porosity of the supports. Such increase in the porosity of the supports is not beneficial for catalyst attrition resistance at all. On the contrary, decrease in the attrition resistance of the catalyst particle is observed with the increase of precipitated silica.

In Figure 9, a broken support particle of catalyst Fe-pSi(15) is shown. As can be seen, this particle is not only porous from an overall view, but also contains inner vacancy. Compared to a broken particle of the catalyst without precipitated silica (Figure 8), such porous structure is not observed. Instead, a much solid structure is found in Figure 8. These results are viewed as strong support of the above speculations. This also explains the "donut"-shape particles observed for the catalysts/supports with precipitated silica. Since the addition of precipitated silica facilitates the formation of a more porous structure and possible inner vacancies, such inner vacancy might be bigger enough that can be seem from outside the particles as a hole into the particle. In brief, it is suggested that the addition of the precipitated silica make it easy for the support to form primary silica particles and form more porous skeletal structure. It is also suggested to facilitate the formation of the structure with inner vacancy (shell type structure).

On the contrary, as seem in Figure 8, when precipitated silica is not added during catalyst preparation, the supports form less porous structure compared to those with precipitated silica. In addition, some silica seems to not form any primary silica particles (granules) but rather exist in an "amorphous" form. This less porous structure of the supports seems to provide better attrition resistance of the catalyst particle compared to the more porous structure of the supports. Another possibility is that the presence of the "amorphous" silica improved the attrition resistance. However, when the catalyst Fe-bSi(12) was studied, it is found that it is less likely

that "amorphous" silica is responsible for the catalyst attrition resistance improvement. Instead, for the support of the catalyst Fe-bSi(12), it is found that the support particles do not agglomerate as much as other supports for the same series of catalysts. A broken support particle of the Fe-bSi(12) catalyst (Figure 10) shows that this catalyst has a relatively more porous but uniform structure compared to other support particles of the same series of catalysts. No inner vacancy was observed for this catalyst even though it is porous. Other supports for the series of catalysts without precipitated silica, except for Fe-bSi(12), were found to have much less porous interior structure.

It is therefore speculated that at the absence of the precipitated silica, the support is less likely to form primary silica particle and therefore form less porous structure. The silica added seems to exist in the particle as an "amorphous" form. This more condensed structure (core type structure) seems to provide a better attrition resistance compared to the supports with shell type structures. However, there seems to be an optimum point between these two different types of structure. The catalyst of Fe-bSi(12) showed that when the porosity of the support is at a optimum point, where the inner vacancies are minimized, the porous structure became uniform through out the whole catalyst particles. At this point the presence of the "amorphous" silica is also eliminated to an amount that is not observable. The attrition resistance is the highest at this point.

Carburized Fe Catalyts

To further investigate the effects of phase change on catalyst attrition resistance, some of the spray dried catalysts were carburized under CO flow (Table 4). Surprisingly, the weight percentage of fines loss during jet cup test was found less compared to the attrition test of the same catalyst under calcined state.

Table 4. Jet cup attrition resistance test results of the spray dried iron catalysts.

Catalyst	Coprecipitaed Silica (pbw)	Binder Silica (wt%)	Fines (wt%) [a]		Bulk density (g/ml)	
			As received	After carburization	As received	After carburization
Fe/bSi(4)	0	4	26.6	--	0.83	--
Fe/bSi (8)	0	8	21.8	21.8	0.81	0.84
Fe/bSi(10)	0	10	4.8	7.7	1.02	1.08
Fe/bSi(12)	0	12	8.5	--	0.90	0.93
Fe/bSi(16)	0	16	18.2	15.5	0.78	1.18
Fe/bSi(20)	0	20	51.6	--	0.64	--
Fe/pSi(5)	5	12	26.6	13.2	0.66	1.09
Fe/pSi(10)	10	12	33.9	--	0.62	--
Fe/pSi(15)	15	12	39.6	--	0.61	--
Fe/pSi(20)	20	12	41.3	32.1	0.59	0.88
Co/SiO_2 [b]	N/A	N/A	31.07	--	0.41	--

(e) Fines wt% = weight of fines collected/weight of total catalyst recovered

(f) Co/SiO_2 is a Davison 952 silica supported 20wt% cobalt catalyst, which was used for develop the procedure.

Figure 10. Morphology of the supports of the catalysts [Fe-bSi(12)] at higher magnification

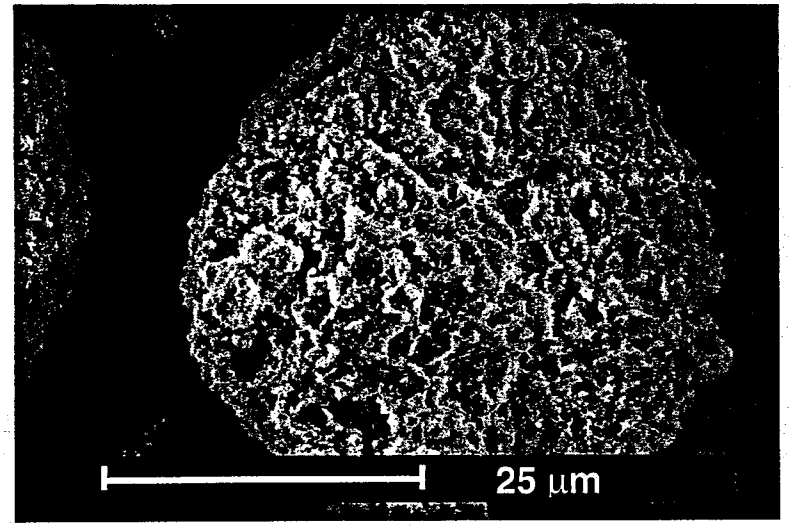

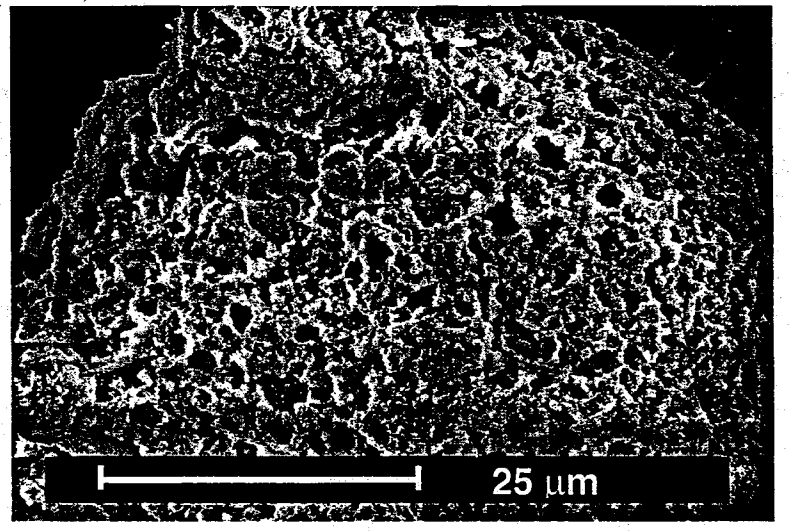

6.0 CONCLUSION

Two series of spray dried iron catalysts were studied in the present research. Both of the series of catalyst were prepared similarly except for the difference in the concentration of the supports (precipitated and binder silica). It is found that the attrition resistances of these catalysts vary in a large range. The XRD results confirmed that all the catalysts after calcination are Fe_2O_3 in phase and similar in crystallinity. TPR results further show a unlike metal and support interaction. Physical properties was thereafter our research focus.

BET surface areas were found to increase with the increase in the concentration of the supports, but less relevant to the catalyst attrition resistance. On the other hand, average pore size of the catalysts seemed to have some impact on the attrition performance, but the effects are not clear from the porosity of the catalysts.

Since the iron oxide is known not to be attrition resistant, the catalysts were therefore treated using acid leaching in order to better study the support with a clearer vision. The XRD results of the supports showed that only silica remains after the acid leaching for all the catalysts. However, SEM micrographs of the support show that there seems to be two different types of silica existing in the catalysts. For the series of catalyst without precipitated silica, there are a type of "amorphous" silica in addition to another type of silica that forms spherical skeletal structure. Such spherical structure are, however, found to be smaller compared to the catalyst particles. This is considered to be a "core" type of structure. On the contrary, the addition of precipitated silica appears to eliminate the amount of such "amorphous" silica, and facilitate the formation of more porous skeletal structure, which even appears to contain inner vacancy. Such structure was found not beneficial for catalyst attrition resistance at all. It is also suggested that such "shell" type of structure is the reason of the formation of the so-called "donut"-shape

particles. With the increase in the concentration of precipitated silica, the skeletal structure of the supports becomes more porous and therefore less attrition resistant.

For the series of catalysts without precipitated silica, it is found that the presence of such "amorphous" silica does not improve the attrition resistance of the catalysts. On the other hand, it is the less porous structure appear to be more attrition resistant compared to the more porous structure of the series of catalysts with precipitated silica. However, such "core" type of structure does not seems to provide the best attrition resistance either. It is found that only when the skeletal structure is porous and uniform can the catalyst particles have the best attrition performance.

Since phase change during reaction has always been a concern for iron catalysts in terms of attrition resistance, some of the catalysts were carburized and tested using the jet cup. The attrition resistance was found to actually improve after carburization in terms of weight percentage of fines lost. Such improvement was considered to be due to the change in catalyst bulk density upon carburization.

7.0 References

Allen T., in "Particle Size Measurement, 5th ed.", Chapman & Hall, New York, 1997, p.45.

Bhatt, B.L., Heydorn, E.C., and Tijm, P.J.A., in "Proceedings of the 1997 Coal Liquefaction & Solid Fuels Contractors Review Conference", US Department of Energy, Federal Energy Technology Center, Pittsburg, Pennsylvania, 3-4 September, 1997, p. 41.

Bukur D.B., Nowicki L., and Patel S., Can. J. of Chem. Eng, 74 (1996) 399.

Bukur D.B. Patel S.A., and Lang X., App. Catal. A, 61 (1990) 329.

Huang, C-S, Xu, L., and Davis B.H., Fuel Sci. Tech. Int'l., 11 (1993) 639.

Jothimurugesan, K., Goodwin, J.G., Jr., Spivey, J.J., and Gangwal, S.K., Syngas Conversion to Fuels and Chemicals, American Chemical Society, 1999.

Kalakkad, D.S., Shroff, M.D., Kohler, S., Jackson N., and Datye, A.K, App. Catal. A, 133 (1995) 335.

Schulz, Nat. Gas Conv. II, Surf. Sci. Sci. Ser., vol. 81, Elsevier, New York, 1994, P.455.

Srinivasan, R., Xu, L., Spicer, R., Tungate, F.L., and Davis B.H., Fuel Sci. Tech. Int'l., 14 (1996) 1337.

Zhao, R., Goodwin, J.G., Jr., and Oukaci, R., App. Catal. A, in press (1999)

APPENDIX B

Attrition Assessment for Slurry Bubble Column Reactor Catalysts

ABSTRACT

Significant interest in 3-phase slurry bubble column reactors (SBCRs) has come about in recent years due to their excellent heat removal capabilities during reaction. However, no evaluation test for catalyst attrition resistance is available in the literature yet for SBCR catalysts, although severe attrition of catalyst particles has actually been encountered in SBCRs. In this work, fluidized bed catalyst attrition tests (fluidized bed and jet cup) and other tests (collision and ultrasound) are evaluated for the first time for their suitability in predicting catalyst attrition in an SBCR. Based on comparisons of particle morphology and size distribution (PSD) of a silica supported cobalt catalyst before and after use in an SBCR with the results from the various attrition assessment tests, it is suggested that the fluidized bed, jet cup and ultrasound tests all provide reasonable and efficient predictions of catalyst attrition. Although the dominant attrition mechanism appeared to be fracture in both SBCR run and collision test, the latter showed too little attrition efficiency to be suitable as an attrition test. Despite the fact that abrasion occurs to a greater degree during the fluidized bed, jet cup, and ultrasound tests compared to during an SBCR run, all these three tests cause particle breakage similar to that in the SBCR, but in relatively short periods of time. Therefore, all three, especially the jet cup test, are suitable tests for predicting catalyst attrition resistance in an SBCR environment.

1. INTRODUCTION

Attrition, defined as the unwanted breakdown of solid particles [1], is a commonly encountered problem in catalytic chemical reactors, especially fluidized bed types [2]. Attrition resistance is one of the critical parameters in the development of catalysts because any attrition of a catalyst causes loss of the catalytic agent and lower product quality. In fluidized bed reactors, attrition can also cause additional filtration and plugging problems and affect the fluidization properties.

Such problems have stimulated many earlier studies [3-15]. Currently, it is believed that attrition processes include both abrasion/erosion (the process during which particle surface layers or corners are removed) and fracture (the fragmentation of particles) [1,2]. These are due to various types of stresses that catalyst particles undergo during reaction, among which the major ones include contact, thermal, pressure, and chemical stresses [2]. For example, in Fischer-Tropsch synthesis (FTS), phase change and carbon deposition have been suggested to be responsible for the nano-scale breakage of iron catalysts [13]. In most earlier studies, however, only attrition due to hydrodynamic forces has been the focus of the research, whereas the other three sources of stress listed above have been assumed to be negligible. In recent reviews and studies by Ghadiri and coworkers on particle attrition [16-18], particle breakdown during impact has been further categorized into different breakage modes according to the impact velocity, particle size and shape, and contact geometry. Particle fracture during impact due to pre-existing internal or surface flaws is classified as brittle failure. Crack initiation, on the other hand, is considered to be semibrittle failure, which can be further categorized by fragmentation or chipping depending on the position of the cracks.

Based on such understanding of attrition processes, several types of attrition assessment methods have been developed and used to evaluate catalyst attrition resistance [3,4,9-11,19-24]. Since it has been concluded that no single particle can represent all the particles involved [2], most catalyst attrition tests involve multiple particles. While tests have been developed for various reactor configurations, such as the compression [19] and rotating drum [20,21] tests aimed mainly at moving bed reactor catalysts, most tests developed have focused on fluidized bed catalysts, which can undergo extensive attrition due to particle-particle and particle-wall collisions. In order to mimic the particle movement and collision inside fluidized bed reactors, Forsythe and Hertwig [3] were the first to use a high-velocity air jet in their attrition test device. This formed the basis of various subsequent tests [4,9,10,12,22,23], including an ASTM (American Standard Test Method) procedure [24]. In a more recently proposed ASTM method, the jet cup test [11], catalyst particles are also fluidized by a high velocity air jet. As mentioned above, physical attrition properties of the catalyst particles are the only ones measured in these tests.

Significant interest in slurry bubble column reactors (SBCRs) has come about in recent years due to their excellent heat removal capabilities during reaction, especially for exthothermic reactions such as FTS. Although it had been suggested that SBCRs are free of catalyst attrition and erosion problems [25], severe attrition problems have been encountered [26]. Due to the complex nature of attrition in three-phase reactors, the attrition mechanisms in SBCRs are still not clear. A suitable evaluation of catalyst attrition resistance is hence a necessity in the SBCR catalyst development. Although, the rotating drum test was modified in order to test a slurry of unsupported precarbided or carbided iron SBCR catalysts in a previous study [15], the results were not compared to attrition in actual SBCR runs. Thus, none of the test methods reported to

date have been developed and qualified for use in assessing the attrition resistance of catalysts for SBCRs.

In the present study, Co/SiO_2 was tested using four different types of attrition assessment methods and the test results were compared to laboratory-scale SBCR results obtained under reaction conditions. The goal was to develop a suitable laboratory test method for predicting the attrition of catalysts under SBCR conditions. Only physical effects have been considered in these comparisons.

2. EXPERIMENT

2.1 Catalyst

The catalyst used was a spray dried silica (Davison Grade 952) supported, Zr promoted, Co catalyst prepared using the incipient wetness technique. After the silica support was pre-calcined at 500°C for 10 hrs and pre-sieved to 38-90 μm (400-170 mesh), Co and Zr salts in an aqueous solution were co-impregnated using incipient wetness in amounts to produce a reduced catalyst having 20 wt% Co and 8.5 wt% Zr. The catalyst precursor was then dried at 115°C for 5 hrs and calcined at 300°C. The prepared catalyst was sieved again after calcination to 38-90 μm using standard sieves. Since particulate materials can undergo size segregation during storage and transportation, such materials have to be mixed as well as possible prior to taking samples. Because the total amount of the catalyst was not very large in this case, this was accomplished by shaking the catalyst container thoroughly in several directions prior to removing a sample.

2.2 Instrumentation and Procedures

2.2.1 SBCR System

The Co catalyst was placed in a 1 inch (1 in = 2.54 cm) diameter, 3 foot (1 foot = 12 in) tall SBCR under Fischer-Tropsch synthesis (FTS) reaction conditions for 240 hrs. All FTS runs

were at 450 psi total pressure (including N_2) and 220-240°C with a CO/H_2 ratio of 2. The slurry initially consisted of Synfluid (Chevron) as the liquid phase and 15 wt% of catalyst presieved to 38-90 μm. After the SBCR run, the catalyst was extracted from the slurry liquid by solvent extraction. The resulting catalyst particles were characterized and compared to those of the catalyst as prepared and sieved.

2.2.2 Air Supply System

Air flow is essential for most of the attrition tests employed. Therefore, a supply system was built in order to supply a steady flow of humidified or nonhumidified air. The flow rate was controlled by a mass flow meter or a rotameter. The humidity and temperature of the airflow was monitored using an on-line Fisher temperature and relative humidity meter. The humidity was able to be adjusted by controlling the volume of air bubbled through a distilled water reservoir.

2.2.3 Collision Test

As illustrated in Figure 1, the instrument for this test consisted of an air supply tube, sealed catalyst reservoir, capillary particle drop channel, and collection assembly. The collection assembly also provided the hard surface (pyrex glass) with which the accelerated particles collided. After loading 1 g of sample into the catalyst reservoir with the air supply tube

Figure 1. Collision or drop shatter system

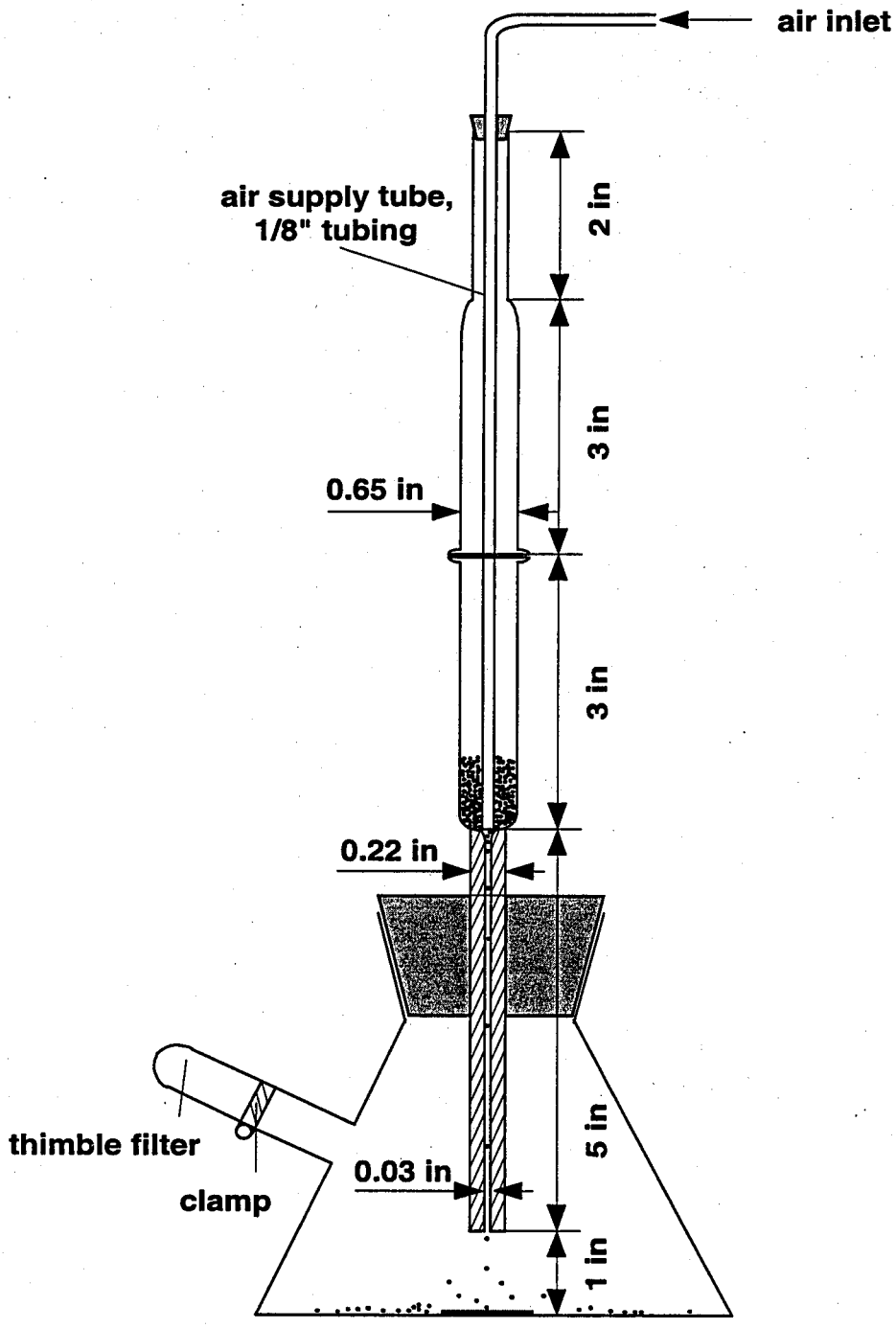

depressed against the entry to the drop channel in order to prevent particle flow out of the reservoir, the reservoir was sealed. After the air jet stabilized at a set flow rate, the air supply tube was raised about 0.5 ± 0.01 mm to provide a gap through which particles could slip into the drop channel. The particles fell into the drop channel and were then accelerated by the air stream before colliding with the inner flat surface of the collection assembly. The speed of the particles striking the hard surfaces was 12 m/s. The gas outlet of the collection assembly was covered with a thimble filter that prevented fine particle loss. The particles collected by the thimble and the collection assembly were removed after the test and analyzed for change in particle size distribution (PSD).

2.2.4 Fluidized Bed Test

A modified fluidized bed test system, based on ASTM D5757-95 [24] but smaller, was employed in this study. This scaled down system is considered superior since less than 5 g of catalyst is required rather than 50 g. The fluidized bed dimensions were calculated using the minimum fluidization gas velocity equation [27]. The gas distributor design was based on the literature [22,23]. The instrument, gas distributor plate and orifice dimensions and setup are illustrated in Figure 2.

In order to prevent the particles from sticking to the tube as a result of static electricity, humidified air (relative humidity of $60 \pm 5\%$) was used as the gas medium instead of using a mechanical tapping system. The fines collection assembly was weighed before the test and its mass recorded. With the air flowing at 0.5 *l*/min and the fines collection assembly removed, 3.0 g of sample were charged into the attrition bed. The fines collection assembly was then replaced and the air flow increased to the desired level. In the procedure given in reference [23], the air

Figure 2. Fluidized bed system

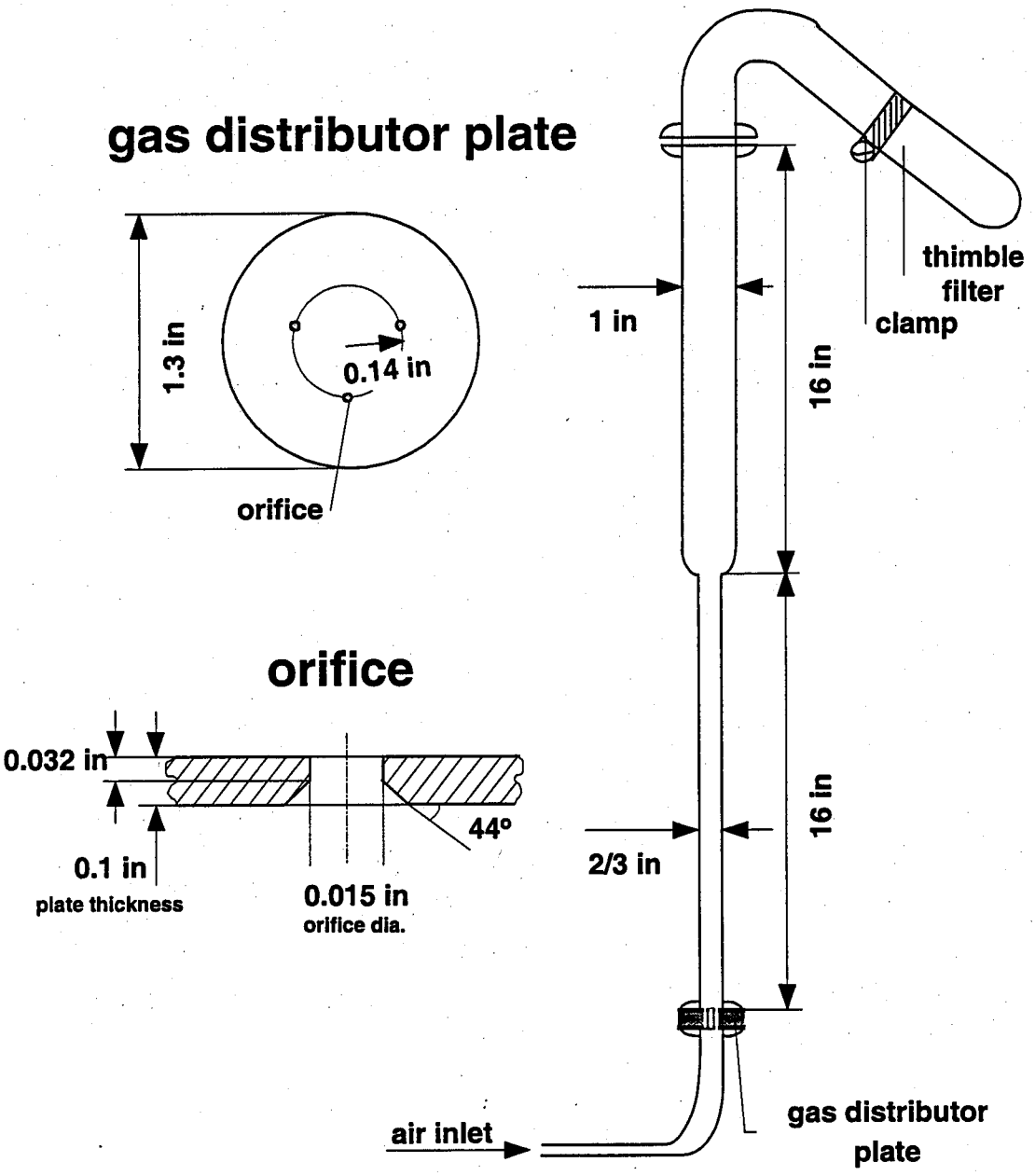

flow is specified to be stopped periodically to measure the rate of loss of fines. However, this potentially leads to turbulence in the fluidization condition and was determined to have an impact on the attrition process inside the fluidized bed. In order to determine the rate of loss of fines without stopping the air flow, two thimbles were weighed and numbered before the experiments in the present study, which is similar to the ASTM procedure [24]. The interchange of thimbles was made quickly to minimize any particle loss. After 6, 12, 18, or 24 hrs time-on-stream, the air supply was stopped. All the catalyst particles were recovered from both the fluidized bed and the fines collection assembly for particle size distribution analysis.

2.2.5 Jet Cup Test

The jet cup test system was based on a proposed ASTM design. As illustrated in Figure 3, the instrument consisted of an air inlet tube connected to the sample cup at the bottom, the settling chamber, and the fines collection assembly. Five grams of sample were weighed and charged into the sample cup. The jet cup was then attached to the settling chamber. After all joints were sealed, humidified air with a relative humidity of $60 \pm 5\%$ was introduced at a controlled flow rate of 10, 15, or 20 *l*/min for one hour. Similar to the fluidized bed test, in order not to interrupt the air flow during experiment, two thimbles were weighted and numbered before the start of the experiment to determine the rate of loss of fines. A thimble, placed on the fines collection assembly, was interchanged with the other quickly at 5 min, 15 min, and 30 min after the start of air flow and its mass recorded. The air flow was stopped after 1 hr on stream, and the fines in the thimbles and the coarse particles in the jet cup were recovered for analysis.

2.2.6 Ultrasonic Test

Figure 3. Jet cup system

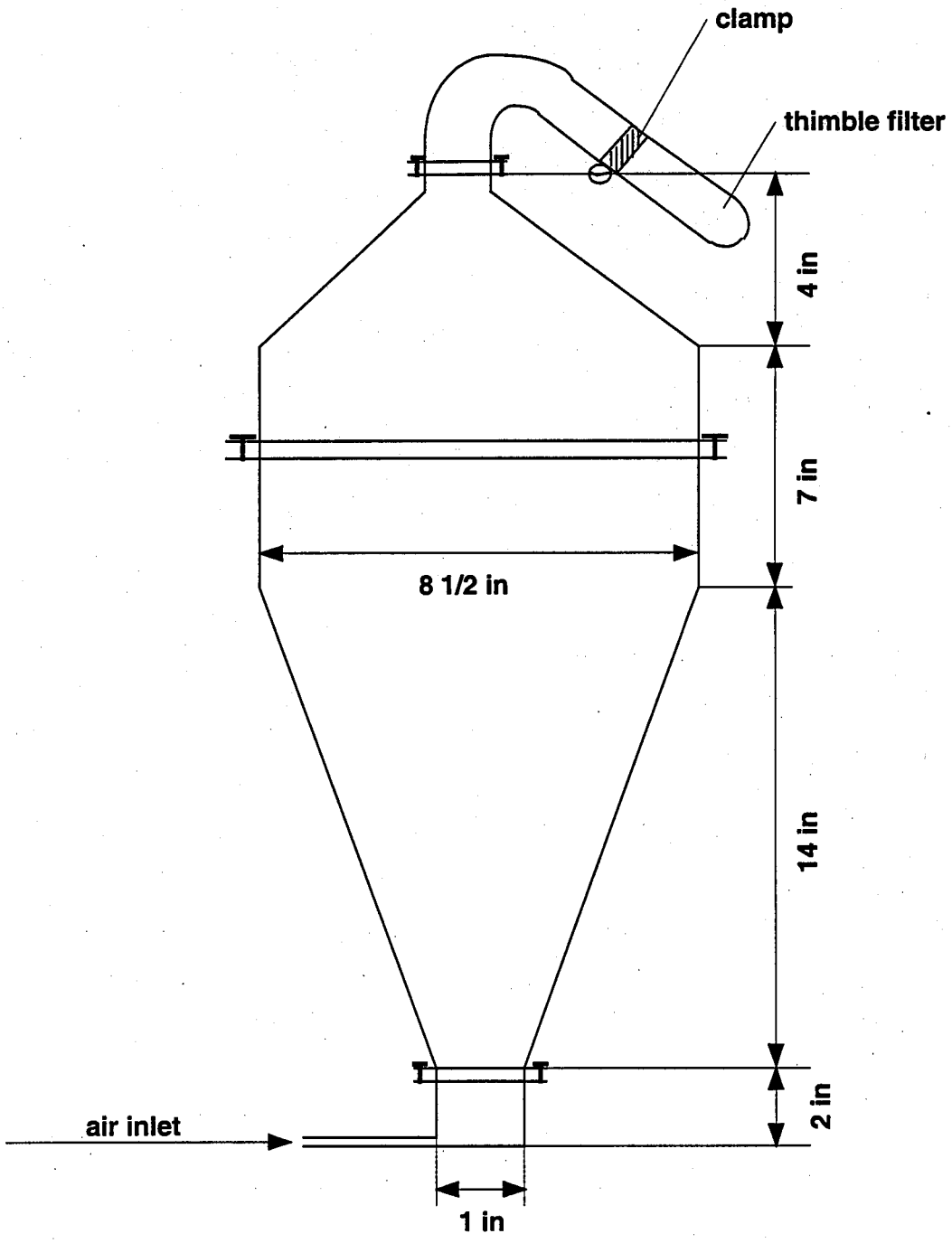

As illustrated in Figure 4, the ultrasonic system consisted of a 20 kHz Tekmar TM501 sonic disrupter with a CV26 horn and a 0.5 inch tip, a container for holding the catalyst slurry, and the horn support frame. Pre-weighed sample was dispersed in the media, which was distilled water in the present study, by stirring. Suspensions were prepared with about 2.5 vol% of solids in a total of 400 ml of distilled water [13,28,29]. The suspension was then treated at a particular energy setting of the sonic disrupter for 15 min. As reported by the system manufacturer, the maximum energy output is 500 W, and the settings correspond to percentages of the total energy output. In the present study, 150 W, 250 W, or 400 W energy settings were used. Since it was reported that temperature is one of the factors affecting ultrasonic energy output, a water bath was used in order to keep a relatively constant temperature of 23°C. After the electronic timer on the ultrasonic generator automatically shut down the system, the slurry was transferred, sampled and characterized using a particle size analyzer. The remainder of the slurry was filtered and dried at 110°C in an oven for SEM analysis.

2.3 Particle Analysis

A Leeds & Northrup Microtrac model 7990-11 laser particle size analyzer was used in order to measure the particle size distributions (PSDs). The original, fluidized bed, jet cup or collision test samples were each was put into 50 ml of deionized water and dispersed using an ultrasonic bath. The approximate 2.5 vol% suspension was then sampled for the Microtrac in order to determine PSD. The suspension from the ultrasonic test was stirred to an even distribution after the test before sampling. Samples were taken from the top, center and bottom of the suspension in order to ensure more accurate analysis. The results of several measurements of the same sample were averaged in order to minimize the error.

Figure 4. Ultrasonic system

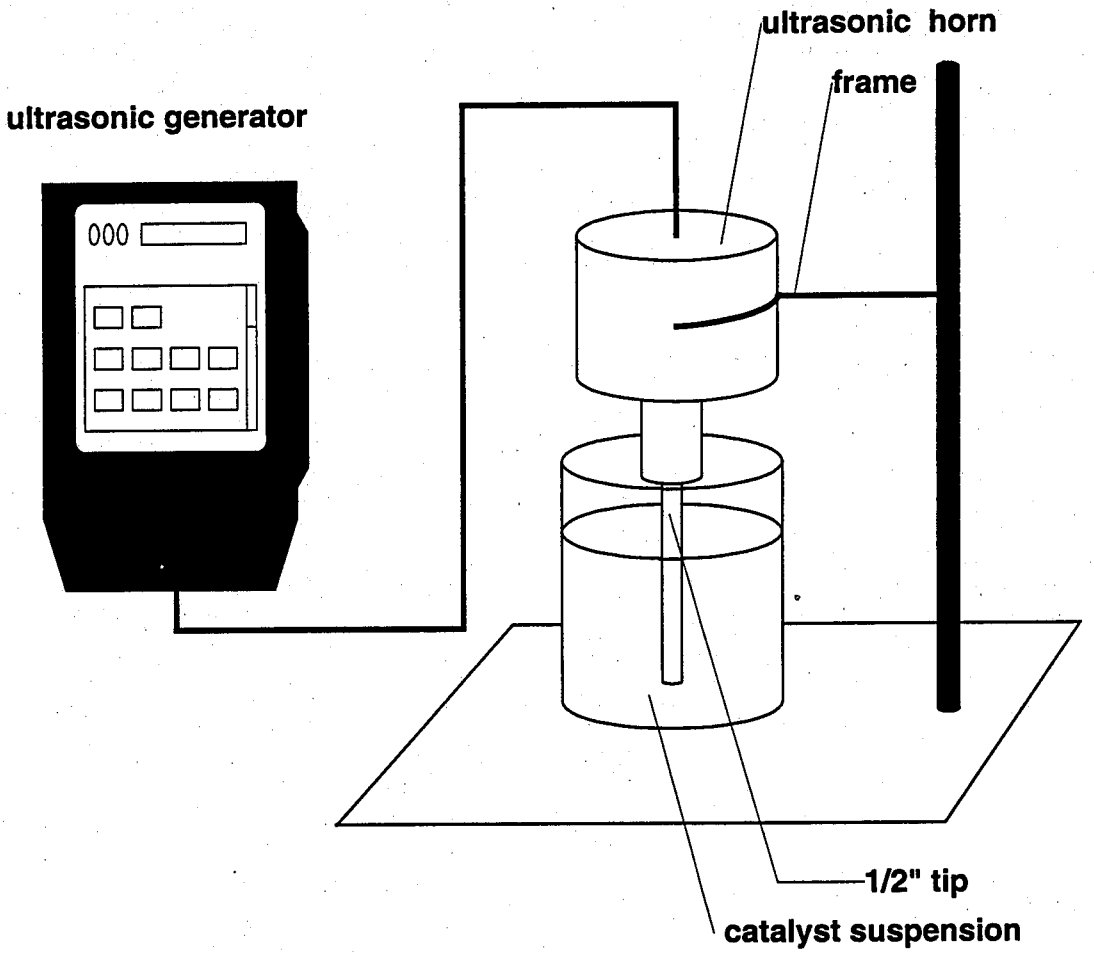

Since size distribution is usually plotted as weight (or volume) percentage versus average projected area diameter of particles in attrition studies, change in the volume moment, a type of average particle size commonly used to represent a particular PSD, has been selected as a useful indicator of the attrition process. The volume moment, x_{VM}, can be calculated by [32]:

$$x_{VM} = x_{WM} = \frac{\sum dM}{\sum dV} = \frac{\sum x^4 dN}{\sum x^3 dN} \quad (1)$$

where, x_{VM} is the volume moment, x_{WM} the weight moment, M the size moment, V the particle volume, and N the number of particles of size (diameter) x.

Particle morphology information was obtained for each sample by using a Philips XL30 FEG Scanning Electron Microscope (SEM). SEM micrographs were further analyzed using Scion Beta 2 image analysis software for determination of areas and perimeters of particle projections.

2.4 Reproducibility

Due to the limited amount of the Co/SiO_2 catalyst available, sieved Davison 952 silica support was used instead to evaluate the reproducibility of each test method. The comparisons are shown in Table 1. Weight percent elutriated and average particle size were used to determine the reproducibility of these attrition tests.

3. RESULTS

The morphology of the catalyst as prepared and sieved is showed in Figure 5. Although the silica support was spray dried, the catalysts as prepared were not as spherical as expected. This is considered to be due in part to particle agglomeration during catalyst preparation – as

Table 1. Reproducibility tests

Test	Run	Flow Rate	Time- on-Stream	Elutriated Fines (wt%)[a]	Volume Moment (μm)
Fluidized Bed	1	1.0 l/min	12 hr	10.85	70.1
	2	1.0 l/min	12 hr	10.39	70.7
	3	1.0 l/min	12 hr	11.17	69.8
Jet Cup	1	10 l/min	1 hr	17.0	46.8
	2	10 l/min	1 hr	18.6	45.2
	3	10 l/min	1 hr	17.0	44.2
Collision	1	1.0 l/min	1 time	NA	72.4
	2	1.0 l/min	1 time	NA	72.6
	3	1.0 l/min	1 time	NA	72.0
Ultrasound	1	250 W[b]	15 min	NA	48.1
	2	250 W[b]	15 min	NA	48.3
	3	250 W[b]	15 min	NA	48.8

a. Elutriated fines wt% = (weight of fines recovered from the fine recollection assembly after test/total weight of catalyst recovered after test) x 100%
b. Ultrasound energy setting: 50% of 500 W.

Figure 5. Morphology of the catalyst as prepared and sieved

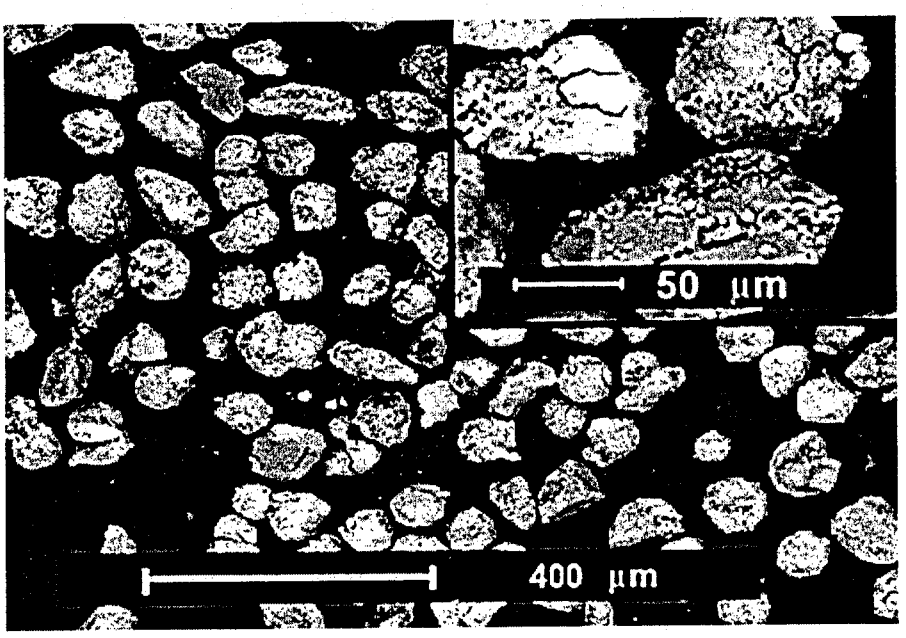

seen by comparing the particle morphology of pre-calcined and sieved catalyst support (Figure 6) and the Co catalyst after preparation (Figure 5). The catalyst support particles before preparation are relatively smaller and more spherical. On the other hand, in addition to particle agglomeration, some fracture and crack formation were also found on the catalyst particles after catalyst preparation. Some of the impregnated cobalt appeared to form cobalt patches on the surface of the silica support particles as can be seen in Figure 5. These patches were found both on and inside the silica support particles when space permitted and had an average size around 2 μm. They appeared at high magnification to be made up of clusters of Co oxide crystals (in the calcined catalysts).

As seen in the SEM micrograph (Figure 7), the catalyst particles after use in the SBCR appeared to be even less spherical than those of the catalyst as prepared (Figure 5). The number of broken particles (fragments and chips) obviously increased after FTS reaction in the SBCR. The external cobalt patches appeared not to be affected during the SBCR run. Obvious fractures could be observed for some of the larger particles. The PSDs of both fresh and used catalysts are given in Figure 8. Continuous curves, instead of bar charts, were chosen to represent the PSDs based on the assumption of continuous size distribution [30-32] for easier data comparison and analysis. The center size of each size interval (i.e., each Microtrac channel) was plotted as the abscissa and the frequency of particles in each interval as the ordinate. As shown in Figure 8, the average catalyst particle size decreased after use in the SBCR. The concentration of particles less than 30 μm obviously increased. Two peaks are apparent for the particles less than 30 μm in the PSD of the catalyst after SBCR use. Considering that fine particles were lost during the SBCR run through the liquid effluent filter with openings of 10 μm, the actual concentration of

Figure 6. Morphology of the catalyst support

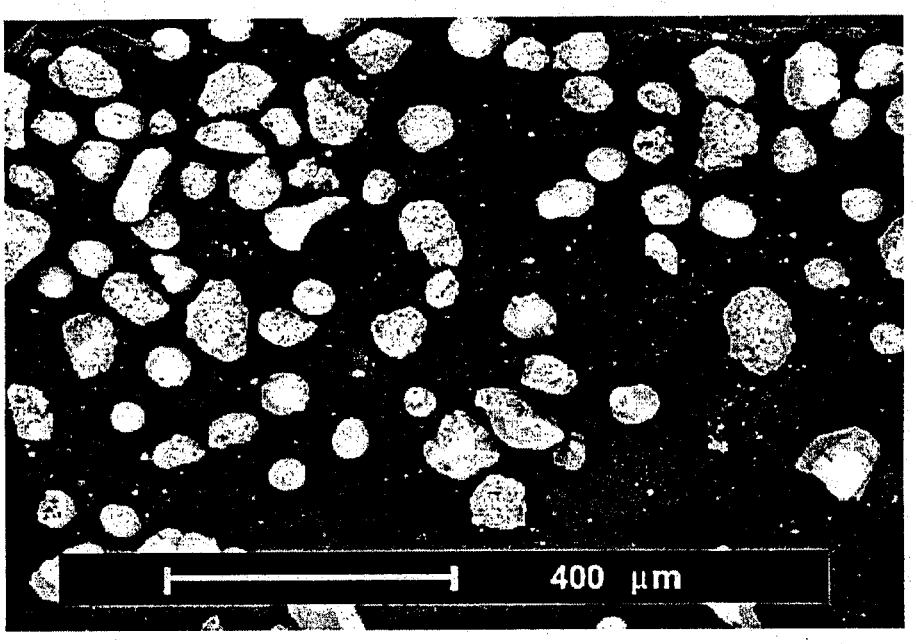

Figure 7. Morphology of the catalyst after SBCR FTS

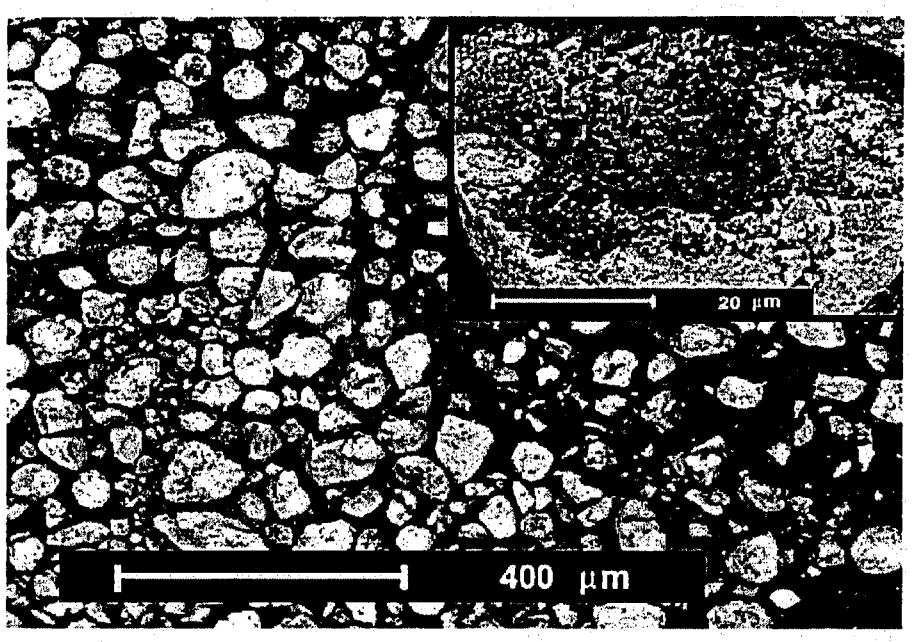

Figure 8. Comparison of PSD before and after the SBCR run

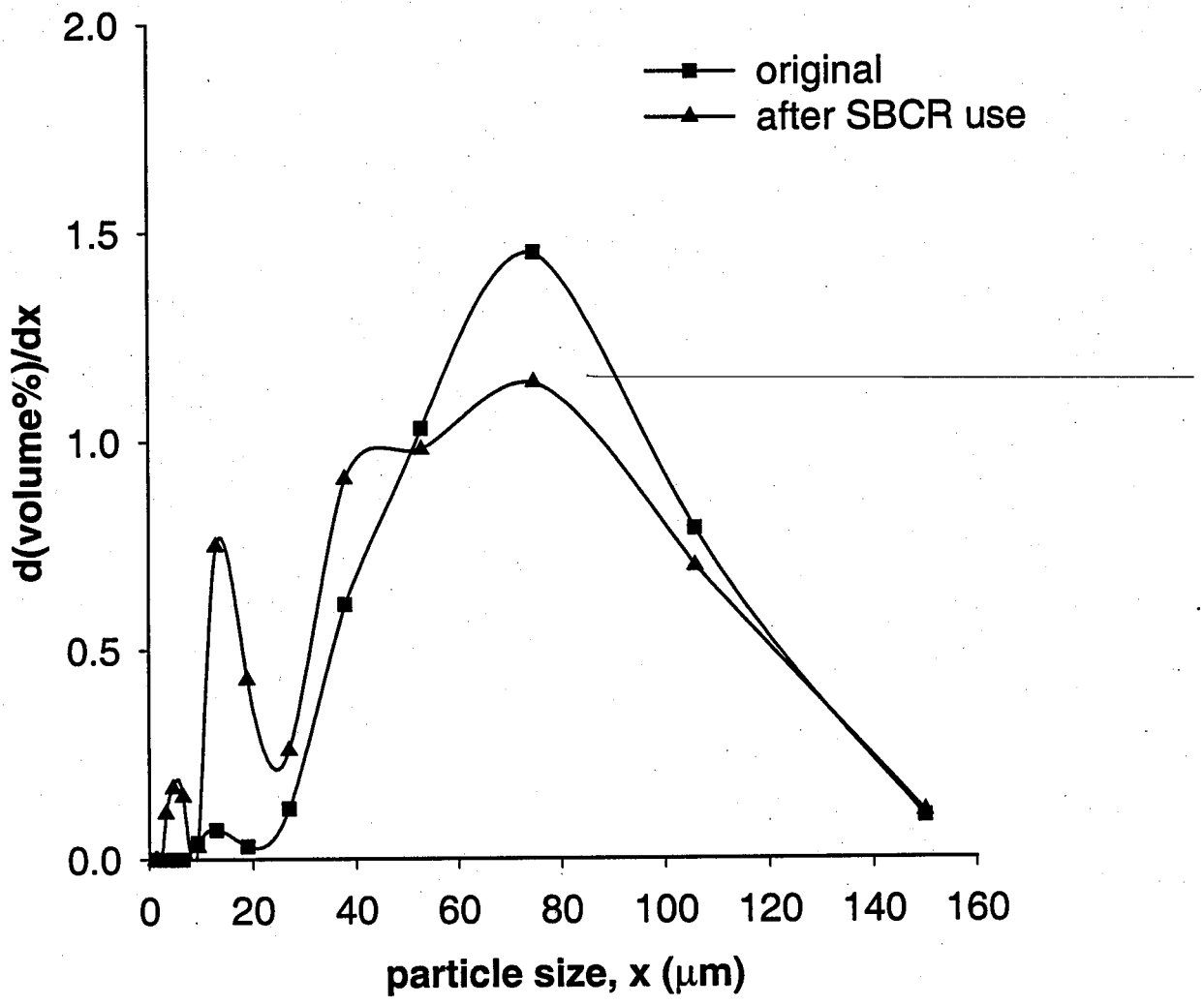

fine particles less than 10 μm should be higher. For particles larger than 30 μm, the PSD of the catalyst after SBCR use appears to have a bi-modal distribution as opposed to the essentially single modal distribution of the catalyst as prepared. Not only the average size, but also the concentration of these larger particles decreased during SBCR operation.

The attrition tests were run under various conditions and the resulting particle characteristics (from SEM) and size distributions were compared to those of the fresh catalyst and after the SBCR run. Figure 9 shows a comparison of the PSDs for the fluidized bed tests (after different lengths of testing time) with the PSDs for the catalyst as prepared and after the SBCR run. Due to the loss of most of fines <10 μm through the downstream filter during SBCR operation, all PSDs of the attrition test results were truncated to > 11 μm before being compared to the SBCR result. Note that all PSDs reported in this work include elutriated fines. The average particle size decreased with increasing time-on-stream in the fluidized bed. Both the weight percent of the elutriated fines (particles exiting the fluidized bed or jet cup and captured by the filter at the top of the system) and the volume moment, as well as other results, are summarized in Table 2. As can be seen by SEM, the particles remaining in the fluidized bed (Figure 10) were more spherical and/or smoother on the surface than those of the fresh catalyst (Figure 5). In addition, the number of cobalt patches on the outside surface of the catalyst particles was much less than that on the fresh catalyst particles. Particles elutriated (Figure 11) were less than 60 μm in size and included fragments and chips, as well as fines.

Similar results were found for the jet cup test. The particles remaining in the jet cup chamber (Figure 12) were more spherical compared to those of the fresh catalyst (Figure 5). However, the particles collected in the fines collection assembly of the jet cup test (Figure 13)

Figure 9. Comparison of PSD for the catalyst after the fluidized bed tests

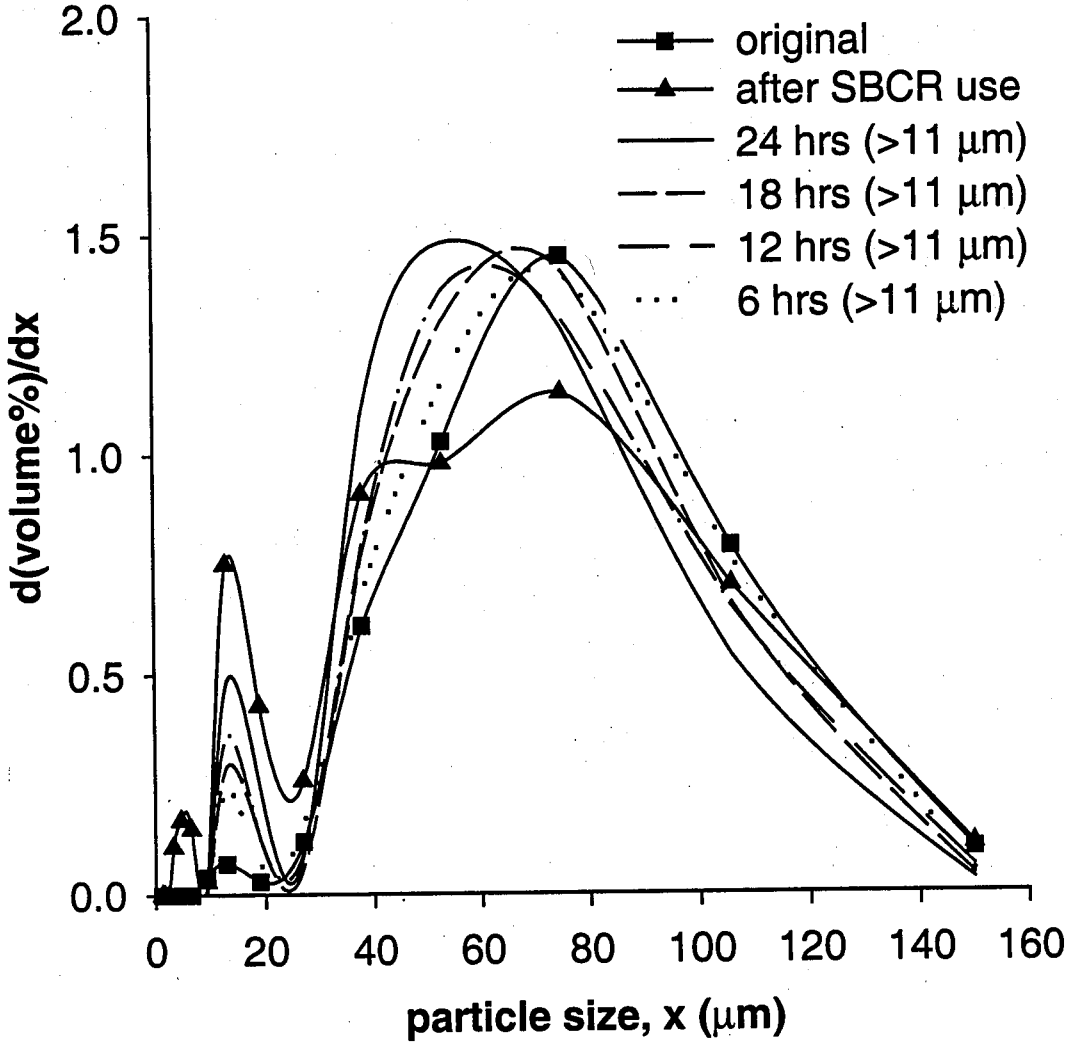

Table 2. Summary of attrition test conditions and results

Test	Flow Rate	Time-on-Stream	Elutriated Fines (wt%)	Volume Moment (μm)		Sphericity [a]	x_{g1}	x_{g2}	x_{g3}	x_{g4}	χ^2
				> 0 μm	> 11 μm						
Original Catalyst	NA	NA	NA	79.9	79.9	1.38	--	--	--	--	NA
After SBCR Run	NA	240 hr	NA	73.4	74.2	1.78	87.6	44.4	15.6	5.6	0.0
Fluidized Bed	1.5 l/min	6 hr	13.5	73.0	76.2	--	83.4	58.3	15.3	5.1	0.24
	1.5 l/min	12 hr	14.3	70.1	73.7	--	--	--	--	--	0.28
	1.5 l/min	18 hr	18.5	69.8	73.7	1.38	83.7	48.3	15.1	5.3	0.32
	1.5 l/min	24 hr	24.7	64.6	68.3	--	90.7	47.7	12.4	4.5	0.31
Jet Cup	10 l/min	1 hr	9.5	63.6	69.2	--	90.2	63.1	16.3	5.7	0.07
	15 l/min	1 hr	31.1	45.2	55.6	1.45	87.3	46.2	17.2	5.5	2.21
	20 l/min	1 hr	80.0	23.7	35.4	--	83.2	43.5	15.7	6.2	14.74
Collision	1.5 l/min	1 time	NA	78.7		--	--	--	--	--	0.45
	1.5 l/min	2 times	NA	78.3		1.36	83.8	52.5	16.0	--	0.35
	1.5 l/min	3 times	NA	78.6		--	--	--	--	--	0.47
Ultrasound	**150 W**	15 min	NA	73.7	73.7	--	86.9	59.5	15.0	2.8	0.42
	250 W	15 min	NA	63.3	65.5	1.46	85.3	55.1	15.3	4.6	0.28
	400 W	15 min	NA	61.4	64.2	--	89.0	55.0	14.5	5.1	0.32

a. sphericity=(circumference)^2 /4π*(projection area of particle outline)

$$\chi^2 = \sum_{i=1}^{k} \frac{(Observed - Expected)^2}{Expected}$$

Figure 10. SEM of the catalyst particles remaining in the fluidized bed (24 hrs time-on-stream)

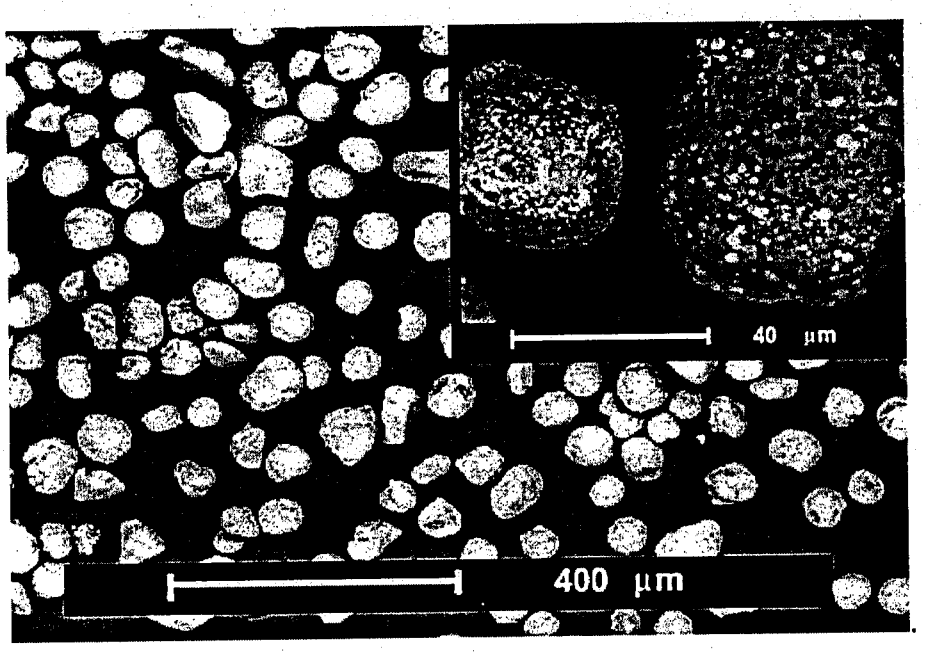

Figure 11. SEM of the elutriated fines of a fluidized bed test recovered in the fines collection assembly (24 hrs time-on-stream)

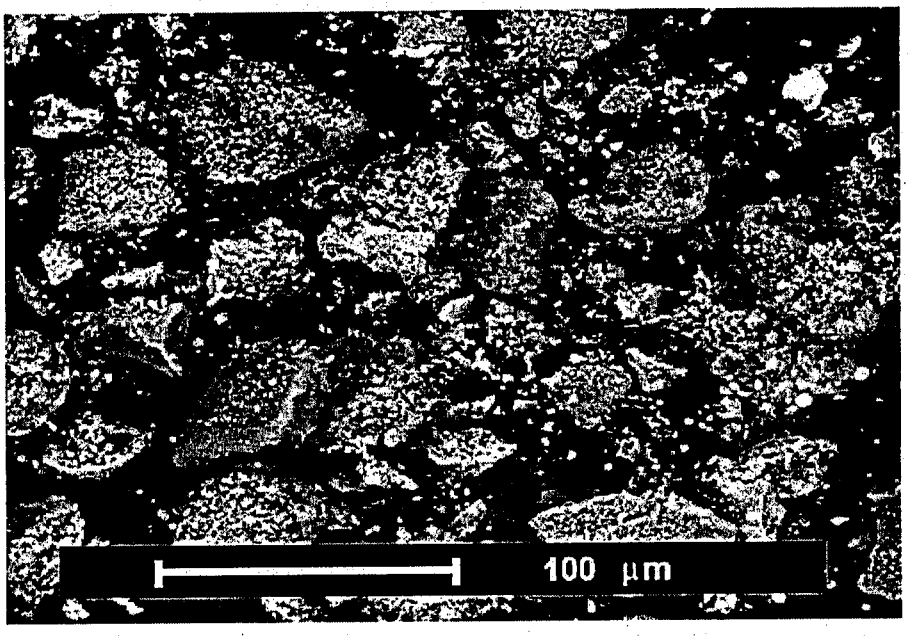

Figure 12. SEM of the catalyst particles remaining in the jet cup chamber (15 *l*/min flow rate)

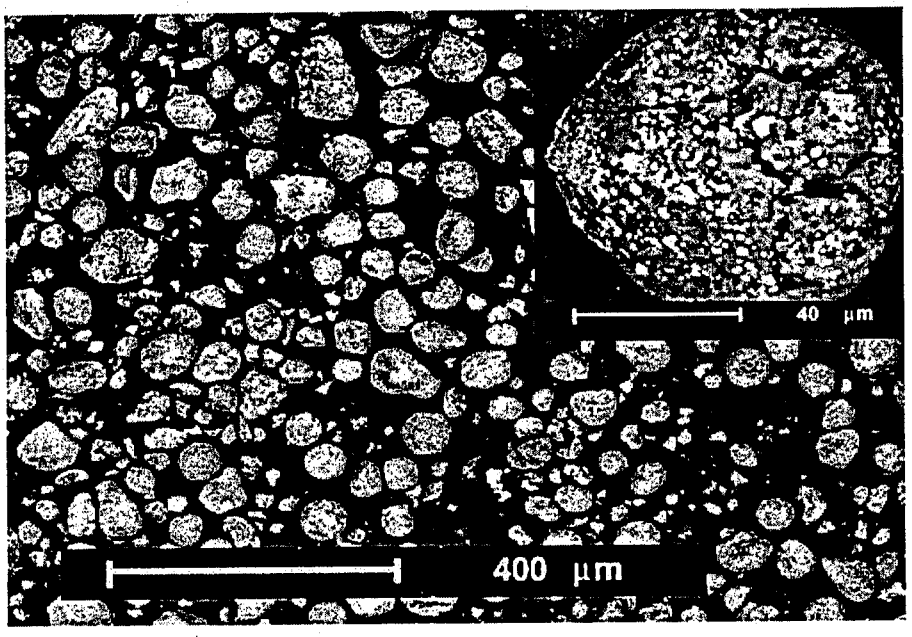

Figure 13. SEM of the fines in the fines collection assembly of a jet cup test 915 *l*/min flow rate)

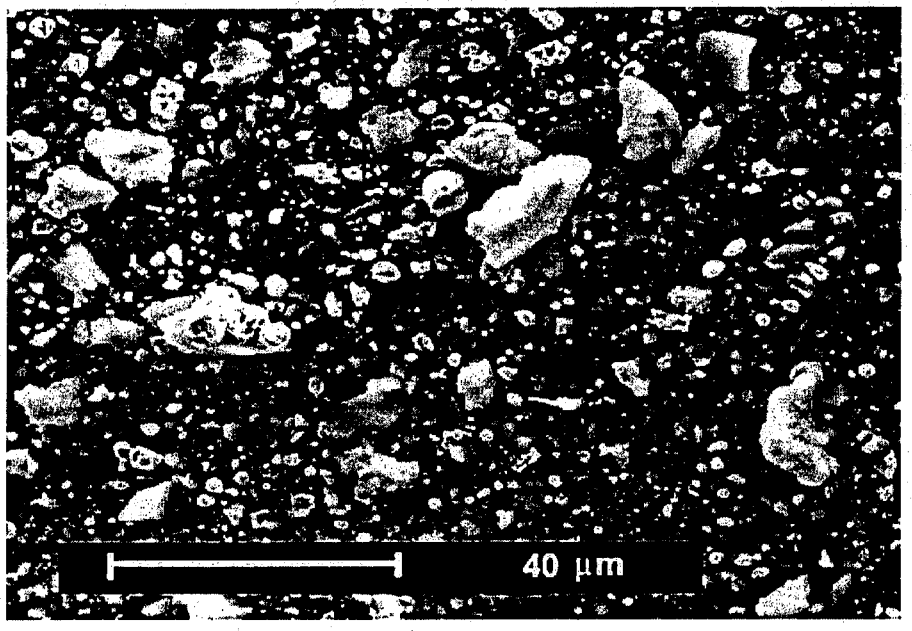

were smaller than for the fluidized bed, mostly chips and fines due to the different fluidization conditions (such as system configuration, flow rate, etc.) in the jet cup. No fragments larger than 30 μm were observed in the fines collected. In Figure 14, the PSDs following several 1 hr jet cup tests using different flow rates are plotted with the distributions of the fresh and the SBCR used catalyst. It is apparent that the mean particle size decreased with an increase in the flow rate.

Different from the results for the fluidized bed and jet cup tests, the change in mean particle size (volume moment) in the collision test, another air jet type test, was small even after multiple runs. The PSDs for different numbers of runs are plotted in Figure 15 and are very close to the PSD of catalyst as prepared. No particles less than 16 μm were observed. The morphology of the catalyst particles recovered after 2 sequential collision tests is illustrated in Figure 16. As expected, the particles after the collision test were similar to those of the fresh catalyst in morphology but contained slightly more chips. The cracks and fracture on larger catalyst particles were also more obvious than those on the fresh catalysts.

The ultrasonic test was the only test employed in the present study that did not involve a high velocity air jet but rather ultrasound. The breakdown of particles is believed to be caused by cavitation via the expansion and subsequent intense collapse of tiny bubbles in the liquid medium [28,29]. The PSDs resulting from different ultrasonic power settings are plotted in Figure 17. It is apparent that the degree of change in mean particle size increased with an increase in ultrasound power setting (or in other words power input), but this trend is not linear with the power input. The PSDs of the catalyst after testing were very close for the runs at power settings of 250 W and 400 W. The morphology of the particles after a 15 min ultrasonic

Figure 14. Comparison of PSD after the jet cup tests

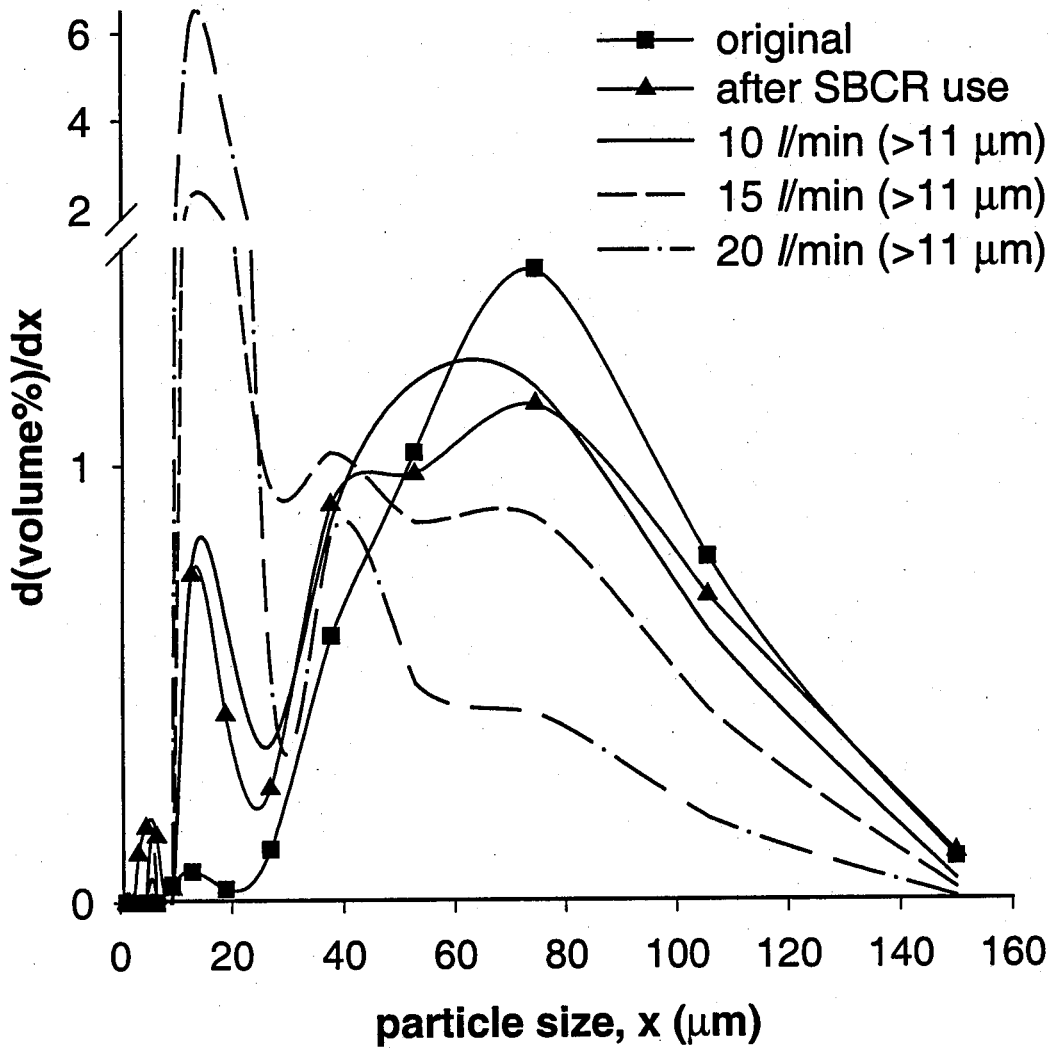

Figure 15. Comparison of PSD after the collision tests

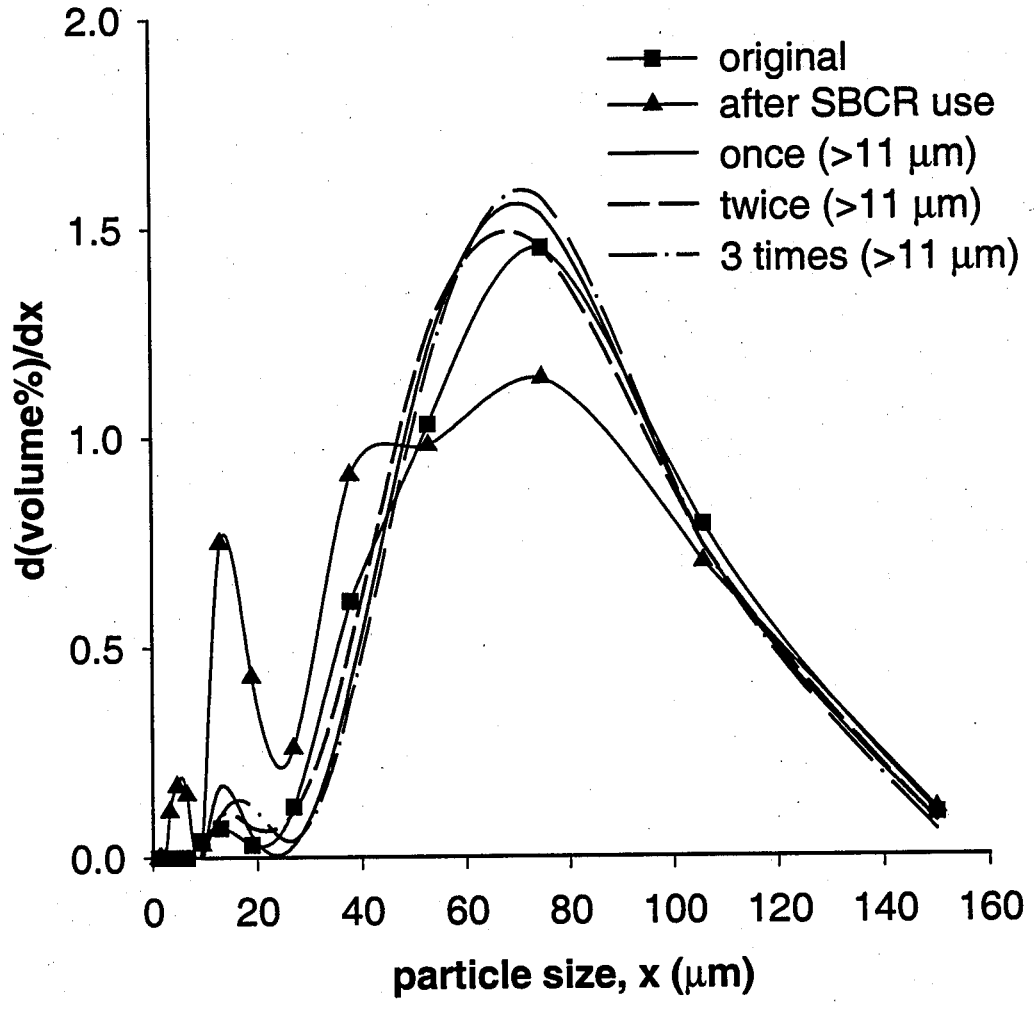

Figure 16. SEM of catalyst particles after a collision test (twice)

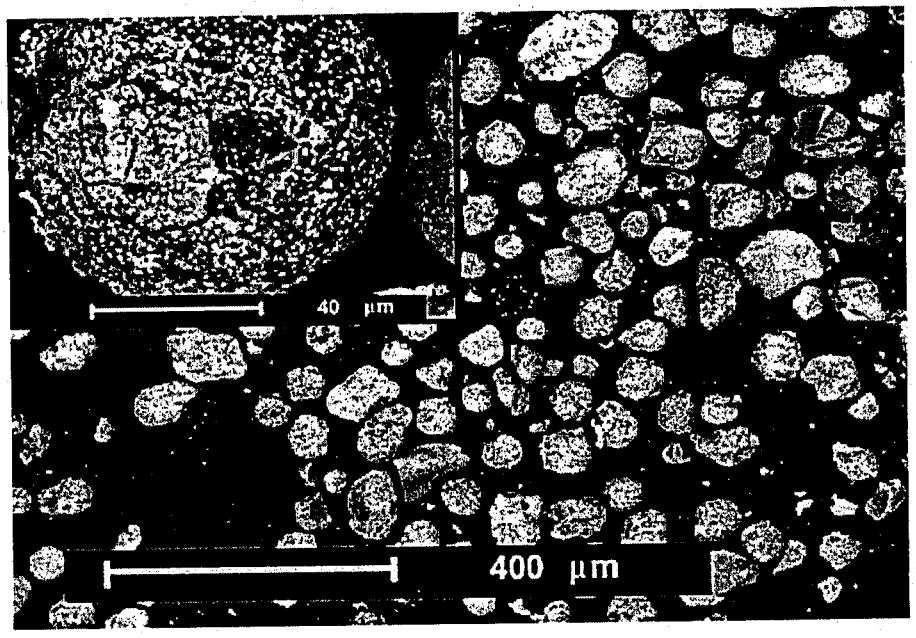

Figure 17. Comparison of PSD after ultrasound tests

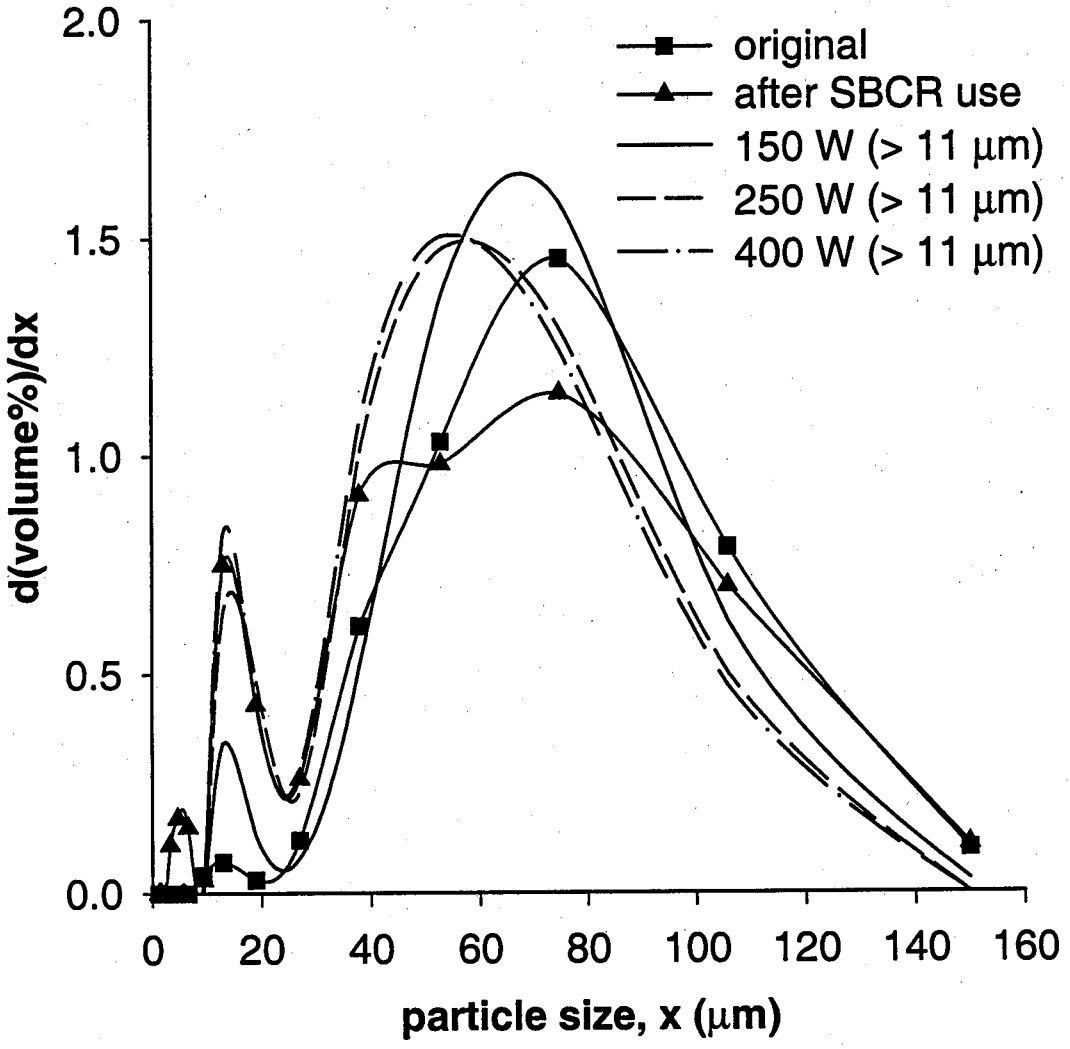

test at a power setting of 250 W is illustrated in Figure 18. The particles are apparently more spherical than those of the catalyst as prepared. Particle breakage may have been a result of crack propagation under pressure, rather than pure impact fractures.

4. DISCUSSION

4.1 Attrition Mechanisms in the SBCR

SEM provides a very powerful and direct determination of attrition mechanism since it is easy to distinguish broken particles resulting from abrasion or fragmentation based on particle morphology. Catalyst particles after the SBCR run (Figure 7) were much less spherical compared to the fresh catalyst (Figure 5). Compared to the fluidized bed and jet cup test results (Figures 10 & 12), surface layer removal was not evident for the SBCR sample (Figure 7) and cobalt patches on the catalyst surface were similar to those of the original catalyst (Figure 5). It is, therefore, speculated that the presence of the dense molten wax served as a "lubricant" between particles during the SBCR run and reduced the abrasion by a considerable degree. In order to quantify the particle morphology, the average particle sphericity was calculated based on the Scanning electron micrographs

$sphericity = (particle \quad circumference)^2 / (4\pi \times particle \quad projection \quad area)]$. The sphericity value for a spherical particle is 1, and this value increases with an increase in particle irregularity. As shown in Table 2, catalyst particles apparently were much less spherical after the SBCR run. This evidence suggests that the mechanisms of chipping and fragmentation, therefore, may have been the primary cause of attrition in the SBCR.

Figure 18. SEM of catalyst particles after an ultrasonic test (250 W power input)

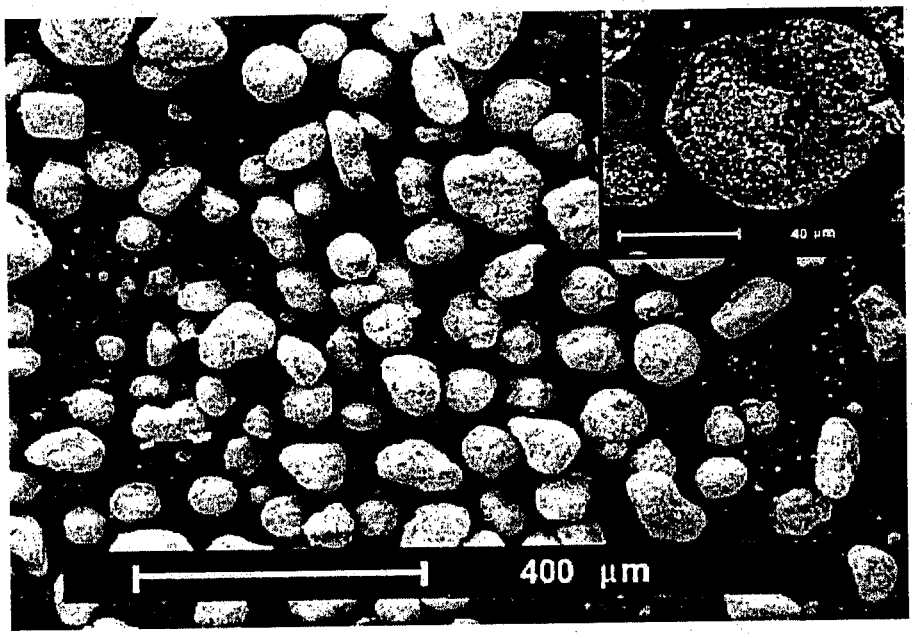

4.2. Attrition Mechanisms in the Attrition Tests

For the fluidized bed, jet cup and ultrasonic tests (Figures 10, 12, & 18), the large catalyst particles remaining were obviously smoother on the surface and more spherical compared to the fresh ones (Figure 5), which suggests that abrasion was much more important than during the SBCR run. Image analysis of these micrographs indicates that samples after the fluidized bed, jet cup and ultrasonic tests did not show any significant change in sphericity (Table 2). This might have been caused by the inclusion of the smaller and irregular fragments during image analysis. For fluidized bed and jet cup, only the SEM micrographs for the particles remaining in the chamber were used for image analysis. Since most of the fragments and chips were elutriated out in the fluidized bed, the sphericity value after this test was found to be relatively lower compared to that after the jet cup test. The higher sphericity value of the jet cup is considered to be partly due to the inclusion during image analysis of considerable amounts of fragments. For the ultrasound test, since all the particles were used for image analysis, a higher sphericity value was also observed.

While abrasion is more apparent for the fluidized bed, jet cup and ultrasound tests compared to that in the SBCR, it could not account for all the attrition. Instead, chipping and fragmentation both must exist in order to achieve the observed particle size reduction. Evidence of the existence of chips and fragments can be seen in the results after fluidized bed, jet cup and ultrasound tests (Figures 10-13, & 18).

It is obvious that the collision test is a different attrition process than the other three methods. As expected, since fracture is the dominant mechanism in this type of test, catalyst particles were less spherical (Figure 16) compared to those after the fluidized bed and jet cup tests (Figures 10 & 12). For the collision test, the change in volume moment was insignificant even after several consecutive runs (Table 2), although chips and small fragments can be

observed in the SEM micrograph (Figure 16). Perhaps only a few flawed particles broke or Microtrac measurement is unable to detect particle change if only a corner of a particle is broken off. This supports the suggestion [16] that there is a necessary velocity required for the threshold of significant particle breakage.

4.2 Comparison of the Different Attrition Tests

It has been shown above that the attrition processes in these tests differ somewhat from each other and also from that of the SBCR run. However, the goal of this work is not to find a test (or a specific experimental condition) that necessarily generates exactly the same attrition result as the 240 hr laboratory SBCR run, since application of a catalyst in a different SBCR would produce different attrition results. Rather, it is to determine a laboratory scale test that is able to reasonably mimic the attrition processes in an SBCR in order to predict the relative attrition resistances of different catalysts developed for SBCR use. Thus, a single attrition parameter cannot define an adequate attrition test. Instead, it is a combination of such parameters that can suggest a suitable test. The various attrition parameters are compared below.

The weight percent of elutriated fines (ratio of weight of fines recovered to total weight of catalyst recovered) was measured for both fluidized bed and jet cup tests and is listed in Table 2. The weight loss of elutriated fines increased with increase in time-on-stream for the fluidized bed test and with the increase in flow rate for the jet cup test, consistent with earlier reports [11,12,33]. In most attrition tests, the weight percent of elutriated fines is used as the sole measure of attrition. It is suggested that such a single measure, while giving a quick result, is inherently flawed due to the fact that elutriation rate is determined by many parameters, such as particle density and shape. In addition, due to different fluidization conditions, it is very difficult to use weight percentage of elutriated fines for comparison between the fluidized bed and jet cup

tests. Moreover, it is impossible to compare such results for these two tests with those of the ultrasonic test, the collision test, or the SBCR run, for which an amount of elutriated fines cannot be measured. Furthermore, similar to other reports [4,11], the attrition rate (weight of fines elutriated per unit time) in the fluidized bed test was found to decrease with time-on-stream, whereas the attrition rate in the jet cup test was relatively constant during the short period of testing (1 hr).

As shown in Table 2, the change in volume moment indicates that all the tests except the collision test were able to generate considerable attrition in relatively short periods of time. The volume moment value determined for the catalyst after the SBCR run is somewhat higher than the actual value since fines lost through the 10 μm filter were not included in the calculation. Thus, to provide a more exact comparison, the values of volume moment for the PSDs truncated at 11 μm are also listed in Table 2 for the SBCR run and all the tests. By comparing these volume moment values, three of the attrition tests can be considered to be reasonable in terms of producing attrition. For the 15 min ultrasonic (at 150 W power input), 1 hr jet cup (at 10 *l*/min flow rate), and 18 hr fluidized bed tests, the volume moments of the catalyst particles decreased approximately the same amount as that for the 240 hr SBCR run. The jet cup and ultrasonic tests appeared to be more aggressive in producing attrition in a shorter time than the fluidized bed test.

The PSDs can be further analyzed in order to determine the suitability of these tests in predicting SBCR attrition. Log-normal is the most commonly used distribution function for particle size in powder technology. In past studies, log-normal distribution was used to describe both the original and the resulting PSDs [32]. It has also been modified to describe samples of truncated or mixed particles [32, 33]. In the present study, a multi-model log-normal distribution was used to fit the experimental data. Considering the attrition mechanisms and the SEM results,

it was assumed that four different types of particles (unbroken/slightly broken particles, fragments, chips and fines) resulted during attrition. Therefore, a quad-model log-normal distribution as given by equation (2) was used to describe the catalyst particles after the SBCR run and attrition tests.

$$\frac{d\phi}{d\ln(x)} = \sum_{i=1}^{k} \frac{P_i}{\sqrt{2\pi}\ln(\sigma_{gi})} \exp\left[-\frac{\{\ln(x)-\ln(x_{gi})\}^2}{2\ln^2(\sigma_{gi})}\right] \qquad (2)$$

Where, ϕ is the general term for the frequency and volume percentage in this present study, σ_{gi} is the standard deviation for each peak, P_i is the percentage of each peak in the overall distribution, x_{gi} is the mean (or center) size of each peak, and x is the particle size. This distribution model fits the experimental data quite well (see Figures 19 and 20). The center values of each peak for the log-normal distributions are also listed in Table 2. The quad-model distribution was not used to deconvolute the PSD of the fresh catalyst because the catalyst as prepared and sieved consisted only of unbroken particles. Although there are only fifteen data points available for the Microtrac results for each sample, this deconvolution analysis is still considered applicable due to the good reproducibility of the Microtrac data points. However, the exact location of the peaks should be considered to be only approximate. As can be seen from Table 2, the center values for x_{g3} and x_{g4} are very similar for all the attrition tests and the SBCR run. Considering the SEM results, this might be a confirmation of the assumed existence of fines and chips (due to abrasion and chipping mechanisms). For the collision test, there was no

Figure 19. Curve fit of the results for the SBCR run

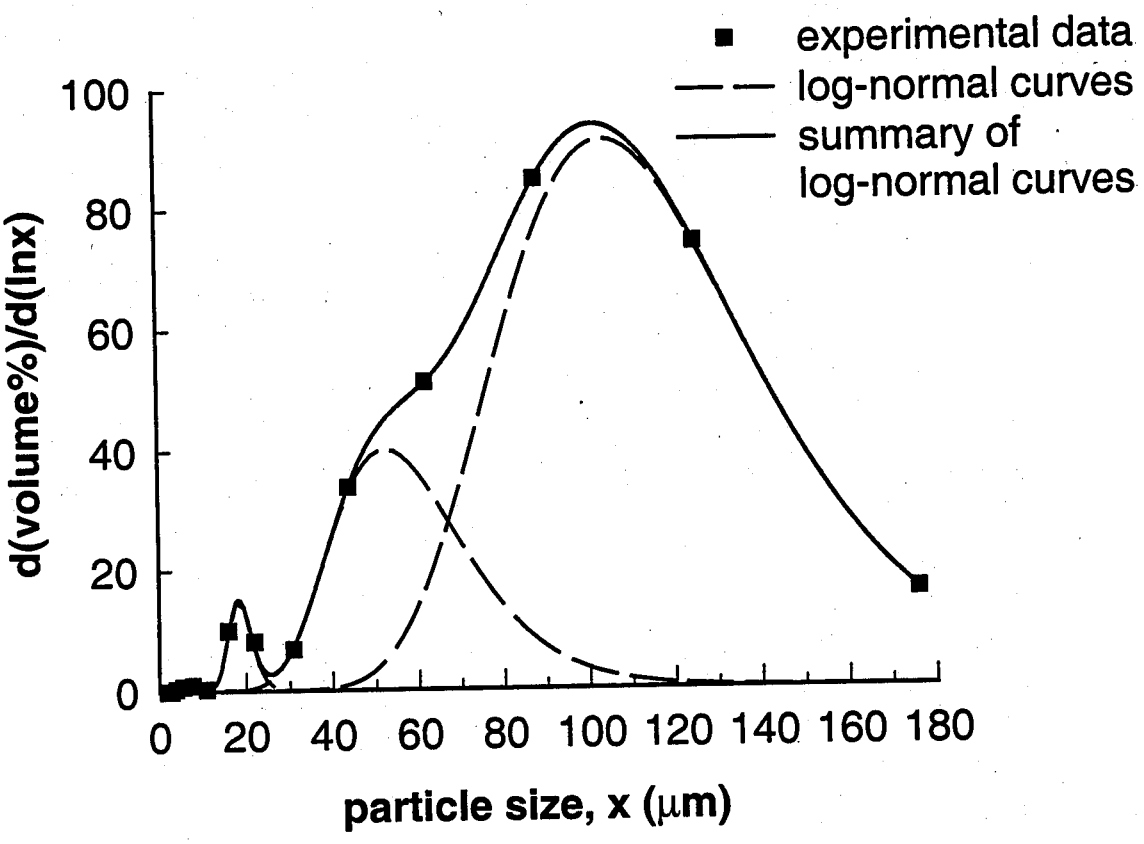

Figure 20. Curve fit of the results for the fluidized bed test for 24 hours time on stream

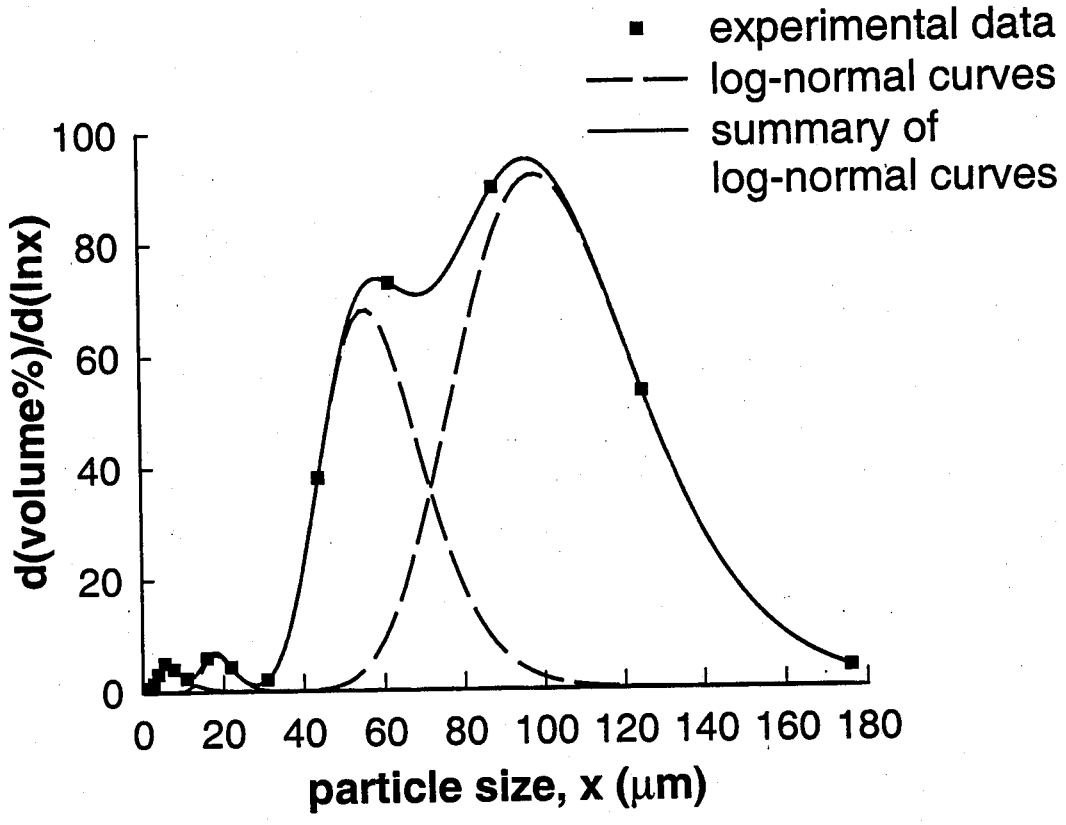

obvious peak for the fines (x_{g4}), suggesting that little abrasion occurred during the particle breakdown. However, the x_{g1} and x_{g2} of the different tests varied significantly. This is considered to be partly due to errors caused by the few data points available in the large particle size range. This difference is also probably partly due to differences in the fracture and abrasion mechanisms for the different tests. It seems that the x_{g2} value after the SBCR run was relatively lower than that after most of the tests. This might be a result of more fragmentation attrition during the SBCR run.

A Chi-squared (χ^2) test [35] was employed to determine the statistical goodness of fit for the PSDs after the various test methods to the PSD after the SBCR run. The χ^2 results are listed in Table 2 for all the tests. The closer the value of χ^2 is to 0, the better the goodness-of-fit and the better the test generated result matches the SBCR result. Only the jet cup test at 10 *l*/min showed near perfect fit. Other jet cup tests at higher flow rate deviated greatly due to aggressive attrition and the high concentration of fines generated. The PSDs from the fluidized bed tests showed poorer fits than the 10*l*/min jet cup test. The χ^2 value for the PSD's after the fluidized bed and ultrasound tests were similar and, as to be expected, better somewhat than those after the collision tests.

5. Conclusion

It was observed that catalyst attrition in a laboratory SBCR run differs somewhat from that in the attrition tests studied. Attrition in the SBCR and the collision test appeared to be fracture dominant, while abrasion was not very important. In the fluidized bed, jet cup, and ultrasound tests, abrasion was more important than in the SBCR, but fragmentation and chipping

also obviously occurred in order to give the particle size distributions (PSDs) which resulted. Although there are some differences in the attrition processes in different systems, the objective of this research was to determine a laboratory scale attrition test which is able to evaluate in a timely fashion the relative attrition resistances of different catalysts developed for SBCR use, rather than to produce exactly the same attrition result as a particular laboratory SBCR run. Therefore, the comparisons of attrition resulting from the different tests and the SBCR run focused on the overall suitability of these tests in mimicking the attrition in the SBCR, especially with regards to the PSD.

Since a single attrition parameter cannot define an adequate attrition test, various attrition parameters were compared. Among the parameters considered, attrition efficiency, i.e, the attrition generated during a certain period of time, was obvious an important criteria for determining the suitability of a test. Although the attrition mechanisms in the collision test appeared to be similar to that of the SBCR run, its attrition efficiency was too low to be suitable for testing attrition. On the contrary, obvious decreases in average particle size were obtained after fluidized bed, jet cup, and ultrasound tests. Using optimum operating conditions, all three tests produced attrition results in terms of change in average particle size, PSD, and % fines quite similar to that produced in the SBCR. Thus, all three tests can be used to study the relative attrition resistance of catalysts developed for SBCR usage. However, the jet cup (10l/min., 1 hr) can be considered slightly superior to the other two based on and in-depth analysis of PSD.

Reference

1. British Materials Handling Board, "Particle Attrition, State-of-the Art Review", Trans Tech, Germany, 1987.
2. Bemrose, C.R., and Bridgwater, J., Powder Tech., 49 (1987) 97.
3. Forsythe, W.L. Jr., and Hertwig, W.R., Ind. Eng. Chem., 41 (1949) 1200.
4. Gwyn, J.E., AIChE Symposium Series, 15 (1969) 35.
5. Zenz, F.A., Hydrocarbon Processsing, 50 (1971) 103.
6. Zenz, F.A., Hydrocarbon Processing, 53 (1974) 119.
7. Wei, J., Lee, W.Y., and Krambeck, F.J., Chem. Eng. Sci., 32 (1977) 1211.
8. Cairatl, L., Dl Flore, L., Forzatti, P., Pasquon, I., and Triflro, F., Ind. End. Chem. Process Des. Dev., 19 (1980) 561.
9. Vaux, W.G., and Fellers, A.W., AIChE Symposium Series, 77 (1981) 107.
10. Pedersen, L.A., Lowe, J.A., and Matocha, C.K., Sr., in "Characterization and Catalyst Development: an Interactive Approach", American Chemical Society, Washington DC, 1989, p. 414.
11. Weeks, S.A., and Dumbill, P., Oil and Gas J., 88 (1990) 38.
12. Werther, J., and Xi, W., Powder Tech., 76 (1993) 39.
13. Kalakkad, D.S., Shroff, M.D., Kohler, S., Jackson N., and Datye, A.K, App. Catal. A, 133 (1995) 335.
14. Fletcher, R., Oil and Gas J., 93 (1995) 79.
15. Srinivasan, R., Xu, L., Spicer, R.L., Tungate, F.L., and Davis, B.H., Fuel Sci. Tech. Int., 14 (1996) 1337.
16. Yuregir, K.R., Ghadiri, M., and Clift R., Powder Tech., 49 (1986) 53.
17. Cleaver, J.A.S., and Ghadiri, M., Powder Tech., 76 (1993) 15.

18. Ghadiri, M., in "Powder Technology Handbook, 2nd Edition", Marcel Dekker, New York, 1997, p. 283.

19. Beaver, E.R., AIChE Symposium Series, 70 (1974) 1.

20. ASTM D-4058-92, Standard Test Method for Attrition and Abrasion of Catalyst and Catalyst Carriers.

21. Dolling, P.K., Gainer, D.M., and Hoffman, J.F., J. of Testing and Evaluation, 21 (1993) 481.

22. Matocha, C.K., Sr., Crooks, J.H., and Plazio, P.P, in "Light Metals", AIME, New York, 1987, p. 129.

23. Matocha, C.K., Sr., and Crooks, J.H, in "Light Metals, Addendum", AIME, New York, 1987, p. 875.

24. ASTM D5757-95, Standard Test Method for Determination of Attrition and Abrasion of Powdered Catalysts by Air Jets.

25. Saxena, S.C., Catal. Rev. Sci. Eng., 37 (1995) 227.

26. Bhatt, B.L., Heydorn, E.C., and Tijm, P.J.A., in "Proceedings of the 1997 Coal Liquefaction & Solid Fuels Contractors Review Conference", US Department of Energy, Federal Energy Technology Center, Pittsburg, Pennsylvania, 3-4 September, 1997, p. 41.

27. Geanskoplis, C.J., in "Transport Processes and Unit Operations, 2nd Ed.", Allyn and Bacon, Boston, 1983, p. 134.

28. Thoma, S.G., Douglas, M.S., and Ciftcioglu, M., Powder Tech., 68 (1991) 53.

29. Thoma, S.G., Douglas, M.S., and Ciftcioglu, M., Powder Tech., 68 (1991) 63.

30. Austin L.G, Powder Tech., 5 (1971) 1.

31. Yu, A.B., and Standish, N., Powder Tech., 62 (1990) 101.

32. Allen T., in "Particle Size Measurement, 5th ed.", Chapman & Hall, New York, 1997, p. 45.

33. Ray, Y.C., Jiang, T.S., and Wen, C.Y., Powder Tech., 49 (1987) 193.

34. Inga, J.R., Ph.D. Dissertation, University of Pittsburgh, Pittsburgh, 1997.

35. Holman, J.P., in "Experimental Methods for Engineers, 3rd Edition", McGraw-Hill, New York, 1978, p. 51.